EXPERIMENTAL AND MODELING OF THE TRANSLATION STIFFNESS OF MAGNETORHEOLOGICAL ELASTOMER

Thesis

Submitted in partial fulfilment of the requirements for the degree of

DOCTOR OF PHILOSOPHY

by

UMANATH R POOJARY

DEPARTMENT OF MECHANICAL ENGINEERING

NATIONAL INSTITUTE OF TECHNOLOGY KARNATAKA,

SURATHKAL, MANGALORE-575025

October, 2018

D E C L A R A T I O N

I hereby declare that the Research Synopsis entitled "**Experimental and modeling of the translation stiffness of magnetorheological elastomer"** which is being submitted to the **National Institute of Technology Karnataka, Surathkal** in partial fulfilment of the requirements for the award of the Degree of Doctor of Philosophy in Mechanical Engineering is a bonafide report of the research work carried out by me. The material contained in this Research Synopsis has not been submitted to any University or Institution for the award of any degree.

Register Number : **123034ME12F08**

Name of the Research Scholar: **UMANATH R POOJARY**

Signature of the Research Scholar:

Department of Mechanical Engineering

Place: NITK-Surathkal

Date:

C E R T I F I C A T E

This is to certify that the Research Synopsis entitled "**Experimental and modeling of the translation stiffness of magnetorheological elastomer**" submitted by **Mr. Umanath R Poojary** (Register Number **123034ME12F08**) as record of the research work carried out by him, is accepted as the Research Synopsis submission in partial fulfilment of the requirements for the award of degree of **Doctor of Philosophy.**

Prof. K V GANGADHARAN
Research Guide
Date:

Chairman-DRPC

Date:

Dedicated
to
my Parents
and
my family

ACKNOWLEDGEMENTS

It has been a great experience to have worked under the guidance of Dr.K.V. Gangadharan Professor, Mechanical Engineering Department for my PhD at NITK, Surathkal. I would like to take this opportunity thank his continuous support, motivation and guidance throughout my research work. He has always been a great motivator to me and made me to realize what research meant to be. His timely inputs were very crucial, which made me to think in a right direction to get the solution for the problem in hand. I am indebted to the opportunity which he had given me to work on industrial projects (consultancy work), which helped me to strengthen my domain knowledge.

I wish to thank The Director, NITK Surathkal and the Head of the Mechanical Engineering Department for allowing me to conduct my research work. I am very thankful to Dr Prasad Krishna for giving an opportunity to work as Post Graduate Research Assistant under TEQIP II. I would like to thank all the teaching and non-teaching staffs of TEQIP II for supporting me throughout my research work. I would like to thank Dr Suresh Hebbar, Professor, Mechanical Engineering Department for his motivation and kind advises. I wish to extend my gratitude to Dr Mervin Herbert for his support during the theses writing.

I would also like to thank my Research Progress Assessment Committee members Dr. Katta Venkataramana (Professor, Department of Civil Engineering,) and Dr. Ravikiran Kadoli (Professor, Mechanical Engineering Department) for their valuable comments and critical inputs which helped in shaping up my Research work.

My sincere thanks to Dr Gururaja Udupa who is always a motivator for me. Special thanks to my dear friend Dr Sriharsha Hegde, who has continuously helped me during my work and also in correcting the thesis and my research papers. Special thanks to Dr Riessom Weldegiorgis for his motivation during my initial stages of my research. Thanks to Mr Giridhar Salian for being my source of inspiration to pursue Ph D. I would also like to extend my gratitude to Avinash B Pai who has been a constant source of inspiration who also happens to be my very good friend. My thanks to Mr Pranith Kumar Reddy and Poornachandra for their kind help in getting the research papers during initial stages of my research. I would like to thank my friend

Katari Kiran for his support in correcting my theses. I would like to I also would like to extend my gratitude to my SOLVE lab mates Pravin Shenoy, Susheel Kumar, Shyam Sundar, Praahas Amin, Kiran Aginthaya, Arun Kumar and Dr. Arun Parameswaran, for their continuous support. Thanks to Dr Vignesha Nayak for his timely help during my stay at NITK, I would like to thank Mrs. Jyothi who helped in many documentation-related activities. I also thank Mr. Jaya Devadiga, and Mr. Pradeep from Machine shop, Mechanical Engineering, for their support in conducting the experiments.

I would like to thank for the facility and funding support from SOLVE: The Virtual Lab @ NITK (Grant number:No.F.16-35/2009-DL Ministry of Human Resources Development) (www.solve.nitk.ac.in) and experimental facility provided by Centre for System Design (CSD): A Centre of excellence at NITK-Surathkal.

Finally and most importantly, I thank my parents, my brothers, my sister, my sisters in law, my nieces and nephew for their patience, their continuous support, and the love. I am indebted to my maternal uncle Late Mr. Thoma Poojary for his support and care towards my family during his entire life span. Also, I would like to extend my sincere gratitude to all the people who directly or indirectly contributed or motivated me to achieve this milestone.

(Umanath R Poojary)

Abstract

Magnetorheological elastomer is a potential resilient element to meet the vibration mitigation demands of a dynamic system over broad-band frequency. It comprises of ferromagnetic fillers dispersed in a non-magnetic elastomer matrix. Under the influence of an external magnetic field, these fillers readily interact and modify the properties of Magnetorheological elastomer. The response of magnetorheological elastomer under dynamic loading includes the contributions from the viscoelastic properties of matrix and the field sensitive characteristics of the filler. These properties are unique for a particular combination of matrix and the filler. The properties of Magnetorheological elastomer are sensitive to the changes in the operating parameters such as frequency and displacement amplitudes. This demands a large number of experiments to characterize the viscoelastic properties of Magnetorheological elastomer. On the contrary, the overall process of dynamic characterization is simplified by adopting a phenomenological modeling approaches based on the theory of linear viscoelasticity. It is important that the model should be able to represent viscoelastic behavior over wide frequency range in a simple form.

The present study is focused on modeling the translation stiffness to realize the concept Magnetorheological elastomer as boundary support damping applications. The dynamic tests are performed on Magnetorheological elastomer under shear mode (volume preserving deformation state) according to the dynamic blocked transfer stiffness method. The viscoelastic properties are evaluated at different frequency, magnetic field and strain amplitudes. These properties are expressed in terms of dynamic stiffness, and the loss factor evaluated from the force-displacement hysteresis loops. The test results indicated that the properties of Magnetorheological elastomer enhanced with an increase in magnetic field and the frequency. The magnetic field dependency is more pronounced compared to frequency. At larger values of frequency and magnetic field, the viscoelastic properties are saturated. For the tested MRE samples, the saturation behavior is observed at 50 Hz and 0.3 T. With an increase in strain the viscoelastic behavior of Magnetorheological elastomer changes from linear to nonlinear. Under magnetized state, the nonlinear behavior occurs at lower strain levels as the matrix-filler frictional energy dissipation is

intensified. In addition, Magnetorheological elastomer exhibits the Payne effect with the variation in input strain amplitude. The Payne effect is more pronounced under non-magnetized state and it diminished under magnetized state due to the contribution from the filler –filler interactions.

The material behavior of Magnetorheological elastomer is modeled by adopting the phenomenological models based on the viscoelastic constitutive relations. In the present study, integer and fractional order derivative based viscoelastic constitutive relations are used. Integer order based model comprises of six parameters, and the fractional order model are represented by five parameters. The parameters of the model are identified by minimizing the error between the response of the model and dynamic compression (translation) test data. Performance of the model is evaluated with respect to the optimized parameters estimated at different sets of regularly spaced arbitrary input frequencies. A linear and quadratic interpolation function is chosen to generalize the variation of parameters with respect to the magnetic field and frequency. The predicted response of the model revealed that the fractional order element model describes the properties of magnetorheological elastomer in a simpler form with reduced number of parameters. The fractional order based model has a greater control over the real and imaginary part of the complex stiffness, which facilitates in choosing a better interpolating function to improve the accuracy of the model. Furthermore, it is confirmed that the realistic assessment of the model performance is based on its ability to reproduce the results obtained from optimized parameters.

The material models based on the viscoelastic constitutive relations are not adequate to describe the amplitude dependent characteristics. These attributes are incorporated in the model by adding a linearized Bouc-Wen element. The proposed model comprised of eight parameters, which are identified by minimizing the least square error between the model predicted and the experimental response. The variations of each parameter with respect to the operating conditions are represented by a generalized expression. The parameters estimated from the generalized expression are used to assess the ability of the model in describing the dynamic response of Magnetorheological elastomer. The proposed model effectively predicted the stiffness characteristics with an accuracy, more than 94.3% and the corresponding

accuracy in predicting the damping characteristic is above 90.1%. This model is capable of fitting the experimental value with a fitness value of more than 93.22%.

Key words: Linear Viscoelasticity, Dynamic stiffness, Loss factor, Payne effect, Maxwell model, Fractional Maxwell model and Bouc-Wen model

TABLE OF CONTENTS

LIST OF FIGURES

LIST OF TABLES

NOMENCLATURE

MRF Magnetorheological fluid

MRE Magnetorheological elastomer

HTV High temperature vulcanization

RTV Room temperatures vulcanization

CIP Carbonyl iron powder

LVE Linear viscoelastic

SEM Scanning electron microscope

SDOF Single degree of freedom

ISO International Organization for Standards

NI-PXI National Instruments-PCI extensions for instrumentation

LabVIEW Laboratory Virtual Instrumentation Engineering Workbench

G Shear modulus

ε Strain

ω Operating frequency

ω_n Natural frequency

M Magnetic saturation

B Flux density

CHAPTER 1

INTRODUCTION

1.1 General background

Vibrations are ubiquitous and can be a cause of concern in many areas of mechanical, civil and aerospace engineering. Vibrations transferred from a dynamic system to the ambient structure is detrimental, and it will result in noise when transmitted to air (Koutsawa and Daya, 2007; Wollscheid and Lion, 2013). Therefore, isolating the structure from the risk of fatigue failure due to the excessive vibrations has posed a major challenge to design engineers. As a consequence, the focus has been shifted to integrating the vibration mitigation device during the design stage of a structure.

Several strategies are utilized for reducing the structure borne vibrations by limiting or altering the vibration response. Modifying the stiffness or mass is a simple approach as long as the excitation frequencies are invariant (Rao, 2004). However, in most cases, the vibrations need to be isolated or dissipated by using an isolator or damping materials (Nakra, 2000). The isolation or absorption of vibration is easy to realize in a simple structure, but its implementation in built-up structures is complicated. In general, a built-up structure is composed of beams, plates and shells, and is often exposed to a wide frequency range of excitations. The conventional vibration mitigation techniques like vibration isolation or absorption fail to yield the desired result as the disturbances excite a number of resonances (Nakra, 1998; 2000). In such cases, the damping plays a critical role in mitigating the vibration and dynamic stresses (Nakra, 1998). So focus has shifted to treating damping as a design

parameter rather than the modification to the system after the problem is encountered.

Damping is the dissipation of input mechanical energy from a vibrating system through heat. The resonant behavior of the structure is controlled as the damping attenuates the traveling waves. The damping in a beam or plate like structure is associated with the internal material damping or external damping (Wren and Kinra, 1992). Internal material damping originates from the internal atomic or molecular reconstructions of the microstructure or from the thermal effects as it is subjected to deformation (Nakara, 2001). The structural damping or external damping includes the mechanisms which are essentially external to a structure (Rao, 2004). The passive damping using viscoelastic materials is an effective way to impart external damping in a flexible structure. Energy dissipation by this technique is attributed to relaxation and recovery of the molecular chains as the coupled structure deforms the viscoelastic material. Passive damping treatments are cost-effective and suitable for high-volume production, which lead to their eventual applications in automotive, aviation, shipping and other industries (Nakra, 1998).

Free and constrained damping layers are the basic configurations of passive damping used in practice (Fan et al., 2009). In free layer damping, a layer of viscoelastic material (VEM) is bonded to an elastic member in the form of sprays or sheets. Constrained layer damping is characterized by a layer of viscoelastic material sandwiched between the constraining layer and the base layer. Both the approaches are successful in reducing the structure borne vibrations and noise, but it is not always feasible or desirable to implement them in real situations depending on the given

constraints. In such cases, the damping treatment at the boundary supports is an alternative solution (Kang and Kim, 1996).

The boundary support damping is augmented by using flexible elements like elastomer inserts between the beam or plate structure and the fixed support (Park et al., 2003). An example for this is an engine cradle and body sub frame, where the engine is connected to the chassis via elastomer supports or a wind shield in an automobile (Noll et al., 2014; Koutsawa and Daya, 2007). Insertion of an elastomer at the boundary support alters the structure's dynamic properties by modifying the boundary condition from fixed-support to elastomer-support (Park et al., 2003). Inclusion of elastomer at the boundary support is beneficial in two aspects: (1) it improves the energy dissipation by the damping and (2) it functions as a passive isolator by decoupling the structure from the disturbing source by interrupting the path of vibration (Tillema, 2003). Elastomer boundary support damping treatment offers a simple and cost-effective way of vibration isolation and damping. Moreover, it offers an inherent stability and reliability. Despite these, passive boundary support possesses an intrinsic drawback. Elastomer exhibits a poor adaptability to the different frequency of excitations and its performance is severely affected at wide frequency of disturbances (Jalili, 2002; Yoshioka et al., 2002).

The need for wide frequency range vibration attenuation cannot be met by a passive system with fixed stiffness and damping (Jalili, 2002). An active vibration control system is an alternative to accomplish such a requirement (Yu et al., 2001). However, the active systems are design-intensive and require sensors, control units and an energy source to provide real-time data to the isolator. As a consequence, weight, cost and energy consumption is increased significantly (Franchek et al., 1995;

Jalili, 2002). These shortcomings are addressed by smart material based semi-active vibration isolation systems (Liu et al., 2008). A semi-active system is a controllable passive device capable of suitably adjusting the stiffness or damping in response to the external excitation and/or from the measured response (Jalili, 2002; Ramallo et al., 2002; Yu et al., 2001). The semi-active system combines the advantages of both active and passive devises. It provides a good performance compared to a passive system, and it can still function as a passive device even when the control system fails (Yao et al., 2002). Semi-active systems are economical and do not require higher-power actuators. The controllable element in a smart material based semi-active isolators include piezoelectric materials, shape memory alloys, electrorheological fluids, magnetorheological fluids and magnetorheological elastomers (Stelzer et al., 2003; Winthrop et al., 2005). Among these, magnetorheological materials are the ideal choice as they have the ability to change the mechanical properties rapidly and reversibly under the action of a magnetic field (Jolly et al., 1996). Moreover, due to the fixed microstructure and the resemblance to a passive resilient element, magnetorheological elastomer is viewed as a potential material for boundary support damping applications (Zajac et al., 2010).

1.2 Magnetorheological Elastomer: A material overview

Magneto Rheological Elastomers (MRE) are smart composite materials comprising of an elastomer matrix and ferromagnetic filler particles (Lokander and Stenberg, 2003a). MRE attains a fixed microstructure as the filler particles are locked in a position after curing the elastomer (Figure 1.1). Fixed microstructure of MRE has an obvious advantage in terms of ease of storage, better strength, reliability and no sedimentation related issues (Caterino et al., 2014). Upon application of a magnetic

field (on-state), the particles acquire a magnetic polarization and from a chain-like structure (Figure 1.2). This process modifies the internal structure and results in the variation of mechanical and electrical properties. These novel characteristics of MRE have created a broad application prospects like smart vibration isolation (Behrooz et al., 2014), adaptive tuned vibration absorber (Sun et al., 2014), magnetic field and force measurement sensors (Li et al., 2009; Du and Chen, 2012) and actuators (Koo et al., 2012).

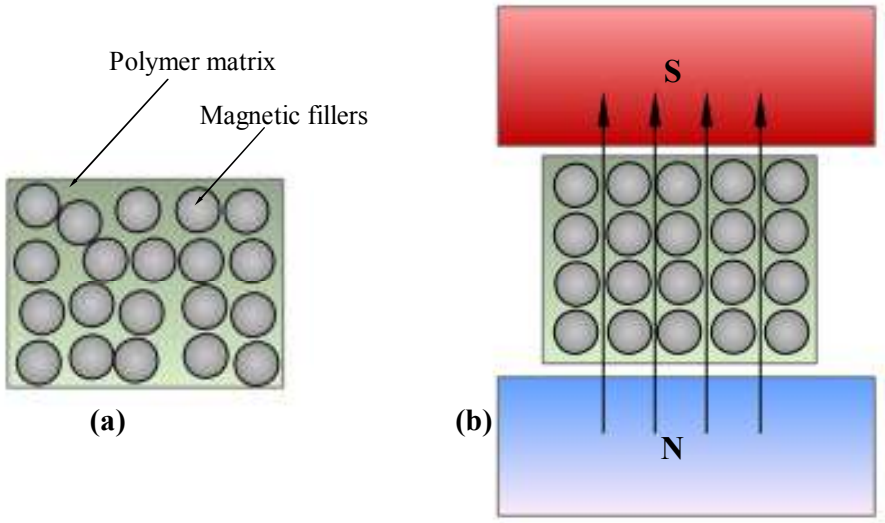

Figure 1.1. Magnetorheological elastomer (a) before and (b) after application of external magnetic field

1.3 Magnetorheological Elastomer as a resilient element for semi-active vibration mitigation device

MRE based semi-active vibration isolation is analogous to a passive vibration control technique, but differs in the sense that the stiffness and damping can be altered in response to the command signals (Behrooz et al., 2014). The semi-active vibration isolation provides a better dynamic performance to a structure over a wide frequency range. The concept of MRE based semi-active vibration isolation is visualized using a

single degree freedom (SDOF) transmissibility model representing the fundamental mode of the structure (Stelzer et al., 2003).

A receiving structure mounted on a vibrating source through a passive isolator with equivalent stiffness (K_P) and passive damping (C_P) is represented in Figure 1.2a. The same structure coupled through a MRE isolator of equivalent stiffness K_{SA} and equivalent damping C_{SA} is represented Figure1.2b.

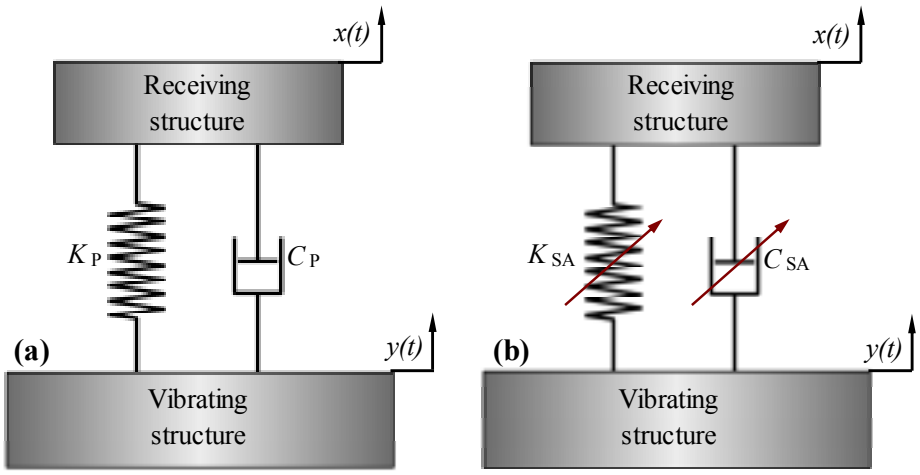

Figure 1.2. (a) Transmissibility model of a SDOF system with passive isolation. (b) Transmissibility model of a SDOF system with semi-active isolation.

A generalized expression for the displacement transmissibility ratio with stiffness K and damping C as a function of excitation frequency ω and receiver mass m is given by (Stelzer et al., 2003),

$$\frac{x}{y} = \frac{K + j\omega C}{K - m\omega^2 + j\omega C} \tag{1.1}$$

The transmissibility response plot of a SDOF system is shown in Figure 1.3. The frequency ω_n, represents the resonance frequency of the receiving structure. In the absence of an isolator, the structure experiences an excessive vibration at ω_n as the path for the transmission of vibration energy is uninterrupted. On the contrary, a passive isolator decouples the path for vibration transmission by modifying the

resonance frequency of the system to ω_{Pn} (where, $\omega_{Pn} < \omega_n$). As a consequence, a significant reduction in the displacement transmissibility at ω_n can be visualized from the graph.

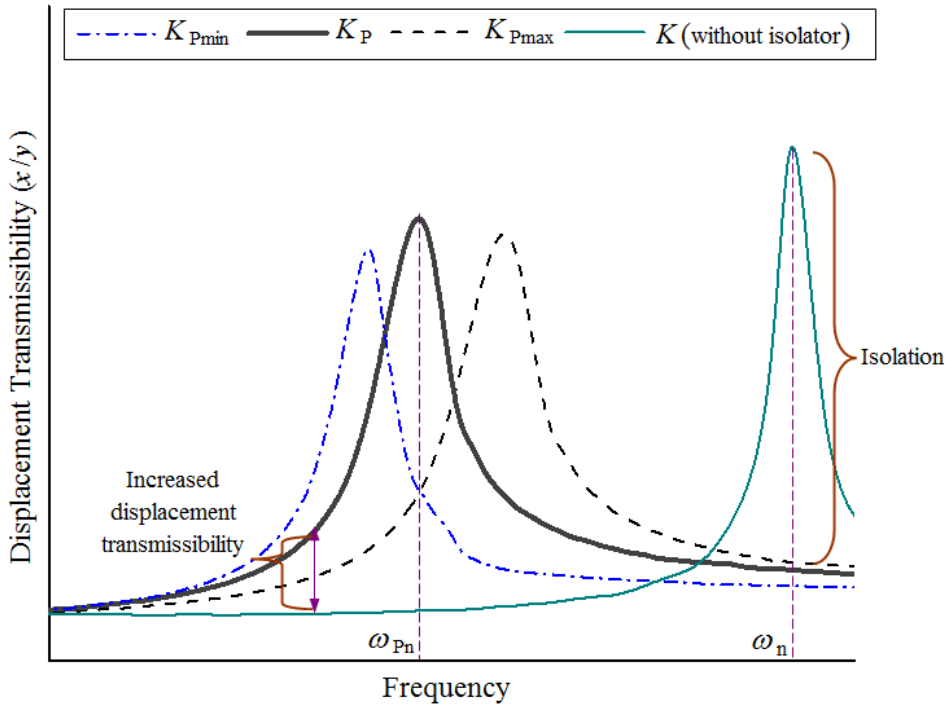

Figure 1.3. Transmissibility response plot of a SDOF system.

The success of passive vibration isolation depends on the properties of the isolators being used. Soft or low stiffness (stiffness K_{Pmin}) isolator yields better vibration isolation at ω_n. But, these isolators are susceptible to heavy loading at lower frequencies by maintaining acceptable displacement in relative to an exciting source. Conversely, a stiff isolator (stiffness K_{Pmax}) could meet the durability and displacement criteria, but its isolation performance at ω_n is lower than the soft isolator. Consequently, the choice of stiffness K_P is an obvious trade-off between the low and high-frequency isolation to meet the durability, displacement and isolation criteria of an isolator.

However, a MRE based semi-active isolator could yield a better isolation performance by modifying the properties under the influence of an external magnetic field. With an efficient control strategy, the stiffness and damping characteristics of MRE isolator are altered to meet the demand for vibration isolation over a wide frequency range. At lower frequencies, stiffness of the MRE is increased by energizing the magnetic circuit to overcome the larger displacements. Subsequently, by de-energizing the magnetic circuit, the stiffness of MRE is lowered to mitigate the vibrations at higher frequencies.

1.4 Concept of a beam on Magnetorheological Elastomer boundary support

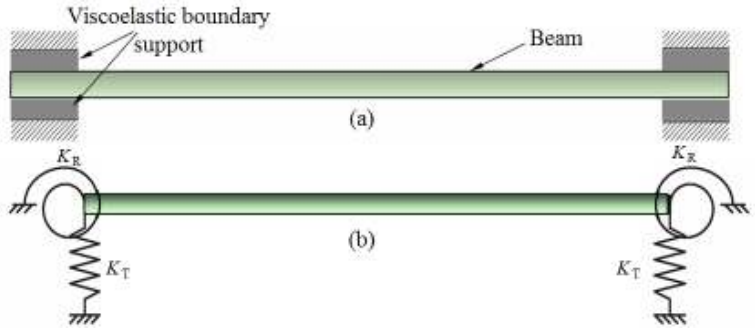

Figure 1.4. (a) Representation of a beam on viscoelastic boundary supports. (b) Simplified representation of a beam with complex stiffness at the support region.

Boundary support (Figure 1.4a) damping by a viscoelastic resilient element is a viable option to overcome the shortcomings of free layer and constrained layer damping (Kang and Kim, 1996). With the inclusion of the boundary support element, the dynamic response of the beam is altered as the modal characteristic of a beam is modified. To simplify the dynamic analysis of a beam, the support masses are often neglected in relative to the mass of a beam (Park et al., 2003). As represented in Figure 1.4b, the boundary support regions are idealized as rotation (K_R) and translation (K_T) springs with complex stiffness (Fan et al., 1998). The support

stiffness K_R and K_T have a significant influence on the modal characteristics of a beam. The natural frequency of a beam changes from free-free to simply-support as the translation stiffness K_T is increased. However, at higher values of K_T, the beam transforms from a simply-support to a fixed-fixed boundary as the K_R is increased from zero (Kang and Kim, 1996).

In case of a beam on MRE boundary support, passive viscoelastic material is replaced by MRE. The support stiffness K_T and K_R, which were invariable, exhibits magnetic field sensitive characteristics. Under the influence of magnetic field, the support stiffness is modified, which alters the modal characteristics of a beam. To understand the dynamic response of a beam on MRE boundary support, the support stiffness K_T and K_R of MRE needs to be represented mathematically.

The properties of MRE are highly complex in nature. It involves the contribution from the viscoelastic properties inherited from the matrix and the field responsive characteristics from the ferromagnetic fillers. In addition, it also exhibits the attributes of a filled elastomer, which is sensitive to the frequency, preload, amplitude and temperature (Olabide et al., 2014).

The characterization of the support stiffness K_T and K_R demands a great amount of preliminary tests. To reduce the cost and time in performing the tests, phenomenological models based on viscoelastic constitutive relations can be implemented. In fact, these models cannot completely replace the experimental investigations, but they can reduce the amount of experiments substantially. However, the research on MREs is still nascent as the data set for the properties of specific class of MRE (type of matrix; filler and its composition) is missing and moreover, no accurate material model for MRE is formulated and verified.

Modeling the support stiffness is decisive to realize the concept of a beam on MRE boundary support. The present work aims at developing an efficient viscoelastic constitutive model to mathematically represent the complex translation stiffness of MRE boundary support over a broad frequency range. The fundamental requirement for the current study can be viewed from two standpoints, which involves understanding the basic viscoelastic behavior of MRE. Later, these results are used to develop a mathematical model for computing the complex translation stiffness of MRE.

1.5 Outline of the thesis

The thesis is grouped into 8 chapters. Chapter 1 provides a general background of the present investigation. An overview of the semi-active vibration mitigation concept by employing MRE resilient element is discussed. The significance of translation and rotation stiffness on the dynamic performance of a beam on viscoelastic boundary support is presented, and the challenges involved in realizing the beam on a MRE boundary support are addressed.

Chapter 2 deals with the thorough and critical review of the existing literature in the field of MRE synthesis, its properties, various approaches to characterize the viscoelastic nature of MRE, the effect of processing and operating parameters on the field sensitive characteristics of MRE and the material modeling aspects of MRE. The literature review points out the research gap and provides the direction for further research. Based on the unanswered questions from the literature survey, the scope of the work is formulated, which is presented at the end of the chapter.

Chapter 3 deals with the experimental characterization of dynamic properties of MRE. The forced vibration tests are performed on MRE to evaluate the frequency

and magnetic field dependent properties. In addition, the effective range of operating frequency and the magnetic field are also assessed.

In chapter 4, the linear viscoelastic region of MRE is evaluated to assess the limiting strain where the models based on the viscoelastic constitutive relations could yield satisfactory results. Furthermore, these studies are extended over the transition region to evaluate the influence of strain on the field-induced characteristics of MRE.

Chapter 5 deals with the dynamic viscoelastic property characterization of MRE under compression (translation) loading. The compression experiments are aimed to develop the phenomenological models of MRE to mathematically represent the compression stiffness of MRE.

In chapter 6, the viscoelastic modeling approaches to represent the frequency and the magnetic field sensitive behavior of MRE are presented. Two types of modeling approaches using an integer and fractional order framework are proposed. Both the models are evaluated based on the predictive accuracy in portraying the viscoelastic behavior over a wide frequency range. These modeling approaches are extended to incorporate the amplitude dependent characteristics, which are discussed in chapter 7. A generalized expression for the translation stiffness of MRE is formulated based on these models, and its effectiveness is tested in terms of the ability to reproduce the experimental results. In the chapter 8 the summary and the major conclusions drawn from the current work are presented.

CHAPTER 2

LITERATURE SURVEY

2.1 Introduction

The demand for vibration mitigation over broad-band frequency calls for the development of a new category of smart materials. MRE is one such material, with the potential to achieve the ultimate objective. The design and development of MRE based device is a complex task, as its properties are distinctly different from the conventional elastic materials. Properties of MRE are viscoelastic in nature, which are sensitive to the variation in the dynamic loading condition. Therefore, the design of MRE device demands a proper understanding of the material properties of MRE and its representation in a mathematical form to implement the control strategies. In recent years, research carried out on the development of MRE and its devices continued the stride to achieve enhanced properties to improve the working range and the effectiveness of a device.

The relevance of a beam on viscoelastic boundary support has been discussed in chapter 1. To implement MRE as a boundary support element, a proper understanding of its material properties, modeling approaches and the limitations are very important. In this chapter, a thorough and critical review of the existing literature on the MRE has been carried out. The literature survey provides a better insight into the MRE synthesis, property characterization and modeling approaches. In addition, the findings from the literature survey provide the direction and the road map for the proposed study. The literature review presented in the chapter is divided into the following broad sections.

1. Basic configuration and modes of operation.
2. Novel field-induced properties of MRE.
3. Viscoelastic property characterization of MRE.
4. Influence of processing parameters on the field-induced characteristics of MRE.
5. Influence of operating parameters on the field-induced characteristics of MRE.
6. Material modeling of MRE.

2.2 Basic configuration and modes of operation

Compared to conventional filled elastomers, MREs have an advantage in controlling the spatial distribution of the fillers inside the elastomer matrix. This can be achieved by applying a strong uniaxial magnetic field during the curing process of the matrix material (Filipcsei et al., 2007). Based on the dispersion of particles inside the matrix, MREs are categorized as anisotropic and isotropic (Bose and Rode, 2009; Xu et al., 2011; Kaleta et al., 2011). Anisotropic or structured MRE is synthesized in the presence of an external magnetic field. The filler particles in an anisotropic MRE have an ordered arrangement, which is originated from its alignment in the direction magnetic field during the pre-cure state (Collette et al., 2010). Formation of a chain like structure in the matrix exemplifies the attempt by the fillers to reach the minimum energy state during the field-induced dipole interactions (Li et al., 2012; Kallio et al., 2005). In contrast, the curing process of an isotropic MRE is carried in the absence of magnetic field, which results in a uniform distribution of the particles in the matrix (Melenev et al., 2011; Han et al., 2011). From the microstructure point of view, both

isotropic and anisotropic MREs are differed significantly, which in turn influences the properties under active as well as the passive state (Bose and Roder, 2009).

Distribution of filler particles during the curing process depends on strength of the magnetic field, initial dispersion of the fillers, the viscosity of the polymer solution, temperature of the melt and the duration of application of external magnetic field (Han et al., 2013). The initial distribution of the particle is associated with the Brownian motion, which makes the particles to arrange themselves in a random direction (Chen et al., 2007a). However, the configuration of the chain structure depends on the intensity of the magnetic field. At lower magnetic field strengths, the dipole interaction between the particles is low, which results in the formation of short and thin chains. Increasing the magnetic field strength, the dipole interaction overcomes the resistance of the matrix, resulting in the formation of a thick and long columnar structure (Chen et al., 2007a). Formation of chain structure also depends on the viscosity of the matrix. A highly viscous matrix provides more resistance during the initial distribution of the particles and also creates an unfavorable condition for the mobility of the particles to align along the direction of magnetic field (Ge et al., 2013; Lu et al., 2012). Moreover, the viscosity of the polymer matrix depends on the temperature of the polymer melt. At higher temperature, the viscosity of the polymer melt is low and it offers a lesser resistance to the formation of columnar structure under the magnetic field (Lu et al., 2012).

Influence of larger pre-cure cycles is insignificant on the properties of MRE due to the formation of equilibrium chain structure. However, it plays a prominent role during the initial stage of the pre-structuring process as it promotes the formation of longer chains (Lu et al., 2012). The pre-cure time is varied with the type of matrix

material, which also depends on the external magnetic field. Past literatures have reported an equilibrium time of 5 min for polyurethane (Gong et al., 2012a) and 20 min for SEBS (Lu et al., 2012) matrix. Apart from the alignment of fillers along the orthogonal direction, the chains can be arranged in a desired direction with respect to the testing magnetic field (Boczkowska et al., 2012). However, the anisotropic MRE is more stable if the testing magnetic field direction is parallel to the iron particle chains (Xu et al., 2011).

Though anisotropic MREs have a superior property than the isotropic MRE, it has several shortcomings in the synthesis process that essentially limit their applications. The synthesis of anisotropic MRE requires a modification in the conventional elastomer fabrication equipment to accommodate the pre-structuring magnetic field during crosslinking. The effectiveness of pre-structuring process depends on the thickness of MRE. Fabrication of a thick MRE is impractical; as the magnetic flux density shows a significant reduction with the increase in thickness. Moreover, it is important to consider the chain direction of MRE, before implementing it in any MRE based devices (Gong et al., 2005).

Based on the direction of deformation and the testing magnetic field, the operational modes of MRE are categorized as shear mode and squeeze mode (Popp et al., 2009; Fu et al., 2013). In the shear mode, the direction of deformation is perpendicular to the direction of the testing magnetic field (Bose and Roder, 2009; Kaleta et al., 2011; Lu et al., 2012; Gong et al., 2012a; Ge et al., 2013). The shear mode can be in oscillatory or rotary shear configuration. The test specimen is subjected to a pure shear loading in oscillatory shear (Kaleta et al., 2011), and torsional loading in rotary shear (Ge et al., 2013). In squeeze mode, the testing

magnetic field and the direction of deformation are parallel (Gordaninejad et al., 2012; Koo et al., 2010). However, in an actual application, combinations of shear and squeeze mode may be encountered. This kind of loading situation is referred to as the mixed mode (Li et al., 2012). Like conventional elastomers, the modes of operation have a significant influence on the properties of MRE. The load-bearing capacity of MRE is higher for squeeze mode when compared to the shear mode (Popp et al., 2009). Moreover, the mechanisms of dipole interaction between the fillers under squeeze mode and shear mode are distinctly different (Liao et al., 2012; Jolly et al., 1996). In comparison to the squeeze mode, the pure shear mode is an effective way of characterizing the property as it represents the volume preserving deformation state (Chazeau et al., 2000).

2.3 Properties of Magnetorheological Elastomer

Magneto mechanical coupling between the polymer matrix and magnetically permeable fillers impart enhanced properties like magnetoviscoelasticity, magnetoresistance, piezoresistance, magnetostriction and pseudoplasticity. With these unique features, MRE can transcend from being a conventional material to a one which open up the possibilities for new technological applications (Behrooz et al., 2014; Sun et al., 2014; Du and Chen, 2012; Li et al., 2009; Koo et al., 2012).

Magnetoviscoelasticity is the magnetic field dependent response of MRE when subjected to an external loading (Lokander and Stenberg, 2003a). Without an exception, MRE is a polymer composite exhibiting viscoelastic behavior. In response to the mechanical loading, it behaves like an elastic solid at some instances and at some instances as a viscous fluid. In general, the property of MRE is intermediate

between the ideal solid governed by Hooke's law and ideal liquid behavior described by the Newton's law of viscosity (Sasso et al., 2011).

The response of viscoelastic material for an external loading comprises of two terms. The first term represents the instantaneous response of the continuous medium, and the second term signifies the delayed response involving the loading history at the preceding instant (Cosson and Michon, 1996). These properties are expressed in terms of complex modulus, creep compliance or relaxation modulus (Roylance, 2001). The complex modulus (G^*) is the response of a viscoelastic material under dynamic loading condition. It represents the resistance offered in response to the applied strain, and it is expressed mathematically as (Shaw and MacKnight, 2005; Lakes, 2009),

$$G^* = \frac{\tau(t)}{\varepsilon(t)} = G' + iG'' \tag{2.1}$$

where, τ represents the applied shear stress, the shear strain is denoted by ε, G' is the storage modulus and G'' is the loss modulus. Storage modulus represents the ability of the viscoelastic material to store the energy during deformation, which could be recovered later. The ability of a viscoelastic material to dissipate the energy is expressed in terms of loss modulus (Boczkowska et al., 2009). The complex modulus is the representation of property in the stress-strain domain, and its equivalent form in the force-displacement domain is referred to as complex stiffness (K^*) (Nadeau and Champoux, 2000), and it is expressed as,

$$K^* = \frac{F(t)}{x(t)} = K' + iK'' \tag{2.2}$$

where, F represents the applied force, x is the displacement, K' is the real part of the stiffness and K'' represents the imaginary part of the stiffness.

The complex modulus/stiffness is also expressed as,

$$G^* = G'(1 + i\eta) \quad (2.3)$$

$$K^* = K'(1 + i\eta) \quad (2.4)$$

where, $\eta = \tan \delta$, represents the loss factor of a viscoelastic material, which measures its energy dissipation capabilities. The loss factor is also expressed as the ratio G''/G' or K''/K' (Lakes, 2009).

Magnetoviscoelatic property characterization studies are focused on the evaluating field-induced changes in G' and G'' or G^* and η (Zhu et al., 2012; Boczkowska and Awietjan, 2009). Variations in these properties are associated with the interaction between the fillers, which alter the internal structure and thereby modify the stress-strain or force-displacement response (Jolly et al., 1996). The property enhancements in MRE under the influence of magnetic field are assessed in terms of absolute or relative MR effect (Lokander and Stenberg, 2003a; Gong et al., 2005; Chen et al., 2010a; Dong et al., 2012). Absolute MR effect measures the property enhancements from the non-magnetized to magnetized state of MRE. The relative MR effect is used to quantify the improvement with relative to the properties under non-magnetized state. Though both the approaches provide the realistic assessment of the smart characteristics of MRE, the relative MR effect is more effective as it depends on the zero field properties (Chen et al., 2010a; Zhu et al., 2013).

The electrical conduction characteristics of MRE depend on the quality of contacts that existed between the conductive fillers in a nonconductive host matrix (Bossis et al., 2001). Under the influence of magnetic field, the electrical properties of MRE are altered, which is referred to as the magnetoresistance (Huang et al., 2015). The magnetoresistive characteristics of MRE are sensitive to the susceptibility of the

fillers to align in the direction of the applied magnetic field. Under magnetized state, the separation distance between the fillers is reduced due to the dipole interaction. Consequently, a conductive path for the applied current is formed due to the tunneling effect (Li et al., 2009; Kchit and Bossis, 2009). The contacts between the fillers are improved at a higher magnetic field as the magnetic force of attraction brings the fillers closer (Tian et al., 2013a; Huang et al., 2015). The rate of enhancement in the electrical characteristics is significant at lower magnetic field strength, but it is reduced at a higher magnetic field strength. This state could be envisioned as the condition where the particles are optimally close enough, in which case the resistance change in the sample is not pronounced (Bica et al., 2014; Huang et al., 2015).

The resistivity of isotropic MRE is higher compared to the anisotropic MRE as the random distribution of fillers is not beneficial to attain the contact between neighboring fillers. However, the conductivity of the isotropic MRE is not varied above a certain level of filler addition, referred to as the percolation threshold of volume fraction. In contrast, for an anisotropic MRE, percolation threshold does not exist rather; the resistivity values are decreased when the volume fraction is increased from 5% to 30% (Bossis et al., 2001; Kchit at al., 2009). The conductive characteristics of MRE are also improved by doping with the additives. The graphite powder (Tian et al., 2013a) and graphene (Bica et al., 2014) are used to enhance the electrical characteristics of MRE.

Unlike magnetic field, the electrical properties of MRE are also sensitive to the external pressure. This attribute of MRE is referred to as the piezoresistivity (Li et al., 2009). The phenomenon of piezoresistivity is similar to the magnetoresistance, where the filler particles are brought closer by the application of mechanical pressure

(Wang et al., 2009; Ausanio et al., 2011). Change in resistivity of MRE depends on the intensity of applied pressure. During initial loading, the rate of reduction in the resistivity under applied pressure is pronounced and it diminishes at an intermediate range of loading (Huang et al., 2015; Tian et al., 2013a). At higher loading, the resistance change is insignificant as the applied pressure brings the filler particles closer where the quality of contact cannot be improved further. These novel characteristics exhibited by MRE under mechanical and magnetic field loading have a great scope in the development of sensing devices (Li et al., 2009).

MRE exhibits a significant change in dimension when subjected to the change in the magnetization state. This phenomenon is referred to as the magnetostriction (Guan, et al., 2008). The mechanism of magnetostriction in MRE is different compared to the rare-earth materials, where the orientation and geometry of the crystals determine the effect (Aga et al., 2008; Ginder et al., 2002). Magnetostriction in MRE is associated with the dipole interactions caused by the alignment of magnetic moments in the direction of applied field. This promotes the displacement and rotation of fillers inside the soft matrix resulting in dimensional variation of the specimen (Guan et al., 2008).

The magnetostriction in MRE is a function of the orientation of the fillers inside the matrix (Guan et al., 2008). Maximum magnetostriction is noticed for MREs pre-structured perpendicular to the direction of the applied field and least for the MREs with chain direction parallel to the direction of magnetic field. The magnetostriction in isotropic MRE is intermediate between the above mentioned cases of anisotropic structures (Guan et al., 2008). The magnetostrictive effect mainly depends on the content of fillers, and it attains a maximum value with the optimum

filler content (Aga et al., 2008, Guan et al., 2008). It is pronounced in MRE with softer matrix compared to the stiffer matrix (Du and Chen, 2012; Aga et al., 2008) and it exhibits hysteretic characteristics. This typical characteristic of MRE depends on the interaction between the filler and matrix at the interface (Du and Chen, 2012; Bednarek, 1999). Like conventional magnetic materials, the magnetistrictive effect in MRE saturates at a higher magnetic field (Ginder et al., 2002; Guan et al., 2008). The rate of increase in magnetostrictive effect is pronounced at a lower magnetic field and it is reduced at higher magnetic field due to the reduction in the relative increase in the field-induced interaction between the fillers (Guan et al., 2008).

Pseudoelasticity in MRE is the irreversible change in the shape under the influence of magnetic field and a complete recovery of the initial configuration once the field is turned off (Nikitin et al., 2004). Under magnetized state, the deformation of the sample under complete shear stress recovery is unchanged with time, and it disappears once the magnetic field is turned off. This phenomenon is associated with the dipole interaction between the fillers, which reserves the new shape under magnetized state; caused by the extension or compression under external mechanical force. Consequently, a complete equilibrium state is achieved, and the samples behave like a plastic material (Stepanov et al., 2008). The dipole interaction between the fillers vanishes as the magnetic field is turned off, which results in the dominance of matrix elasticity (frozen under the magnetized state) to regain the original shape of the sample (Stepanov et al., 2007).

2.4 Viscoelastic property characterization of MRE

The properties of MRE are characterized by adopting conventional viscoelastic property measurement techniques. These tests are performed under the influence of an

external magnetic field to assess the field sensitive characteristics (Lokander and Stenberg, 2003a). Generally, the properties of viscoelastic solids are characterized by static or dynamic mechanical analysis techniques (Kumar et al., 2012). The static tests are focused on measuring the creep or relaxation response of a material for the unit step input. In creep test, the time-dependent strain resulting from the constant stress is measured. The stress relaxation is an alternative form of the static test, which involves, monitoring the time-dependent stress resulting from the steady-state strain (Lakes, 2009). Static tests are performed under tensile or torsion loading or by using indentation techniques (Roylance, 2001; Basdogon and Dikmen, 2011; Li et al., 2010a). Creep and relaxation tests are more convenient for studying the material response at a longer time, but it is less accurate at a shorter duration. On the contrary, the dynamic mechanical analysis offers a suitable means to investigate the viscoelastic properties, which are well suited for the short time range response (Roylance, 2001).

The response of a viscoelastic material under dynamic loading is distinguished as linear and nonlinear (Ng et al., 2010; Gong et al., 2012a). Linear viscoelastic behavior implies that the response stress/force is proportional to the input displacement/strain (Deshpande et al., 2010; Tariq et al., 1998). Within the linear viscoelastic region, the response stress in a material is described by a single trigonometric function (Cho et al., 2005). The onset of nonlinearity appears as the strain is increased beyond a certain limit (Gong et al., 2012a; Renou et al., 2010). At larger strain, the stress-strain responses no longer exhibit linear relation due to the contribution from the high-order harmonics. In the nonlinear region, the complex modulus, which represents the elastic and viscous characteristics, loses its physical

significance (Cho et al., 2005). Moreover, the appearance of nonlinearity is relevant in the applications of MRE, and it needs to be addressed to predict the performance of a device.

Generally, the material properties in the linear viscoelastic region are characterized by small amplitude oscillatory shear test (SAOS) (Deshpande et al., 2010; Uthayakumaran et al., 2002). The large amplitude oscillatory shear (LAOS) method is often used to probe the nonlinear behavior of a material (Ewoldt et al., 2010). However, the LAOS is also used to assess the transition from linear to the nonlinear viscoelastic response in a material (Deshpande et al., 2010;Gong et al., 2012a; Ewoldt et al., 2010). In this approach, the onset of nonlinearity is assessed by the change in elliptical shape of stress-strain Lissajous plots (Gong et al., 2012a). Alternatively, the nonlinear response is also assessed from the deviation in the linear relationship between stress-strain curves (Ren and Krishnamoorti, 2002; Uthayakumaran et al., 2002; Glenn, 1963) or by the appearance of higher harmonics (odd) in Fourier transforms rheology (Wilhelm et al., 2003). The hysteresis loop approach of assessing transition behavior is an effective, and most widely used strategy as it provides the real-time graphical representation of nonlinear behavior in a material (Cho et al., 2005; Ewoldt et al., 2010). Moreover, the linear viscoelastic behavior is also affected by the contribution from other sources like the inertia of the test setup. Therefore, it is essential that the source of nonlinearity should be solely from the material response, and the contribution of other harmonics needs to be eliminated (Gong et al., 2012a; Collyer and Clegg, 1998).

The linear viscoelastic response of a material is represented in the form of a strain-independent complex modulus evaluated from SAOS test (Menard, 1999). This

approach involves the measurement of delayed harmonic force response for the known input harmonic displacement. Generally, these tests fall under two categories, i.e resonant and nonresonant method (Gade et al., 1994; Medilia, 1978). In the resonant method, viscoelastic property measurements are focused on the resonance region of the dynamic system. However, this approach is not effective to characterize the properties in nonresonant region as the viscoelastic behavior of a material is sensitive to the frequency. On the contrary, the properties in the nonresonance region are characterized by nonresonant method (Ooi, and Ripin, 2011; Thomson, 1998). The DMA, Rheometry and conventional forced vibration tests are the widely used techniques to evaluate the nonresonance characteristics of a viscoelastic material. These methods are based on the measurement of response for the known steady-state harmonic input (an excitation contains only a single frequency of the sine wave) or a swept sine input (frequency of excitation of sine waves is continuously varied within the frequency range of interest). The DMA and rheometer based measurements evaluate the properties under a sine swept input (Romrio et al., 2003; Lu et al., 2012; Chen et al., 2007b; Li et al., 2010b; Olabide et al., 2014). But, the conventional forced vibration tests are employed with either frequency sweep or steady-state excitation signals for characterizing the properties (Mallik et al., 1999; Romrio et al., 2003, Koblar and Boltezar, 2013; Nadeau and Champoux, 2000). The steady-state input yields better results as it excludes the errors associated with the frequency sweep (ASTM E756-04). Moreover, the forced vibration test methods are economical as it avoids the need for the costlier test set up.

The conventional forced vibration tests on a viscoelastic material are performed by using a hydraulic pulsator (Lokander and Stenberg, 2003a; Zhu et al., 2012) or an

electrodynamic shaker (Mallik et al., 1999; Romorio et al., 2003) as per the ISO standard 10846-1. Alternatively, an impact hammer is also used to provide the external excitation. According to the standard, the forced vibration tests are categorized as direct stiffness measurement (ISO 10846-2) or indirect stiffness measurement (ISO 10846-3). The direct stiffness method includes two different types of dynamic stiffness estimations; dynamic drive point stiffness and dynamic blocked transfer stiffness. The dynamic drive point stiffness estimates the stiffness with respect to the force at the drive point end. Stiffness assessed from the drive point measurement is often affected by the inertial mass, which limits its applicability over higher frequencies (Nadeau and Champoux, 2000; Ooi and Ripin, 2011). In contrast, the dynamic blocked transfer stiffness could overcome the limitations of drive point measurement by estimating the stiffness with respect to the blocked force (Ooi, and Ripin, 2011). This approach allows to carryout the viscoelastic property characterization studies at higher frequencies (Thomson, 1998).

The viscoelastic property estimation from dynamic blocked stiffness method is through the measurement of receptance (Lin et al.,2003; Ooi, and Ripin, 2011), transmissibility (Mallik et al., 1999; Ramario et al., 2003; Koblar and Boltezar, 2013) or hysteresis behavior (Ju et al., 2012; Zhu et al., 2012). In receptance measurement, the dynamic stiffness is obtained from the response plot corresponding to the receptance vs excitation frequency. The phase difference between the force and displacement signal yields the loss factor. The transmissibility measurement includes the measurement of dynamic response in terms of force or displacement transmissibility. The displacement transmissibility is the ratio of the displacement/velocity/acceleration at the output side to the input side (Ramorino et

al., 2003; Koblar and Boltezar, 2013). Correspondingly, the force transmissibility is the ratio of the force at the output side to the input side (Hegde et al., 2014). Both approaches have the same response function but differ with the system of reference (Rao, 2004). The displacement transmissibility is preferred when the device is to be protected from the vibrations arising from the point of attachment. Conversely, the force transmissibility is considered when a vibrating source has to be isolated from the system of concern. The receptance and transmissibility based property measurements can be performed under steady state or frequency sweep excitations. On the contrary, the hysteresis loop based measurement approach is purely based on steady-state excitations. In this method, the material properties are evaluated by the measurement of output response for steady-state harmonic excitations (Lakes, 2009). The response lags the input excitation; resulting in an elliptical shaped hysteresis loop. These plots are represented in the force-displacement domain (Zhu et al., 2012; Li et al., 2013) or stress-strain domain (Li, 2010b; Ju et al. 2012). In particular, the process of estimating the stiffness and damping are simpler as the slope yields the dynamic stiffness, and the damping characteristics are computed from the area of the hysteresis loop (Brown, 1996).

2.5 Processing parameters of MRE

The key ingredients of MRE are matrix and the filler, which are mixed during the pre-cure state. The composition of the key ingredients can be varied to during synthesis, which modifies the properties under magnetized and non-magnetized state. The present section is focused on the influence of operating parameters like the type of matrix, type of filler, the content of fillers, additives and size / shape of the fillers on the field-induced performance of MRE.

2.5.1 Matrix Material

MRE is a solid analog of Magnetorheological fluid (MRF), where the carrier oil is replaced by an elastomer matrix. The solid matrix has an obvious advantage in overcoming the sedimentation and leakage problems often encountered in MRF devices. The choice of matrix for MRE include; silicone, natural rubber, polyurethane, butyl rubber and SEBS (Chen et al., 2007b; Boczkowska and Awietjan, 2009; Gong et al., 2012a; Zhu et al., 2013; Olabide et al., 2015; Khairi et al. 2016; Perales-Martínez et al., 2017). Matrix materials used for the synthesis of MRE are categorized as high temperature vulcanized (HTV) rubber and room temperature vulcanized (RTV) rubber. HTV matrix of MRE is distinguished by the temperature at which crosslinking process is carried out (Chen et al., 2007b). The RTV elastomer matrix based MRE is prepared by mixing polymer melt with the ferromagnetic particles and curing under room temperature conditions, initiated by a curing agent (Perales-Martínez et al., 2017). Mixing process of matrix and filler entraps the air bubbles into the mixture, which could result in a defective MRE sample. Entrapped air in the matrix is removed by a vacuum degassing process before the curing process is initiated (Li et al., 2010b). Synthesis of HTV MRE involves blending of matrix and fillers by mastication via double-roll mill or conventional mixing process (Chen et al., 2007b; Zhang et al., 2010). The curing process of HTV MRE is carried at a temperature higher than the room temperature. Depending on the type of matrix, the curing temperature varies, which in turn influences the viscoelastic properties of MRE (Chen et al., 2007b).

The elastomer matrix has a significant influence on the overall properties of MRE. A matrix of MRE comprises of long chains of molecules joined together by a

crosslinking process. Based on the crosslink density, the properties of elastomers vary significantly, which is distinguished by the shore hardness (Zhu et al., 2013). Higher the crosslink density of the elastomer, larger will be the shore hardness value. The shore hardness of a particular type of MRE is enhanced by the increase in the content of filler (Rajhana et al., 2013; Yunus et al., 2016; Zhu et al., 2013), which in turn modify its field sensitive characteristics. The mobility of the molecular chains have a considerable influence on the alignment of a filler under the magnetic field (Lokander and Stenberg, 2003a; Rabindranath and Böse, 2013; Zhu et al., 2013). Molecular chains of a softer matrix have higher mobility, which experiences a least resistance for the motion (Lokander and Stenberg, 2003a; Rabindranath and Böse, 2013; Zhu et al., 2013). As a consequence, it yields a larger MR effect than the harder matrix based MRE (Wang et al., 2006). However, the absolute MR effect is independent of the hardness of the matrix material (Lokander and Stenberg, 2003a; Li et al., 2010b; Yang et al., 2015). Apart from the cured state properties, the field-induced performance of MRE is also a function of viscosity of the matrix under pre-cure state (Lu et al., 2012; Ge et al., 2013). Lower the viscosity of the matrix, easier will be the particle movement to form a chain like structure along the direction applied magnetic field (Boczkowska and Awietjan, 2009). This results in an improved interaction between the fillers under the magnetized state and enhances the MR effect (Ge et al., 2013; Lu et al., 2012). Furthermore, the matrix material also has an influence on the transition from linear to nonlinear viscoelastic behavior (Olabide et al., 2015). In a harder matrix, the influence of the particles is not pronounced; hence, the transition from linear to nonlinear response occurs at a lower strain level. While, the MRE based on softer matrix, the LVE region is relatively larger.

The field sensitive characteristics of MRE are enhanced by introducing a plasticizer (Lokander and Stenberg, 2003a, 2003b; Chen et al., 2007; Kaleta et al., 2011; Rabindranath and Böse, 2013; Khairi et al., 2016) or by preparing a hybrid polymer matrix (Hu et al., 2005; Wang et al., 2007; Gong et al., 2012b; Wang et al., 2015). The plasticizer is a kind of addition in the rubber technology in which, it can be dissolved in the rubber after mixing. Plasticizer acts like a lubricant which allows the molecular chains of rubber to glide easily. Addition of the plasticizer modifies the flexibility of the matrix and enhances the MR effect by improving the filler interactions under the magnetic field (Ge et al., 2013; Khairi et al., 2016). The choice of plasticizer depends on the chemical affinity with the particular type of matrix material. On the contrary, the hybrid matrix is a polymer blend obtained by mixing two or mode elastomers. The salient feature of a hybrid matrix is to synergize the properties of resulting polymer with the characteristics it inherited from the constituent matrix material. For example, silicone polymer with good elasticity, blended with polystyrene having a high modulus might yield a polymer with excellent elasticity and larger modulus (Wang et al.,2007). However, the property of a hybrid matrix depends on the compatibility between the constituent matrix materials. An incompatibility results in the immiscibility between the two constituents in the pre-cure state and forms a conglomeration of one matrix inlaid within the other (Hu et al., 2005; Wang et al., 2007). Additionally, an incompatible hybrid matrix results in a distinctively different filler distribution when compared to a MRE with single matrix. In such hybrid MRE, a majority of the filler particles are distributed in the relatively softer matrix. This increases the effective filler concentration compared to the single matrix based MRE and enhances the MR effect (Hu et al., 2005). Moreover,

the agglomeration of particles intensifies with the increased incompatibility of the matrix. As a consequence, the fillers disperse at the surface of the relatively rigid phase or at the interior the holes of the matrix. The particle agglomerations are beneficial as it functions as a single larger particle to enhance the magnetic force of attraction (Hu et al., 2005). Furthermore, presence of a harder matrix surrounded by the softer matrix enhances the zero field modulus by imparting additional reinforcing effect (Wang et al., 2013). The compatibility between the matrices in a hybrid matrix can be improved by adding the Inter Penetrating Network (IPN). This promotes the formation of network among the immiscible polymer, which improves the particle-matrix interaction to attain superior field-induced characteristics (Yu et al., 2015). Although the hybrid matrix based MRE performs better than the single matrix MRE, its properties deteriorate above the optimum limit as the compatibility between the matrix is lost (Yu et al., 2015).

Like conventional filled rubbers, the damping characteristics of MRE also depends on the intrinsic properties of the matrix (Yang et al., 2012). The inherent damping differs with the type of matrix, and it governs the overall damping properties of MRE. A matrix with larger damping results in a higher loss factor compared to MRE with lower damping matrix material. For example, a reinforcement of 70 wt % of fillers, the loss factor of MRE based on Bromo butyl rubber is 0.64, while for a natural rubber based MRE, the loss factor is 0.189. The corresponding properties of Bromo butyl and natural rubber under unfilled state are in the range 0.05 - 0.5 and 0.01 - 0.08 respectively (Zhu et al., 2013).

The damping in the matrix originates due to the movement of the adjacent molecular chains under the applied deformation (Ju et al., 2015). For an unfilled state

of elastomer or the MRE with a lower percentage of filler addition, the distance between the fillers is larger. As a consequence, the rubber molecules readily interact under the applied strain (Ge et al., 2013; Wang et al., 2015) and contribute to the damping of MRE. At larger content of fillers, the mobility of the molecular chain is hindered by the presence of more particles. As a consequence, the matrix-filler interface friction dominates the molecular chain friction (Yang et al., 2012). On the contrary, the mechanism of damping in hybrid MRE is different than that of MRE with single matrix. In addition to the intrinsic damping of the matrix, an incompatible hybrid matrix contributes to damping by the existence of matrix-matrix interface friction (Gong et al., 2012b). However, this effect can be neglected when a good affinity between the matrices is formed, which results in a neat blend similar to the MRE with a single matrix material (Yu et al., 2015).

2.5.2 Types of fillers

Magnetically sensitive fillers distinguish MRE from the conventional filled elastomers. The reinforcing fillers used for the synthesis of MRE are categorized as magnetically hard and magnetically soft (Kramarenko et al., 2015). Hard fillers are magnetically anisotropic with a specific magnetization direction. This implies that the hard fillers have non-zero magnetization in the absence of an external magnetic field (Kramarenko et al., 2015; Lockette et al., 2011). Accordingly, the MREs synthesized using hard fillers attains the attributes of a permanent magnet. In contrast, MRE reinforced with magnetically soft particles do not have a net magnetization; therefore, it demonstrates usual viscoelastic behavior in the absence of an external magnetic field (Lokander and Stenberg, 2003a; Zajac et al., 2010).

The response of MRE driven by an external magnetic field is distinctly different for magnetically hard and soft fillers. Existence of magnetic anisotropy in a hard filler based MRE (HMRE) results in the rotation of a filler in a semi-rigid matrix (Stepanov et al., 2017). This imparts a field-induced variation in the properties which opens up the possibility of realizing MRE based actuators (Lockette et al., 2011; Koo et al., 2012). The list of fillers for HMRE includes: barium hexaferrite, strontium ferrite, samarium cobalt and neodymium magnet (Lockette et al., 2011; Koo et al., 2012; Borin et al., 2013). Moreover, HMRE has the advantage to vary the properties in two ways by applying a field in opposite directions, which is in fact beneficial to attain larger bandwidth of field sensitivity (Stepanov et al., 2012). Furthermore, the response of HMRE under shear loading is complex as the orientation of particle magnetization with respect to the applied field is altered. This results in a rotation of embedded particles inside the matrix, which in turn affect its bulk material properties. The resulting behavior is magnetically hysteretic in nature, which limit its relevance as a resilient material for vibration mitigation applications.

On the contrary, the fillers used for synthesizing the MRE for vibration mitigation applications must have high permeability, high magnetic saturation and low remnance (Lokander and Stenberg, 2003a; Zajac et al., 2010). For an anisotropic MRE, higher permeability and saturation lead to the better alignment of fillers along the direction of applied magnetic field. Correspondingly, for an isotropic MRE, these attributes are beneficial to attain maximum molecular attraction and a larger magnetorheological effect. Commonly used soft fillers for synthesizing MRE include carbonyl iron, Nickel and cobalt (Song et al., 2009; Padalka et al., 2010; Lokander

and Stenberg, 2003b). The carbonyl iron powders (CIP) have the maximum magnetic saturation of about 2.1 T (Jolly et al., 1996).

The properties of soft fillers have a significant influence on the viscoelastic behavior of MRE. Under non-magnetized state, response of MRE is governed by the mechanical properties of the filler. For the same level of filler content, MRE loaded with Ni particles exhibits superior properties compared to the CIP reinforcement (Padalka et al., 2010). However, under magnetized state, the enhancement in stiffness and damping depends on the magnetic properties of soft filler. The MR effect is larger for CIP based MRE than the Ni-based MREs. This difference is attributed to the permeability and magnetic saturation of the fillers to align along the direction of applied magnetic field. Particles with a higher permeability have a greater particle-particle interaction in response to the applied field. Meanwhile, the ferromagnetic fillers with lower permeability will not line uniformly under the magnetic field and exhibits lower field-induced property enhancement. Consequently, the larger MR effect is observed for CIP, and lower for MRE reinforced with Ni (Padalka et al., 2010). Therefore, CIP is contemplated as the ideal choice of filler to synthesize MRE for vibration mitigation application.

The field-induced characteristics of CIP based MRE is sensitive to the presence of carbon content (Yu et al., 2012). Magnetic properties are deteriorated significantly with the increase in carbon content. Larger variation in the field-induced shear modulus and damping is registered for MRE reinforced with low carbon content CIP fillers. However, the field-induced enhancements are relatively reduced as the increased carbon content hinders the alignment of the domain wall of the fillers. This

phenomenon results in a relative reduction in the permeability of the fillers and modifies the field-induced characteristics of MRE (Yu et al., 2012).

2.5.3 Content of Fillers

The field dependent characteristics of MRE are associated with the interaction between the magnetically sensitive fillers. Under the influence of magnetic field, these fillers function as magnetic dipoles (Stepanov et al., 2008). The total number of dipoles present in MRE depends on the amount of fillers present in the matrix. The content of fillers are generally expressed in terms of weight percentage or volume percentage (Lokander and Stenberg, 2003a; Chen et al., 2007b; Sun et al., 2008; Boczkowska and Awietjan, 2009). Weight percentage signifies the weight of the fillers present within the sample and volume percentage represents the total volume of the fillers within the matrix. Weight percentage or volume percentage is unique for a particular type of MRE as its conversion depends on the density of the elastomer matrix. For example, the content of filler with 60% by weight corresponds to 15% for a natural rubber based MRE and 11% for a RTV silicone based MRE (Gong et al., 2007).

Addition of fillers into the matrix modifies the properties of MRE under magnetized as well non-magnetized state. The enhancement in the modulus under non-magnetized state is attributed to the reinforcing effect, which can be represented by the modified Guth-Gold equation (Yu et al., 2015). The reinforcing effect is not pronounced at lower filler concentration, but the variations are significant at large fractions of filler addition (Gong et al., 2005; Molchanov et al., 2014). Meanwhile, the tensile strength and the tear strength of MRE are reduced at large filler content (above 60 wt %) as it attains a discontinuous structure compared to an unfilled rubber

(Chen et al., 2007b; Wu et al., 2009). Apart from modifying the zero field properties, the content of filler has a significant influence on the field dependent characteristics of MRE. At lower particle content, the distance between the fillers is relatively larger and the amount of free rubber occupied between the fillers are more (Fan et al., 2011; Wang et al., 2015). However, with the increase in the content of filler, the distance between the fillers is relatively reduced and the magnetic force of attraction is increased. This improves the properties of MRE under the magnetic field and thereby enhances the MR effect (Stepanov et al., 2007; Boczkowska and Awietjan, 2009; Fan et al., 2011; Ge et al., 2013). Variation in the field sensitive characteristic of MRE is correlated to the changes in the magnetic permeability of MRE by the addition of fillers. The permeability of MRE is increased as the matrix is loaded with large content of ferromagnetic fillers, which offers a path for the flow of magnetic field (Wang et al., 2007). The permeability of MRE is relatively low for the addition of smaller quantity of fillers and it improves as the amount of fillers in the matrix is increased. For a silicone-based MRE, permeability varies from 1.6 to 4.3 for the increase in particle content from 10 to 30 percentage by volume (Schubert and Harrison, 2016).

At very large filler concentration, the properties of MRE are deteriorated (above 80 wt %) (Sun et al., 2008; Chen et al., 2007). With the increase in filler content, the amount of elastomer present in MRE is reduced. Subsequently, the toughness of the MRE is decreased, and it becomes brittle (Gong et al., 2005). Moreover, increase in the content of fillers reduces the separation distance between the particles. Consequently, the amount of free rubber trapped between the fillers is reduced, and a contact is established between the fillers. This creates an unfavorable

condition for the interaction between the fillers and thereby diminishes the MR effect (Gong et al., 2005; Chen et al., 2007b; Sun et al., 2008). Additionally, at higher particle content, the zero field modulus of the MRE is larger, which has a significant influence on the relative MR effect (Chen et al., 2007b; Gong et al., 2007). These aspects of MRE substantiate the existence of an optimum quantity of filler, which maximizes the relative MR effect. Past literatures have reported the influence of content of fillers on the field-induced performance of MRE. These studies confirm the existence of optimum content of fillers in the range of 25 to 35% by volume (Lokander and Stenberg, 2003b; Stepanov et al., 2008; Zając et al., 2010; Yang et al., 2013a; Hegde et al., 2015; Wang et al., 2015; Böse and Röder, 2009), which was verified theoretically by Davis (1999). The corresponding values in terms of weight percentage are 60-80% (Gong et al., 2005; Sun et al., 2008; Ju et al., 2012; Yang et al., 2012; Ge et al., 2013). Like a conventional ferromagnetic material, MRE also exhibits the magnetic field-induced saturation behavior. The saturation condition refers to the state where there is no increment of magnetization due to the alignment of all magnetic moments in the direction of magnetic field flux lines (Kashima et al., 2012). This attribute of MRE depends on the content of fillers present in it. At a higher percentage of fillers, the saturation magnetization of MRE is increased. However, these variations are not pronounced for the particle content above 50% by weight (Yunus et al., 2016).

Influence of particle content on the field-induced characteristics of isotropic and anisotropic MRE are distinctly different. An anisotropic structure is characterized by the formation of ordered arrangement of the fillers due to the pre-cure magnetic field (Ge et al., 2013; Fan et al., 2011). For the same level of filler loading, the

distance between the fillers in an isotropic MRE is larger than the anisotropic MRE. This results in an enhancement of magnetic force between the fillers and yields a larger magneto induced modulus (Böse and Röder, 2009). At lower filler content, larger distance exist between the adjacent chains, and it reduces as the content of fillers is increased. For the particle content above 33% by volume, the microstructure of isotropic and anisotropic is indistinguishable as the fillers are closely spaced (Boczkowska and Awietjan, 2009). The distribution of filler particles is uniform in isotropic MRE but in an anisotropic MRE, effective filler content is varied throughout the cross section. Due to trapped elastomer between the particles, the effective filler content is higher inside the particle chain and away from the chain it is relatively lower (Boczkowska and Awietjan, 2009).

The filler particles in MRE tend to agglomerate as the content of fillers increased above 70 wt % (Fan et al., 2011; Aloui and Klüppel, 2015; Yunus et al., 2016). Compared to anisotropic structure, the particle agglomerations are more pronounced in isotropic MRE. Moreover, the smaller-sized fillers are susceptible to agglomeration (Fan et al., 2011). The particle agglomerations are beneficial in enhancing the MR effect when its orientation is along the direction of the applied magnetic field (Lokander and Stenberg, 2003a). Furthermore, the particle content has a significant influence on the LVE region. The LVE limit is decreased with the increase in particle content (Tian et al., 2013b; Olabide et al., 2015) which is explained by the filler reinforcement experienced by the matrix due to physical interactions.

Apart from enhancing the stiffness, addition of fillers influences the damping characteristics of MRE. These contributions are associated with the intrinsic damping

of the fillers and the damping arising from the matrix-filler interface (Fan et al., 2011; Chen et al., 2008a; Sun et al., 2008; Jian-feng and Gong, 2009). Since the particle size is smaller, its contribution on the damping of MRE is negligible (Ju et al., 2012). However, the influence of matrix-filler interface is significant as the content of fillers is increased (Sun et al., 2008). The contribution of matrix-filler interface is originated due to the interface friction between the particle and matrix under the external loading (Yang et al., 2012). At a larger content of fillers, the incompatibility between the matrix and filler intensifies, which is characterized by the formation of loosely a bonded interface. As a consequence, the matrix-filler interface friction is increased, which enhances the overall damping characteristics of MRE (Hu et al., 2005; Yang et al., 2012). In contrast, under the external magnetic field, the mechanism of interface friction is different as the movement of the fillers is restricted by the magnetic field, which modifies the mechanism of interface damping of MRE (Chen and Gong, 2008; Sun et al., 2008; Jian-feng and Gong, 2009; Chen et al., 2008a).

2.5.4 Additives

Response of MRE under dynamic loading, depends on the intrinsic properties of individual constituents and the interface interaction between the matrix and filler (Yang et al., 2012). Based on the nature of interactions, the interface is categorized as, strongly bonded interface and a weakly bonded interface (Yang et al., 2012). A strongly bonded interface is characterized by the existence of strong interaction between the matrix and the filler. The energy dissipation in a strongly bonded interface is low as the relative motion between the matrix is not pronounced. Meanwhile, a weakly bonded interface comprises of a weak link between the matrix

and fillers, which is not effective in load transfer as the part of energy is lost by interface friction (Yang et al., 2012; Yu et al., 2017).

The interface interactions are critical for MRE as the matrix and particle are organic and inorganic respectively. An immiscibility between the hydrophobic and hydrophilic nature of the constituents results in an incompatibility between the magnetic particle and polymer matrix (Malecki et al., 2015; Chen et al., 2016; Yu et al., 2017). As a consequence, the mechanical properties are deteriorated. The relative motion between the particle and matrix is also increased, which results in an enhancement in the damping characteristics of MRE (Malecki et al., 2016; Yang et al., 2012; Chen et al., 2016). Moreover, a weakly bonded interface results in the loss of magnetic energy at the gaps between the matrix and the fillers, which could diminish the field sensitive characteristics of MRE (Wang et al., 2006).

The compatibility between the matrix and the fillers can be improved by the inclusion of additives as the properties of iron particles, and the matrix is inherently fixed (Chen et al., 2008b; Li and Sun, 2011; Malecki et al., 2015; Damiani and Sun, 2016). Additives modify the interface regime between the matrix and the particle, and change the properties such as oxidation resistance and stiffness due to an applied magnetic field (Behrooz et al., 2015). Property enhancement of MRE by the inclusion of additive is either by modifying the properties of a matrix or by enhancing the surface properties of the ferromagnetic filler (Chen et al., 2008b; Kaleta et al.,, 2011; Qiao et al., 2012; Ge et al., 2013; Malecki et al., 2015; Ismail et al., 2016). Generally, these additives are in the form of liquid or powder.

Liquid form additives improve the properties of MRE by inducing plasticizing (Kaleta et al., 2011; Ge et al., 2013; Rabindranath and Böse, 2013) or coupling effect

(Wang et al., 2006; Kashima et al., 2012; Qiao et al., 2012; Chen et al., 2016) between the matrix and filler. The plasticizing effect is created by adding the plasticizers into the matrix during curing, which enhances the properties of MRE not only by altering the rubber mechanisms but also by modifying the surface of a filler particle. The choice of plasticizer for MRE depends on the chemical affinity with the parent polymer matrix. For example, silicone oil for silicone rubber (Gong et al., 2005), paraffin oil for Tefabloc polymer (Kaleta et al., 2011), glycerine for natural rubber (Ge et al., 2013), diisooctyl phthalate for polyurethane (Wu et al., 2012) and so on. The plasticizers also improve the compatibility between the iron particles and polymer matrix and promote the homogeneous dispersion of filler in the rubber matrix (Kaleta et al., 2011; Ge et al., 2013; Khairi et al., 2016).

In an unmodified MRE matrix, the short linkage between the matrix and the fillers offers a limited mobility and reduces the freedom of movement for the fillers under the applied field. Conversely, by introducing a plasticizer, the viscosity of the matrix is reduced. Subsequently, the sliding of molecular chains of the matrix is improved and the storage modulus is reduced (Rabindranath and Böse, 2013). This attribute of MRE results in a pronounced structuring and more dense arrangement of the particles under magnetic field, and leads to a higher storage modulus and larger MR effect (Gong et al., 2007; Kaleta et al., 2011; Wu et al., 2013; Rajhana et al., 2013; Rabindranath and Böse, 2013). In addition, the plasticizer also enhances the contribution of intrinsic damping of the matrix as the dissipative heat loss due to the enhanced mobility of the polymer chains is increased (Rabindranath and Böse, 2013).

Alternatively, the compatibility between the matrix and the fillers can be enhanced by the addition of a coupling agent. The coupling agent improves the metal–polymer interaction by coating the magnetic particles surface with a functional polymer (Behrooz et al., 2015; Malecki et al., 2015,2016; Chen et al., 2016). Adsorbed coupling agent enhances the interfacial compatibility between the particles without losing the original toughness and softness of the pristine MRE (Qiao et al., 2012). A coupling agent promotes the formation of closer connections between the fillers and matrix through covalent bonds, which improves both chemical and physical properties of MRE (Behrooz et al., 2015; Yu et al., 2017). Most often, silane coupling (Wang et al., 2006; Behrooz et al., 2015) and titanate coupling agents (Qiao et al., 2012) are used as coupling agents to enhance the properties of MRE. Additionally, these coupling agents improve the dispersion of the fillers and enhance the tensile strength of the MRE when compared to the samples with unmodified CIP (Qiao et al., 2012; Chen et al., 2016). The filler surface modification resulted from the coupling agent alleviates the stress concentration by reducing the defects like bubbles and other interface defects (Chen et al., 2016). Additionally, the coupling agent also lowers the actual content of CIP. The distances between the fillers are relatively increased with the addition of coupling agent, which diminishes the field-induced interactions between the dipoles (Malecki et al., 2015).

The mechanical properties of MRE are remarkably enhanced by the addition of a powdered form of additives, as it improves the bonding between the elastomer and filler (Wang et al., 2015). Generally, nano sized powders are used as additive due to higher surface activity and the reinforcing effect (Li and Sun, 2011). The powdered form of additives are adsorbed on the surface of CI particles, which enhances the

matrix-filler interaction by occupying the gaps at the interface (Chen et al., 2008b). Inclusion of powdered form of additives increases the storage modulus of MRE by inducing the hydrodynamic reinforcement effect (Aishah et al., 2016). Often used powdered form of additives are: carbon black (Chen et al., 2008b), carbon nanotube (Li and Sun, 2011), graphite (Tian et al., 2011), graphene (Bica et al., 2014) and silicon carbide (Yang et al., 2013a). Apart from enhancing the mechanical properties, the electrical properties of MRE is also improved by doping with the additives. For example, graphite and graphene particles are added to enhance the magnetoresistance of MRE.

Enhancement in the overall magnetorheological properties of MRE depends on the magnetic characteristics of the additive. Magnetically insensitive additive functions only as a reinforcing medium. However, a magnetically active additive has an obvious advantage in contributing to the field-induced characteristics of MRE apart from serving as a reinforcing medium. CNT is one such additive, which not only improves the interface but also contributes to the enhancement in magnetic characteristics of MRE (Aishah et al., 2016). The saturation magnetization of CNT doped MRE is relatively higher than the unmodified MRE as CNT inherits magnetic properties attained during the CVD process (Zhang et al., 2001; Zilli et al., 2005). However, for MRE doped with non-magnetic additives, the actual weight ratio of the fillers is lower than unmodified MRE, which results in a decrement of field-induced characteristics (Yang et al., 2013a).

The overall property enhancement by an additive depends on its size. A strong filler aggregate structure is formed when the CIP is doped with smaller-sized fillers. The bonding is weakened as the size of the additives is increased and the

corresponding aggregate structure is easily damaged (Yang et al., 2013a). With an increase in size of additive, a locking effect is created to obstruct the motion of matrix chains, which overweigh the field-induced enhancements. Moreover, the particle chains are stronger for the MRE doped with the additive of smaller size (≤ 0.06 μm), and the chain structure is slimmed and shortened for larger size (≥ 0.6 μm) owing to the obstruction to the alignment of fillers in response to the magnetic field.

The field-sensitive properties attain a larger values for MRE doped with optimum quantity of additives (Yang et al., 2013a; Tian et al., 2011). This signifies the existence of a larger fraction of strongly bonded interface between the matrix and fillers. Corresponding to the optimum level of additive, the internal structure of MRE is strengthened and the modulus is increased. The flexibility of MRE is affected as the degree of molecular motion and slippage at the matrix-filler interface is reduced (Aishah et al., 2016; Yu et al., 2017). As a consequence, the contribution from intrinsic damping and the interface damping on the overall damping of MRE is reduced. However, the MR effect may be compromised owing to the improvement in absolute MR effect as it is unrealistic to target for high relative MR effect (Li and Sun, 2011). As the content additives exceed the optimum level, the aggregate structure of filler and matrix is deteriorated, and the interface is dominated by weak bonds. Subsequently, the stress transfer between the particle and matrix is weakened due to increased dissipation caused by the discontinuous structure (Yang et al., 2013a). Therefore, it is quite possible to develop MRE, tailor-made to suit a particular application by a proper combination of matrix, filler and the additives.

2.5.5 Size and shape of fillers

The size and shape of the reinforcing fillers have an important influence on the properties of MRE under active as well as the passive state. In general, the geometry of the fillers used for MRE is in the form of nanowire, spherical and irregular shape (Lokander and Stenberg, 2003b; Song et al., 2009; Li and Zhang, 2010). The diameter of the spherical particles ranges from 6-40 μm (Demchuk and Kuzmin, 2002; Böse and Röder, 2009) and the dimensions of nanowire are 15 μm long and 298 ± 40 nm diameter (Song et al., 2009). The size of irregularly shaped fillers varies from 60-200 μm (Lokander and Stenberg, 2003b). For all the geometries of fillers, the stiffness of MRE is increased monotonically with an increase in weight fraction (Stepanov et al., 2007; Böse and Röder, 2009). However, increased contact area between the fillers and elastomer matrix yields a larger stiffness for nanowire reinforced MRE than the spherical particles (Song et al., 2009). The nanowire geometry of filler could lead to a densely packed structure resulting from the reduced inter particle spacing. In addition, the nanowire based MRE composites have higher dynamic stiffness and equivalent damping than the spherical microparticle-based MRE composites due to the larger matrix-filler interface (Song et al., 2009). Furthermore, for the same level of filler reinforcement, MRE reinforced with nanowire exhibits greater sensitivity to increased weight fraction which results in a larger controllable stiffness range. Nanowire based MRE composites have a greater specific modulus, which allows MRE to perform better with a lesser weight. Though nanowire fillers impart superior characteristics, the reinforcement level cannot be increased beyond 30 wt% as the pre-cure mixture becomes too viscous (Song et al., 2009). Moreover, the optimum performance of MRE is reported for the filler reinforcement in the range of 60-70 wt%, which cannot

be achieved by reinforcing with the nanowire. Therefore, nanowire based MRE is not common in MRE based devises.

The micron-sized fillers with regular and irregular geometry are most often used in the synthesis of MRE (Lokander and Stenberg, 2003b; Zając et al., 2010). The irregular shaped fillers are larger in size (above 60 μm) compared to the regular spherical shaped fillers. As a consequence, the reinforcing effect is more pronounced in spherical shaped fillers, which results in relatively higher zero field modulus. However, for the same level of reinforcement, the field-induced properties are larger for MRE with irregular shaped fillers (Lokander and Stenberg, 2003b). This difference is associated with the increased energy interaction due to the larger dipoles and lower separation distance. Moreover, compared to irregularly shaped fillers, the spherical shaped fillers are more susceptible to agglomeration, which affect their distribution in the matrix. The studies by Lokander and Stenberg (2003b) confirmed that the agglomerations were beneficial if it formed along the applied field direction, where it functions as a larger irregular shaped filler. Though irregular shaped fillers have superior properties, spherical shaped particles are most preferred due to ease of mixing during the synthesis process (Aishah et al., 2016).

The field dependent characteristic of MRE is sensitive to the size of spherical shaped fillers embedded in it. For the same level of filler reinforcement, finer particles have a larger surface area, which results in a higher storage modulus (Fan et al., 2011). Meanwhile, the storage modulus of MRE with larger particles exceeds that of the smaller sized filler under magnetized state (Demchuk and Kuzmin, 2002; Böse and Röder, 2009; Fan et al., 2011; Jin et al., 2014). Additionally, larger matrix and filler interface in MRE with the finer particles results in higher loss factor. However,

with an increase in filler content, the smaller particles tend to agglomerate. This reduces the interfacial area between the free rubber and the particles and thereby contributes to variation in stiffness and loss factor (Fan et al., 2011).

The size of the filler also has a significant influence on the properties of isotropic and anisotropic MRE. For an isotropic MRE, the field sensitive characteristics are higher with larger particles (Böse and Röder, 2009). The differences are not significant in case of anisotropic MRE as the smaller particles also generate a greater MR effect due to reduced separation distances from their immediate neighbors (Böse and Röder, 2009). Furthermore, the larger-sized particle has a softening effect, which increases the MR effect.

The field-induced characteristics are higher for MRE reinforced with larger-sized fillers. On the contrary, MRE with smaller-sized fillers experiences a lesser resistance to overcome the elastic forces to get closer under magnetic field (Jin et al., 2014). These effects are opposite in nature, which indicates the existence of an optimum size for the fillers to attain higher MR effect. For MRE reinforced with the fillers of size 5,14, 38, 74 and 150 μm, the optimum performance is registered for the sample with 74 μm (Jin et al., 2014).

The size of the filler influences the hysteresis behavior of MRE. With larger sized filler, the hysteresis behavior is pronounced and it reduces for smaller-sized fillers. This implies, the size of fillers have a control over the remnant characteristics of MRE (Stepanov et al., 2009; Aloui and Klüppel, 2015). The formation of filler network inside the matrix has a reversible character, which depends on the magnetic field strength. The fillers are displaced from their initial position due to the application of magnetic field. Upon removal of magnetic field, these fillers return to

their initial positions under the influence of the elastic forces. With decrease in magnetic field strength, samples containing larger particles experience more resistance from elastic forces to overcome the inter particle interactions (Stepanov et al., 2009). This phenomenon could influence the sensitivity of MRE devices in response to the change in the magnetic field.

Like particle size, its distribution also influences the field-induced property enhancement of MRE (Stepanov et al., 2007; Li and Zhang, 2010). MR effect is pronounced for the MRE reinforced with wide particle size distribution than that corresponding to the monodispersed particles (Stepanov et al., 2007). The particle chains with monodispersed magnetic fillers have some fraction of the regions filled with pure elastomer. However, in case of polydispersed magnetic powders, these regions are reduced as the smaller particles can fill the voids which otherwise would have remained unfilled. For the same particle content, the field-induced shear modulus of MRE is much higher for bimodal particle distribution than that for the monodispersed particles. This enhancement is associated with the higher degree of particle packing in chain-like aggregates, which substantially reduces the loss of magnetic energy. Moreover, in MRE with bimodal particle distribution, a higher fraction of larger-sized fillers yield a pronounced MR effect than that corresponding to smaller-sized fillers (Li and Zhang, 2010).

2.6 Operating Parameters

Apart from processing parameters, the dynamic characteristics of MRE are also influenced by the variation in operating conditions. A proper knowledge on the response of MRE under different operating environments is essential for the design of MRE based devises. In general, viscoelastic materials exhibit the properties which are

sensitive to loading frequency, strain amplitude, temperature and pre-compression. In addition, properties of MRE also depend on the magnetic field, which elevates it from conventional viscoelastic materials. Moreover, these basic operating parameters also influence the characteristics of MRE under magnetized state.

The dynamic properties of MRE are evaluated under non-homogenous and homogeneous magnetic field varying from 0 T to 1 T (Jolly et al., 1999; Fan et al., 2011; Liao et al., 2012). Non-homogeneous magnetic field magnetizes only a specific portion (Hu et al., 2011a) and the homogeneous magnetic field covers the entire geometry of the MRE (Stepanov et al., 2007). The homogenous magnetic field is beneficial for effectively utilizing the novel field-induced characteristics. The field dependency in MRE is associated with the alignment of filler in the direction of the magnetic field, which displaces the fillers from its initial position to cause a localized deformation in the matrix. As a consequence, the microstructure of MRE is altered which results in the variation of rheological properties (Stepanov et al., 2008). The field-induced changes in the properties of MRE are evaluated in terms of MR effect, which measures the range of force that can be controlled in a MRE device (Jung et al., 2009).

The storage modulus of MRE is progressively increased with an increase in the intensity of magnetic field. At a magnetic field below 0.1 T (Hu et al., 2011a), the property enhancements are not significant but these variations are pronounced as the magnetic field strength is increased (Jolly et al., 1999; Lokander and Stenberg, 2003b; Chen et al.,2007b; Li et al., 2010b; Ju et al., 2012). However, these property enhancements are at the cost of a reduction in linear characteristics (Stepanov et al., 2007; Li et al., 2010b; Gong et al., 2012a; Olabide et al., 2015). Under non-

magnetized state, the stress-strain relations are fairly linear but with an increase in magnetic field, the linear range of MRE is reduced. Additionally, at a higher magnetic field, the field-induced enhancements are not significant, as MRE is magnetically saturated. Moreover, the attraction between the particles is not affected further by the increase in magnetic field strength (Jolly et al., 1999; Lokander and Stenberg, 2003a; Chen and Jerrams, 2011; Lu et al., 2012). Saturation state also depends on the interface interactions, where the magnetic force does not create any significant variation in the microstructure (Yunus et al., 2016). Past studies reported that the saturation magnetization depends on the type of matrix and it is observed in the range between 0.3 T to 0.8 T (Demchuk and Kuzmin, 2002; Chen et al., 2007b; Chen et al., 2008a; Sun et al., 2008; Ju et al., 2012; Lu et al., 2012; Yu et al., 2015).

Like storage modulus, the damping characteristics of MRE are also influenced by the magnetic field. The field dependent variations in damping reported by the past literatures are not consistent. Few studies reported that the damping characteristics of MRE exhibit a positive trend with the increase in magnetic field. Few literatures also reported that the loss factor was decreased with an increase in magnetic field (Gong, et al., 2012a; Wei et al., 2010; Aishah et al., 2016). Lokander and Stenberg (2003a) concluded that the field-induced variation in the damping characteristics of MRE was not significant (Lokander and Stenberg, 2003a). There are few literatures, which concluded that the loss factor exhibits a peak at a magnetic field around 0.25 T to 0.4 T (Gong, et al., 2012a; Wei et al., 2010; Aishah et al., 2016). The variations in the field-induced damping characteristics depend on the contributions from the interface damping and magneto-mechanical damping (Chen et al., 2008b; Chen et al., 2016). Compared to the interface damping, contribution of magneto mechanical damping is

not significant. However, the intensity of magnetic field influences the mechanism of interface damping. At a lower magnetic field, the force of attraction between the fillers is very low, and the interface pressure between the matrix and filler are not pronounced. This results in an enhancement in the loss factor of MRE. With an increase in magnetic field, the force of attraction between the fillers is altered. The interface friction is enhanced due to the increased interface pressure. As a consequence, relative motion between the matrix and filler is reduced (Chen, et al., 2008a; Jian-feng and Gong, 2009; Ju et al., 2012; Rabindranath and Böse, 2013; Yu et al., 2017). Therefore, MRE exhibits an increasing and decreasing trend in the damping characteristics. Past literatures have reported this behavior for the magnetic field in the range of 0.3 T to 0.4 T (Jian-feng and Gong, 2009; Ju et al., 2012; Rabindranath and Böse, 2013; Yu et al., 2017).

MRE exhibits rate dependent properties inherited from the relaxation characteristics of the matrix. Generally, the frequency dependent properties of MRE are characterized within the frequency range of 1 Hz to 100 Hz (Jian-feng and Gong, 2009; Fan et al., 2011; Tian et al., 2011; Gong et al., 2012; Khairi et al., 2016; Perales-Martínez et al., 2017; Yu et al., 2017). For any structural vibration control applications, the viscoelastic response up to 80 Hz is very critical (ISO 10846). Past literatures reported that the storage modulus of MRE exhibits a positive trend with the increase in frequency (Li et al., 2010b; Chen and Jerrams, 2011; Gong et al., 2012a; Zhu et al., 2012; Tian et al., 2013b). This implies that a higher loading frequency results in a larger storage modulus. The frequency dependent enhancement in the storage modulus can be related to the speed mismatch between the slower movement of polymer chains, and the frequency of excitation (Chen et al., 2008a; Yu et al.,

2017). Frequency dependency in MRE can be represented in terms of strain rate effect. At lower frequency, the strain rate effect is increased exponentially but at higher frequencies, these enhancements are not pronounced (Jung et al., 2009). This indicates that the effect of frequency is significant at lower frequencies (less than 5 Hz) but gradually reduced with the increase in frequency (Li et al., 2010b). Moreover, the field-induced enhancements represented in terms of absolute MR effect are independent of the frequency (Lokander and Stenberg, 2003a; Chen et al., 2007b; Damiani and Sun, 2016). However, the relative MR effect depends on the excitation frequency.

The damping characteristic of MRE is a function of operating frequency. The loss modulus of MRE exhibits a positive trend with the increase in frequency (Li et al., 2010b; Tian et al., 2011, 2013b). But, the loss factor is reduced as the storage and loss modulus are enhanced simultaneously with the increase in frequency. Compared to an unfilled rubber, the influence of frequency on the variations in loss factor of MRE is minimal as the embedded fillers obstruct the rubber molecules under the applied cyclic loading (Jian-feng and Gong, 2009). At higher frequencies, the loss factor of MRE is low, which indicates that less energy is dissipated during the sliding of molecular chains in the rubber matrix (Khairi et al., 2016). Moreover, Chen et al (2008a) reported that with an increase in frequency, the influence of magnetic field on the damping characteristics of MRE was reduced. They had correlated this phenomenon to the lack of time available to show the field-induced effect as the driving frequency is increased to larger values (Chen et al., 2008a). Furthermore, the dynamic characteristic of MRE is also affected by the configuration of the testing

system. As the driving frequency is increased, the inertial contributions are amplified, which results in the nonlinear response of MRE (Gong et al., 2012a).

The temperature dependency is a typical characteristic of a polymer composite, which is categorized as glass transition temperature (T_g), room temperature (T_R) and melting point(T_M) properties (Sun et al., 2008; Gong et al., 2012a). The glass transition temperature is referred to the temperature where the polymer transforms from a hard, glassy material to a soft, rubbery material (Lakes, 2009). A drastic change in the properties of MRE is noticed as the temperature is increased from T_g to T_R. The loss factor is maximum corresponding to T_g and reduced as the temperature is increased up to the room temperature (Sun et al., 2008; Yu et al., 2015). The temperature-dependent property of MRE is sensitive to the magnetic field as it affects the mobility of rubber molecules. Rubber matrix becomes relatively softer with the increase in the temperature, and it offers a lesser resistance for the alignment of fillers under the applied magnetic field (Liao et al., 2012; Ju et al., 2015). As the temperature is increased beyond the melting point of the matrix, the reorientation of the fillers alters the original microstructure (Gong et al., 2012a). For example, this process might function as a pre-structuring process and results in a new anisotropic structure.

Increase in temperature enhances the field sensitive characteristics of MRE up to the critical temperature (Liao et al., 2012). This phenomenon is associated with the temperature-dependent magnetization characteristics of MRE. At higher temperatures, the matrix stiffness is reduced but at the same time, the magnetization of fillers is also diminished. Both phenomenon are opposite in nature which results in a critical temperature. Corresponding to the critical temperature, field sensitive characteristics

of MRE attains a maximum value. Moreover, temperature has an adverse effect on the linear range of MRE (Olabide et al., 2015). With the increase in temperature, the matrix-filler interactions are enhanced, which relatively reduces the LVE limit of MRE.

Pre-compression has a significant influence on the properties of MRE under magnetized and the non-magnetized state (Jung et al., 2009; Lejon and Kari, 2009; Dong et al., 2012). The storage modulus of MRE is enhanced with an increase in the compressive preload. Under the influence of magnetic field, the storage modulus exhibits an increasing trend, which signifies the existence of field sensitive characteristics in MRE under the pre-compressed state (Dong et al., 2012). These enhancements are larger under pre-compressed state than that corresponding to the uncompressed state (Jung et al., 2009; Dong et al., 2012). This phenomenon is associated with the increased interaction between the fillers as the inter particle distance is reduced. Though preload enhances the field sensitive characteristics, the relative MR effect is reduced due to the larger zero field modulus.

Like conventional filled elastomers, the properties of MRE are also sensitive to the input displacement (Gong et al., 2005; Li and Sun, 2011; Yu et al., 2017). In a filled elastomer, two general types of interactions arise, namely, particle-matrix and particle-particle (Yu et al., 2017). Both interactions have a significant influence on the storage and loss modulus of MRE. The mechanisms associated with these interactions are altered under the applied strain, which in turn influence the storage and loss modulus. The storage modulus of MRE shows a decreasing trend with an increase in applied strain (Jung et al., 2009; Gong et al., 2012a; Tian et al., 2013b; Olabide et al., 2015). Generally, the strain induced variation in the properties of MRE are

distinguished with respect to the critical strain (Olabide et al., 2015). Within the critical strain, the storage modulus shows a near-linear relationship with the strain. Beyond the critical strain, the storage modulus is drastically reduced (Tian et al., 2013b; Yu et al., 2017). This phenomenon is associated with the destruction of the matrix-filler structure under the action of external load. At lower strain amplitudes, the matrix-filler structure is slightly disturbed. This results in a mild decrease in the storage modulus as the MRE still retains the linearity (Gong et al., 2012a). Therefore, the linear viscoelastic region of MRE is often interpreted as the strain corresponding to 10% deviation from the strain independent storage modulus from SAOS test (Olabide et al., 2015). However, at higher strain amplitudes, the interface is damaged resulting in a larger reduction of storage modulus (Molchanov et al., 2014).

The damping characteristics of MRE have a greater dependency on the dynamic strain amplitude which is equivalent to a filled elastomer (Sun et al., 2008; Jian-feng and Gong, 2009; Fan et al., 2011). Filled elastomer exhibits an initial increasing and decreasing trend with the variations in strain amplitude (Chazeau et al., 2000). The damping in MRE originates due to the discontinuous phase created by the fillers embedded in an elastomer matrix (Chen et al., 2008; Jian-feng and Gong, 2009; Fan et al., 2011). At smaller strain, the damping is lower as the microstructure of MRE is not disturbed. However, with an increase in strain, the relative motion between the particles is intensified, which enhances the damping (Molchanov et al., 2014). With a further increase in strain, the microstructure of MRE is completely destroyed. As a consequence, contribution from the interface friction is reduced, which decreases the loss modulus significantly (Chazeau et al., 2000; Yu et al., 2017). Subsequently, the loss factor is also affected, as it depends on the storage and loss

modulus. The loss factor exhibits a peak with the increase in strain (intermediate strain levels), and it reaches a stable value at higher strain levels.

Under magnetized state, the strain has a significant influence on the properties of MRE as the fillers are displaced from their initial position (Chen et al., 2007b; Zhu et al., 2013). Few studies have reported the strain dependent characteristics under the influence of magnetic field. Nevertheless, these studies are not conclusive as the findings were contradictory. Studies by Molchanov et al. (2014) illustrated that the strain amplitude destroyed the internal filler structure formed under the action of the magnetic field. Under the non-magnetized state, this effect is not pronounced as the filler-structure is not present. However, in the presence of magnetic field, the breakage of magnetic coupling caused by the input strain displaces particles from their initial positions by overcoming the energy barrier and restructure. Chen et al. (2007a) reported that the magneto induced modulus was decreased with an increase in strain as the distance between the fillers were reduced, which in turn reduced the interaction energy between the fillers. Lokandar et al. (2003a) reported that within the tested strain range, the MR effect decreased rapidly with an increase in strain. The studies by Yu et al. (2017) interpreted that the amplitude dependent behavior in MRE was analogous to the phenomenon of Payne effect, generally found in filled rubbers (Chazeau et al., 2000). The Payne effect is measured in terms of the difference between the modulus observed at lower strain and the maximum strain (Yu et al., 2017). Payne effect is pronounced under the magnetized state as the modulus which corresponds to larger strain is least sensitive to the variations in the magnetic field. Above literatures are mainly focused on the influence of larger strain on the field-induced enhancements. However, the effects of magnetic field on the response of

MRE under moderate strain levels (the critical strain region) are overlooked. In the critical strain region, field-induced interactions between the fillers are critical as iron particles are impelled by the magnetic force to move from their initial positions (Gong et al., 2012a). This phenomenon may have a significant influence on the strain dependent response of MRE.

2.7 MRE modeling

Success of MRE based device depends on its ability to modify the properties in response to the control signals. This demands a mathematical formulation, representing the field-induced characteristics of MRE. The properties of MRE are viscoelastic in nature (Lakes, 2009; Li et al., 2010a; Zhu et al., 2012), which is distinguished by the time-dependent response, and it cannot be expressed mathematically by the laws of fluid or solid alone (Sasso et al., 2011). Moreover, these properties vary with magnetic field, preload, strain amplitude and frequency of excitation. Therefore, a great amount of effort is required to represent this behavior in the form of a mathematical model. In general, material modeling approaches of MRE are either parametric or nonparametric (Hu and Wereley, 2007; Wei et al., 2009; Cesmeci and Engin, 2010; Yang et al., 2013b). A nonparametric technique is used to construct models that require a large number of parameters. The parameters of nonparametric model do not have a definite meaning but they are strongly correlated with the experimental data. The list of nonparametric models includes the polynomial model, the neural network model and the fuzzy model, and so on (Hu and Wereley, 2007; Kaldas et al., 2012; Yang et al., 2013b). Applications of the nonparametric models are limited due to the lack of physical conception, and also it needs a large amount of experimental work. On the contrary, parametric modeling is a robust

technique that characterizes the materials behavior as a collection of physical elements like springs and dampers (Cesmeci and Engin, 2010; Yang et al., 2013b). The parametric modeling approach for representing the viscoelastic behavior includes an integral or differential form (Lectez and Verron, 2016; Pritz, 1996). The integral form of representation is based on the Boltzmann superposition principle (Lakes, 2009; Markovitz,1977) and the differential form of approach uses the framework of standard spring-dashpot mechanical models (Sasso et al., 2011). Spring represents the elastic behavior, obeying Hooke's law. The viscous dashpot depicts the time dependent behavior, which relates the relaxation characteristic as described by Newton's law of viscosity (Payne, 1966; Emri and Gergesova, 2010). A classical form of differential order viscoelastic modeling approach involves a combination of linear spring and dashpot, often referred to as Kelvin-Voigt model. The other form of classical model is the Maxwell model, which comprises of an elastic spring in series with a viscous dashpot (Christensen, 1982). These models represent the basic viscoelastic behavior, but fail to describe both creep and relaxation behavior independently (Aho, 2011). The Maxwell model allows for an indefinite deformation with no limiting crosslink to model the equilibrium state after the deformation. On the contrary, the Kelvin-Voigt model represents the viscoelastic behavior of a solid, but it fails to predict the frequency dependent damping characteristics. Furthermore, the Kelvin-Voigt model do not retain the time history, which is a typical characteristic of a polymer (Aho, 2011). In order to improve the ability of a model to concur the viscoelastic behavior of a solid, the classical models are expanded by including additional springs and dashpots in a specific order. Such models are referred to as standard linear solid models (SLS). Zener and the Poynting-Thomson (Lectez and

Verron, 2016; Bruni and Collina, 2000; Roylance, 2001) are the examples for SLS models. The SLS models are defined by a fixed a set of parameters, which are identified by minimizing the error between the modeled and experimental data (Kim and Lee, 2009; Lewandowski and Chorążyczewski, 2007).

Generally, a polymer composite exhibits complex frequency dependence characteristic. The storage modulus increases with an increasing in frequency, and the damping behavior is neither fully viscous nor fully hysteretic (Bruni and Collina, 2000). These attributes cannot be portrayed by SLS models as the damping characteristics have either overestimated at higher frequencies or underestimated them at lower frequencies (Park, 2001; Pritz, 2003). These limitations can be addressed by connecting several springs and dashpots in a specific order such as generalized Maxwell and generalized Kelvin-Voigt models (Bruni and Collina, 2000, Lewandowski and Chorążyczewski, 2007; Park, 2001). The generalized viscoelastic models give a close reality of the viscoelastic solids as each element can describe the relaxation spectrum of each length of the molecule chain (Aho, 2011). As the model includes more elements, the computation process becomes complex due to increased number of parameters (Gil-Negrete et al., 2009). Additionally, recent studies in this domain revealed that a generalized Maxwell model with two Maxwell element is effective in representing the static and dynamic characteristics of real elastomer isolation systems (Zhang and Richards, 2006). The performance of this model is evaluated based on its ability to portray the viscoelastic behavior of a weather-strip seal system over wide frequency range (Basdogon and Dikmen, 2011).

Fractional order based viscoelastic modeling is an alternative approach to overcome the weakness of integer order based models (Pritz, 2003; Berg and Kari,

2003; Makris et al., 1992). In recent years, the fractional derivative order models have gained the popularity due to the simplicity in modeling the dynamic behavior of a vibration mitigation device (Bagley and Torvik, 1983; Torvik and Bagley, 1983; Zhu et al., 2012). These models predict the properties that are intermediate between a Hookean solid and a Newtonian fluid (Meral et al., 2010). A generalization of these characteristics in a fractional order model is conceived by a new kind of element named as spring-pot (Gil-Negrete et al., 2009; Shen et al., 2013). The spring-pot comprises of a fractional power α having the values between zero to one. Appearance of fractional order in a viscoelastic model has a sound physical meaning as the damping characteristics of polymers do not exhibit a strong frequency-dependency (Koh and Kelly, 1990; Schmidt and Gaul, 2009). Compared to integer order, the fractional order based models are capable of accurately predicting the frequency-dependent behavior. Moreover, the fractional order models could concur the wide spectrum of viscoelastic behavior in a simple form involving fewer parameters (Bagley and Torvik, 1983; Gil-Negrete et al.,2009). Similar to the classical models, the fractional models are represented in the form of fractional Kelvin-Voigt (Eldred et al., 1995; Zhu et al. 2012) or fractional Zener (Guo et al. 2014; Pritz, T. 1996). Fractional Kelvin-Voigt model comprises of an elastic spring in parallel with a spring-pot, and the Zener model includes an elastic spring in parallel with a fractional Maxwell element (Pritz,1996). Like the integer order based models, the parameter estimation process becomes more complex with increasing the number of elements. Most often, fractional Zener and fractional Voigt are preferred for dynamic characterization of the rubber component. However, few studies have reported about

the generalized models of fraction Maxwell to improve the fidelity of the predicted response of a viscoelastic material (Pritz, 2003; Shen et al., 2013).

Material models based on classical viscoelastic relations effectively portray the frequency-dependent characteristics. But, these models are not fully adequate to describe the properties of MRE as the amplitude of dynamic deformation is varied. The input strain is an important parameter, which has a significant influence on the properties of MRE. Due to the variation in the strain amplitude, the dynamic stiffness of MRE is decreased, which cannot not be captured by the conventional viscoelastic models (Gil-Negrete et al., 2006; Gil-Negrete et al., 2009). As a consequence, the control strategies developed based on this framework fail to yield satisfactory results. Therefore, it is an absolute requirement to incorporate amplitude dependent effects while designing the MRE based devices. This situation calls for an extension of a conventional viscoelastic model by incorporating the amplitude dependent effects.

A general approach involves connecting spring-Coulomb elements in parallel with the viscoelastic models. This element represents the stick-slip phenomena resulting from the interface slippage with the increase in the amplitude (Bruni and Collina, 2000; Chen and Jerrams, 2011). However, the estimation of the parameters of a frictional element is a cumbersome process as it involves many variables and demands a large amount of experimental data. The limitations of Coulomb friction element can overcome by Berg's friction models comprising of lesser parameters. Although Berg's model predicts the amplitude dependent characteristics, its accuracy is significantly affected by the selected testing conditions (Sjöberg and Kari, 2002; García-Tárrago et al., 2007; Gil-Negrete et al., 2009; Lijun et al., 2010). These limitations are addressed by the modified approach proposed by Thaijaroen et al.

(2010), where the parameter estimation process is carried in two stages. The approach based on an addition of friction element is simple, but its parameter estimation process requires low-frequency and high-amplitude tests, which are difficult to perform in a simple forced vibration test apparatus. Moreover, the measurement condition under high displacement amplitude is always affected by the stiffening effect due to geometrical constraints (Thaijaroen and Harrison, 2010; Lijun et al., 2010). Alternatively, a new visco-tribological model comprising of generalized Maxwell model and Dahl friction model is used to represent the amplitude dependent behavior. However, this model is having limited application due to a large number of parameters, which makes the parameter identification process more complex (Jrad et al., 2013).

In addition, the hysteresis models based on Ramberg-Osgood model and Bouc-Wen are used to describe the nonlinear characteristics of MRE (Eem et al., 2012). The Ramberg-Osgood model is successfully employed to tune the amplitude dependent characteristics of MRE. However, its effectiveness relies on the process of capturing the transition curve from elastic to the plastic response of a material (Sireteanu et al., 2013). This makes the parameter estimation process as path dependent and it has an influence on the identified parameters. On the contrary, Bouc-Wen models could overcome these limitations and are often used to represent the nonlinear characteristics of an isolator system. The advantage of this model is that it does not necessitate the initial path of the target hysteresis loop to estimate the parameters. Compared to other hysteresis models, the Bouc-Wen model comprises of more number of parameters (Ismail et al., 2009), but it can effectively capture the strain stiffening and strain softening behavior often observed in the filled elastomers

(Yu et al., 2016; Carboni and Lacarbonara, 2015). However, at intermediate strain levels, the distortion in the shape of the hysteresis curve is not significant. In such cases, a modified Boucwen model with stochastic linearized random variable is sufficient to describe the amplitude dependent characteristics (Hurtado and Barbat, 2000; Sireteanu et al., 2009; Sireteanu et al., 2010). The simplified models based on linearized Boucwen is reported in many literatures, and it is often used to model the dynamic characteristics of base isolation systems (Marano and Greco, 2003; Love et al., 2011).

Apart from the frequency and amplitude dependent characteristics, the model should incorporate the field sensitive attributes. The material modeling of MRE is an extension of viscoelastic modeling technique by incorporating the magnetic-field dependency (Li et al., 2010b). Most often, these attributes are encompassed in the model by incorporating the field-induced interactions between the adjacent fillers or the particles in a chain of periodically spaced dipoles (Jolly et al., 1996; Shen et al., 2004). The cumulative contributions of dipole interactions are addressed by adding a magnetic spring element in parallel with the viscoelastic models (Zhu et al., 2012; Guo, et al., 2014). Inclusion of this element is essential for the mathematical representation of smart characteristics of MRE isolator as it allows the model to portray the variation in field-induced characteristics (Yang et al., 2013c; Behrooz et al., 2014).

2.8 Summary of Literature Survey

MREs are categorized as anisotropic or isotropic based on the orientation of the fillers in the post cured state. The anisotropic structure comprises of an ordered arrangement of fillers, and the isotropic MRE is characterized by the random

arrangement of the fillers. Though anisotropic MRE possesses better field-induced properties, the isotropic MRE is most preferred due to the simpler synthesis process.

Generally, MRE is operated in shear or squeeze mode based on the loading direction and testing magnetic field direction. The mechanism of field-induced interactions differs under the influence of magnetic field. As a consequence, it is not realistic to perceive the inter conversion between the shear and compression characteristics.

The properties of MRE can be tested by adopting the conventional viscoelastic property measurement approaches. These characteristics are influenced by many processing parameters but the quantity of filler is a decisive factor, which is responsible for the field-induced behavior of MRE. MRE yields a maximum field-induced performance for the addition of fillers in the range of 25-33% by volume. Under the fixed set of processing conditions, the properties of MRE are varied significantly as the operating environment is altered. In general, the performance of MRE is evaluated under different frequency, strain and the magnetic field. These properties of MRE are unique in nature, which vary significantly with the change in the composition of the fillers and matrix. The properties of MRE are evaluated by the dynamic rheological experiments. This approach involves repeating the dynamic tests for different sets of operating conditions. The viscoelastic material modeling approach is an alternate method to simplify the MRE property characterization studies. Most often, viscoelastic models based on constitutive relations are used for the mathematical representation of the material behavior of MRE. An efficient viscoelastic model is the one which can accurately portray the behavior of a material over broad-band frequencies in a simpler form. The relations based on the integer, and

fractional order derivatives are used to model the viscoelastic behavior of MRE. These models are effective in portraying the frequency and field dependent characteristics but fail to predict the amplitude dependent behavior simultaneously. Amplitude dependent attributes are integrated into the model by incorporating friction or hysteresis damping characteristics.

2.9 Research gap and the Scope of the Present Work

Developing a material model for a MRE device demands a proper understanding of its properties. The properties of MRE are unique in nature as it varies significantly with the different combination of matrix and filler. It is also important that there should be a clear distinction between the LVE limit of MRE for the control strategies to yield a better result. For an ideal model, simplicity is a vital parameter, which can be addressed by the proper combination of viscoelastic modeling elements. The model should be able to predict the viscoelastic behavior of MRE over a broad-band frequency in a simple form. Moreover, the model should account for the amplitude dependent characteristics, which is inherent to MRE. To address these aspects, the work undertaken aims at modeling the dynamic translation (compression) characteristics of MRE, which pursues the following specific objectives.

- Experimentally evaluating the dynamic viscoelastic properties of MRE under different magnetic field and excitation frequency.
- Experimentally investigate the influence of strain, its influence on the linear viscoelastic range and assess the effect of magnetic field and frequency on the strain dependent properties of MRE.
- Develop an efficient viscoelastic model to represent the frequency and magnetic field dependent dynamic compression characteristics of MRE over wide frequency range.

- Formulate a mathematical expression to represent the frequency, magnetic field and strain dependent behavior of MRE simultaneously.

CHAPTER 3

EXPERIMENTAL INVESTIGATION ON THE INFLUNCE OF MAGNETIC FIELD AND FREQUENCY ON THE VISCOELASTIC PROPERITES OF MRE

3.1 Introduction

The novel field-induced properties make MRE as a potential material for semi-active vibration isolation devices. As revealed by the literature survey presented in chapter 2, the properties of MRE are sensitive to the operating parameters like frequency and the magnetic field. These characteristics are inherent to particular combination of matrix and fillers, and they attain saturation at larger values of frequency and magnetic field. The present work investigates the effective range of frequency and magnetic field with respect to the variations in field-induced characteristics of MRE. Experiments are performed as per the dynamic blocked transfer stiffness approach on a RTV silicone-based isotropic MRE sample filled with an optimum quantity of ferromagnetic fillers. Its properties are characterized over the frequencies below 80 Hz (representing the low-frequency region as per ISO 10846-1) and a magnetic field up to 0.4 T. The properties of MRE are represented in terms of dynamic stiffness and loss factor computed from force-displacement hysteresis loops, which provides the real time indication of the linear viscoelastic response. An overview of the present investigation is listed below.

1. Synthesis of RTV silicone-rubber based isotropic MRE samples and confirming the particle distribution by SEM observation.

2. Develop an experimental setup to characterize viscoelastic properties of MRE as per the dynamic blocked transfer stiffness method.
3. Evaluate the frequency and magnetic field dependent viscoelastic properties of MRE and analyze the influence of these factors on its saturation behavior.

3.2 Theoretical background for direct blocked transfer stiffness method

3.2.1 Dynamic stiffness

Dynamic stiffness represents the response of a viscoelastic material under cyclic loading condition. According to ISO 10846-1 standard, the dynamic stiffness is the ratio of force response of an isolator for the given input displacement (ISO 10846-1).

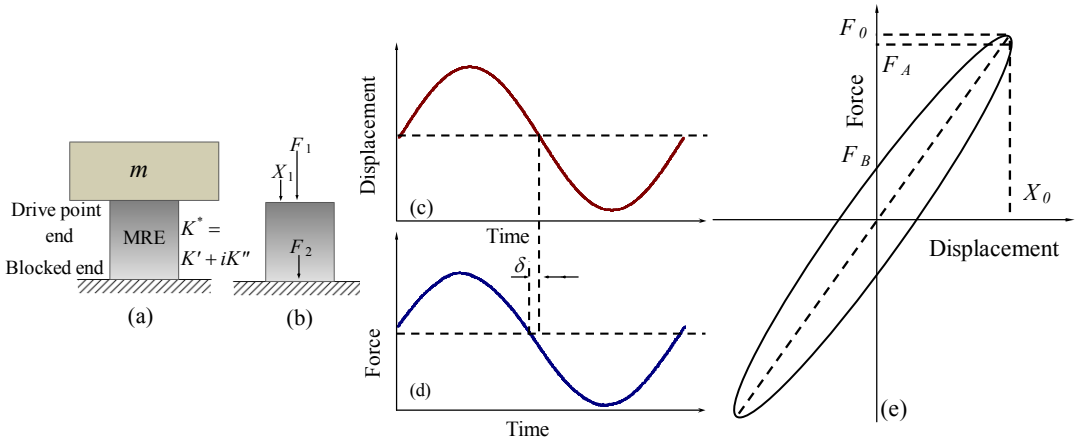

Figure 3.1. (a-b) Schematic representation of direct stiffness measurement approach. (c-e) Graphical representation of the force-displacement hysteresis loop.

The viscoelastic property measurement approach of MRE through direct stiffness method is schematically illustrated in Figure 3.1a and 3.1b. Input harmonic excitation to MRE induces a force, F_1 at the input end and a blocked force, F_2 at the blocked end. The ratio, F_2/X_1 represents the dynamic blocked transfer stiffness, which is a complex quantity depicting the partly viscous and partly elastic nature of a material (Lakes, 2009).

The mathematical representation of dynamic blocked transfer stiffness is given by (Nadeau and Champoux, 2000),

$$K^* = (K' + iK'') = \frac{F_2(t)}{X_1(t)} \tag{3.1}$$

where, K^* represents the dynamic blocked transfer stiffness. The in-phase component (K'), represents the stiffness of MRE (real part of the dynamic blocked transfer stiffness) and the out-of-phase component (K''), signifies the energy dissipation (imaginary part of the dynamic blocked transfer stiffness). The in-phase and out-of-phase components of the dynamic stiffness are evaluated from the response of a system to sinusoidal input. In the linear viscoelastic region, the response blocked force for the sinusoidal input displacement (equation (3.2) and Figure 3.1c) is also sinusoidal (equation (3.3) and Fig 3.1d) in nature with a phase lag of δ.

$$X_1(t) = X_0 \sin \omega t \tag{3.2}$$

$$F_2(t) = F_0 \sin(\omega t + \delta) \tag{3.3}$$

The in-phase and out-of-phase components of dynamic blocked transfer stiffness are expressed as,

$$K' = \frac{F_0}{X_0}\cos\delta \text{ and } K'' = \frac{F_0}{X_0}\sin\delta \tag{3.4}$$

The modified complex force-displacement response is expressed as,

$$F_2(t) = K'(1 + i\eta)X_1(t) \tag{3.5}$$

where, η= tan δ is the loss factor of MRE.

The viscoelastic response of MRE is represented in the form of a force-displacement hysteresis loop by eliminating the parameter t in equation (3.5). The mathematical expression to evaluate the dynamic stiffness and loss factor from the force-displacement hysteresis loop (Figure 3.1e) is given by, (Brown, 1996),

$$K^* = \frac{F_0}{X_0} \tag{3.6}$$

$$\text{Loss factor, } \eta = \frac{F_B}{F_A} \tag{3.7}$$

3.2.2 Energy dissipation

The phase lag between the input displacement and response force results in an elliptical shaped hysteresis loop. The area within the hysteresis loop represents the energy dissipation. The energy absorbed per unit volume by the material due to deformation up to time *t* (one cycle) is given by (Lakes, 2009),

$$W = \int_0^{\frac{2\pi}{\omega}} F_2(t)\dot{X}(t)dt \tag{3.8}$$

From the equations 3.2 and 3.3, the energy dissipation can be written as,

$$W = \omega F_0 X_0 \int_0^{\frac{2\pi}{\omega}} (\cos\omega t \sin\omega t \cos\delta + \sin^2\omega t \sin\delta)dt = W_s + W_d \tag{3.9}$$

The stored and dissipated energy are denoted by W_s and W_d respectively. Negligible inertial effects in dynamic blocked transfer stiffness approach completely restore the energy stored during stretching of the molecular configuration (Luo et al., 2010). Under this condition, the second term of equation (3.9) solely represents the energy dissipation.

The amount of energy dissipation estimated from the dynamic blocked transfer stiffness for one complete cycle of deformation is expressed as,

$$W_d = \pi F_0 X_0 \sin\delta = \pi K'' X_0^2 \tag{3.10}$$

The energy dissipation associated with the equivalent viscous damping in the material is given by (McConnel, 1995)

$$W_d = \pi C \omega X_0^2 \tag{3.11}$$

where, $K''=C\omega$; C represents the equivalent viscous damping of MRE.

3.3 Experimental studies

3.3.1 MRE Synthesis

MRE samples were prepared with 27% by volume CIP (diameter 5 μm; BASF; Type CN) and 73% by volume of two-component RTV silicone matrix (base to crosslinker ratio 100:5 from Dow Corning). The corresponding matrix-filler ratio represents the optimum level of reinforcement to attain maximum field-induced enhancements (Davis, 1999). The details of the ingredients used for preparing the MRE sample are listed in table 3.1.

Table 3.1. Particle ingredients for MRE preparation

S No	Material	Source	Density (Kg/m^3)
1	Silicone rubber	Dow Corning Corporation, United States.	884.57
2	Carbonyl iron particles (average diameter 5μm)	BASF, Type CN	7850

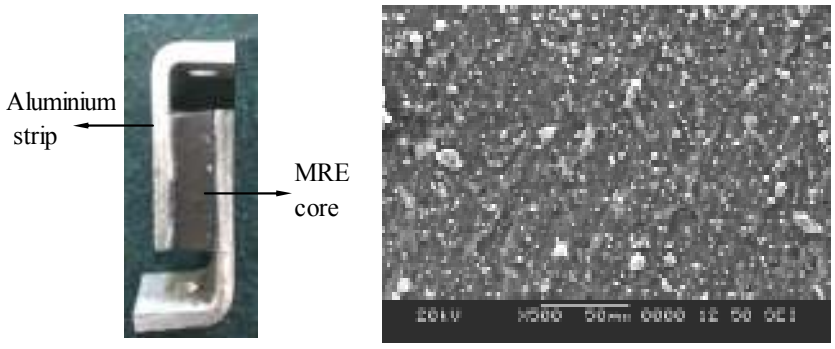

Figure 3.2. (a) MRE sample in single shear mode configuration. (b) Microstructure image of MRE sample

Synthesis process of isotropic MRE involved of two steps: mixing and curing. The ingredients were put into a beaker and stirred for 15 mins. The mixture was then poured to an aluminium mould of size 20 mm x 20 mm x 6 mm and degassed in the vacuum chamber for 5 mins. MRE samples were cured at room temperature under constant pressure for 15 hours (Gong et al., 2005; Li et al., 2010; Fu et al., 2013). Completely cured samples then bonded to an aluminium strip to prepare single lap

shear test specimen (Li and Sun, 2011) as shown in Figure 3.2a. Microstructure of the sample was examined at different locations to verify the distribution of fillers in the matrix. The image shown in Figure 3.2b revealed the uniform distribution of CIP in the matrix indicating the isotropic nature of the prepared MRE sample.

3.3.2 Experimental setup

The schematic and actual images of experimental setup to measure the dynamic viscoelasticity property of MRE are shown in Figure 3.3 and 3.4 respectively. Sinusoidal signals generated from NI PXI-5412 function generator were fed to the electrodynamic shaker though a power amplifier system. MRE test sample was fixed to the electrodynamic shaker through a stinger. The magnetic field was provided by an electromagnet and the field intensity was measured by a Tesla gauge (Lake Shore Cryotronics, Inc; Model 410). Force at the blocked end was measured by a force transducer (KISTLER, type 9712). The input displacement to MRE was monitored by the signals from an accelerometer (KISTLER, K-shear) attached to the input end (ISO:10846-2). The signals were sampled at a rate of 25.6 kS/s and acquired through 24-bit NI PXI-4496 data-acquisition system. The displacement signals were converted to corresponding strain for the ease of representation.

Viscoelastic property measurements of MRE were performed under steady-state harmonic excitation to exclude the errors associated with frequency sweep (Hegde et al., 2014). The experiments were performed at frequencies: 6 Hz, 10 Hz, 20 Hz, 25 Hz, 40 Hz, 50Hz, 60Hz, 70Hz and 80 Hz. The influence of magnetic field was evaluated by extending the viscoelastic property measurement studies at different magnetic field strengths (0 T, 0.2 T, 0.3 T and 0.4 T). To ensure linear viscoelastic response, the experiments were performed at 1.25% strain. MRE samples were

subjected to preconditioning cycles to exclude the effect of stress softening on the measured blocked transfer stiffness (Lion and Kardelky, 2004; Hofer and Lion, 2009). These cycles were repeated until the steady-state hysteresis loops obtained.

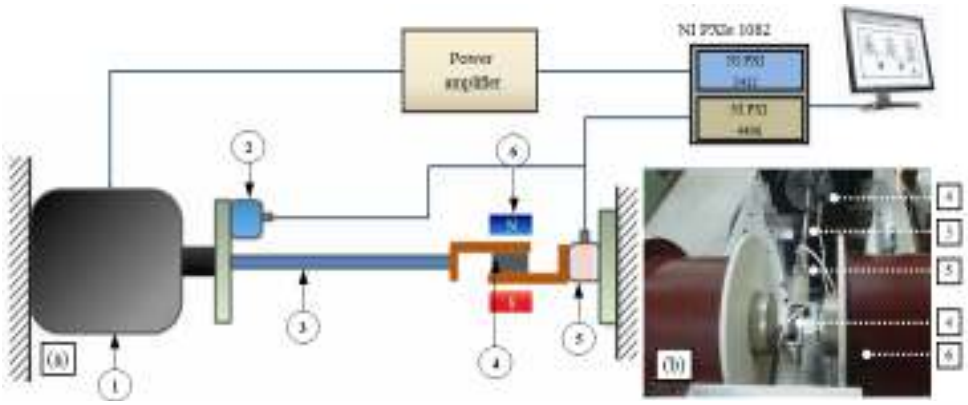

Figure 3.3. (a) Schematic representation of dynamic viscoelastic property measurement experimental set up. (b) An image of the main apparatus.**1.** Electrodynamic shaker, **2.** Accelerometer, **3.** Stinger, **4.** MRE sample, **5.** Force transducer, **6.** Electromagnet

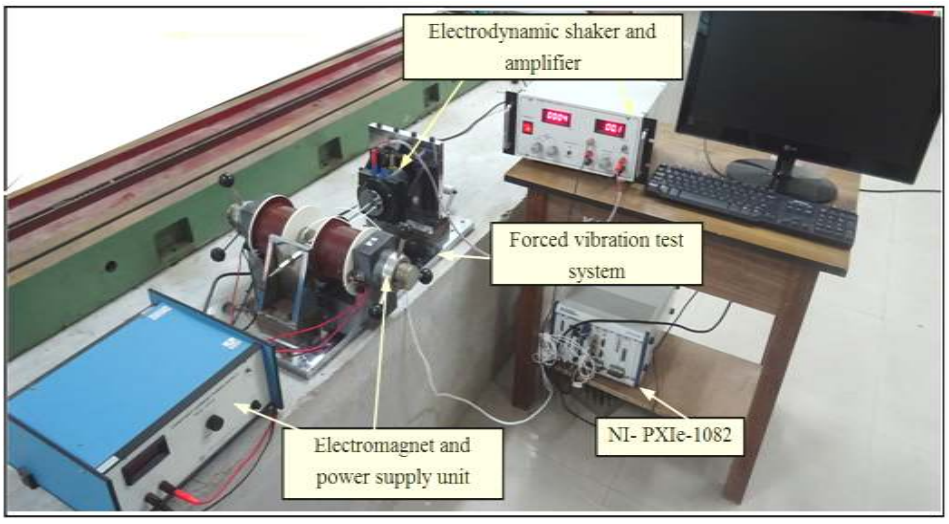

Figure 3.4. A view of a dynamic viscoelastic property measurement experimental setup.

Consistency and accuracy in the viscoelastic property characterization were ensured by performing the experiments on three identical MRE samples. Each set of experiments was repeated 10 times, and the average value has been considered for the analysis. The stable response of the system was ensured by measuring 10 cycles for each loading case. The error bar representation was adopted to indicate the uncertainty in dynamic stiffness and loss factor estimation. MRE samples were

allowed a recovery period of 15 min (Stacer et al., 1990) between successive measurements to exclude the effect of deformation history on the computed viscoelastic properties.

3.4 Results and discussion

Hysteresis loops corresponding to the force-displacement system were plotted based on real-time data recorded during the experiments. Figure 3.5a and 3.5b represent the frequency dependent hysteresis loops registered at 0 T and 0.4 T respectively. The variations in magnetic field and frequency dependent hysteresis behavior are assessed from the resistance force offered by the MRE at the blocked end. The maximum resistance force offered by MRE at 6 Hz and 0 T magnetic field is 0.3416 N and the corresponding force at 80 Hz is 0.429 N. As evident from the Figure 3.5, the effects of frequency on the variation in hysteresis characteristics are not pronounced, and it is diminished above 50 Hz. This behavior of MRE is attributed to the rate dependent relaxation characteristics of the polymer matrix and the inclusion of ferromagnetic fillers. The polymer matrix of MRE comprises of long polymer chains interconnected by chemical crosslinks. At lower excitation frequencies, the bulk polymer chains are flexible and move easily under the imposed deformation. However, these polymer chains gain the stiffness (Osman and Atallah, 2006; Chen and Xu, 2011; Ginic et al., 2000; Funt, 1988) with the increase in excitation frequency, which reduces the mobility of polymer chains by imparting a pseudo-solid behavior (Osman and Atallah, 2006; Jong, 2005). Moreover, the frequency dependent characteristics of MRE are also influenced by the presence of fillers. In an unfilled rubber, the frequency dependent stiffening behavior is pronounced but with the addition of fillers, MRE transforms from a soft elastomer into a rigid composite. As a consequence, the

movement of bulk polymer chains under harmonic loading is inhibited, which in turn diminishes the rate dependent characteristics (Funt, 1988; Leopoldes, 2002; Fuente et al., 2002; Osman and Atallah, 2006).

Figures 3.6(a-f) represent the hysteresis loops corresponding to 0 T, 0.2 T, 0.3 T and 0.4 T magnetic field. Hysteresis behavior of MRE varies with the change in the magnetic field. These variations are pronounced up to a magnetic field of 0.3 T and for an increase in the magnetic field from 0.3 T to 0.4 T, the property enhancements are not significant. These results substantiate the existence of field-induced saturation behavior in MRE around 0.3 T (Chen et al. 2008a, 2008b; Jian-Feng and Gong, 2008). The field-sensitive characteristics of MRE can be attributed to the modifications in the internal microstructure, which leads to the variation of its mechanical properties (Stepanov et al., 2008).

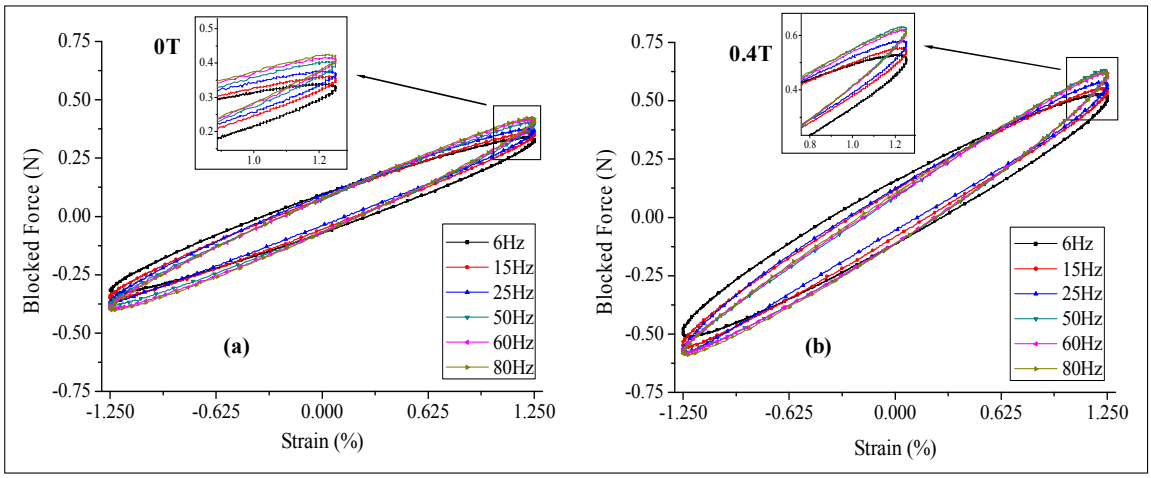

Figure 3.5. (a-b) Steady-state hysteresis loops of MRE at different frequencies corresponding to 0 T and 0.4 T magnetic field.

From the force displacement plots, it is evident that the field dependent variation in hysteresis behavior of MRE is unaffected by the increase in frequency. Corresponding to 6 Hz, maximum resisting force experienced by MRE is increased from 0.337 N at 0 T to 0.571 N at 0.4 T. The cumulative increase in resisting force is

53.33%. Under similar conditions, at 80 Hz, the resisting force is enhanced by 49.12%.

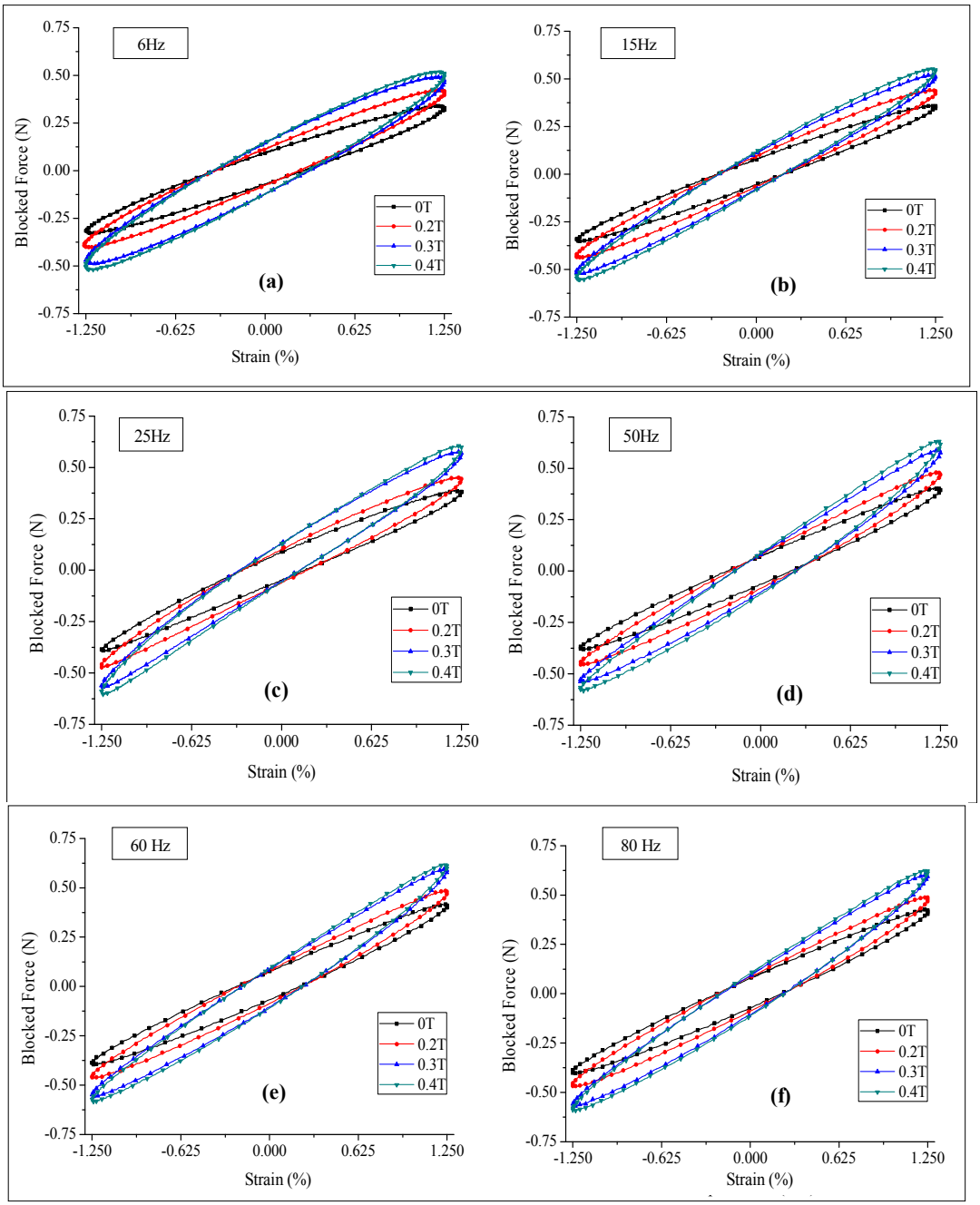

Figure 3.6. (a-f) Magnetic field dependent hysteresis characteristics of MRE at different frequencies.

3.5 Dynamic stiffness of MRE

Figure 3.7a represents the variation in dynamic stiffness at different frequency and magnetic field. The dynamic stiffness of MRE enhances with the increase in magnetic

field and the frequency. The field-induced enhancement in the dynamic stiffness is consistent for all the tested frequencies.

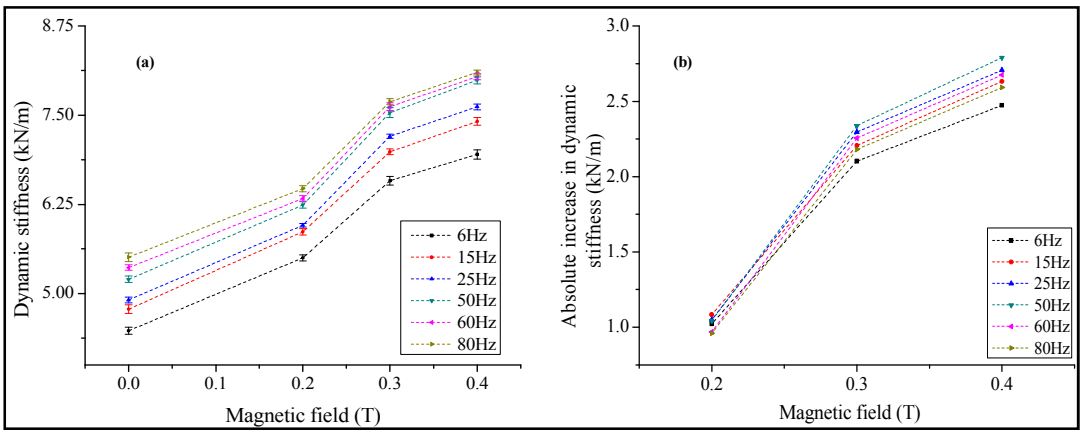

Figure 3.7. (a) Magnetic field-induced dynamic stiffness measured at different frequencies. (b) Absolute increase in dynamic stiffness at different magnetic field and frequency.

Changes in the dynamic stiffness with respect to the magnetic field is expressed in terms of MR effect. The variation in MR effect is depicted in Figure 3.7b and the corresponding values at 0.4 T are listed in table 3.2. Dynamic stiffness of MRE under non-magnetized state and at 0.4 T magnetic field are denoted by K_0 and $\Delta K_{0.4}$ respectively. The ratio $\Delta K_{0.4}/K_0$ represents the MR effect. As evident from table 3.2, the variation in MR effect with the increase in frequency is not pronounced, which signifies the weak dependency of frequency on the field-induced property enhancements of MRE.

Table 3.2. MR effect (dynamic stiffness enhancement) of MRE at different frequencies

Frequency (Hz)	K_0 kN/m	$K_{0.4}$ kN/m	$\Delta K_{0.4}$ (kN/m)	$\Delta K_{0.4}/K_0$ (%)
6	4.48	6.95	2.47	55.24
15	4.78	7.41	2.63	55.07
25	4.91	7.62	2.71	55.11
50	5.20	7.99	2.79	53.65
60	5.37	8.04	2.68	49.86
80	5.51	8.10	2.59	47.00

Enhancement in the stiffness of MRE under the magnetic field can be attributed to the localized compression of the matrix caused by the magnetic force in

the vicinity of the filler. The mechanism of magnetic field-induced localized compression of the matrix is schematically represented in Figure 3.8. Interactions between the fillers under magnetized state are analyzed on a unit cell of MRE (Jolly et al., 1996). A unit cell representation is an enlarged view of a section of the microstructure image (Figure 3.8a), which comprises of a pair of ferromagnetic fillers separated by polymer matrix. Figure 3.8b and Figure 3.8c depicts the schematic representation of MRE unit cell under non-magnetized and magnetized state respectively. As illustrated in Figure 3.8c, under magnetized state, the magnetic force of attraction due to the dipole interactions results in localized compression of the matrix (Leng et al., 2015). This results in an increase in the stiffness of matrix at the vicinity of the fillers, and contributes to the overall stiffness enhancement when bulk effect is considered. As evident from Figure 3.7b, the enhancement in the dynamic stiffness of MRE is pronounced up to a magnetic field of 0.3 T but these variations are not significant as the magnetic field is increased from 0.3 T and 0.4 T.

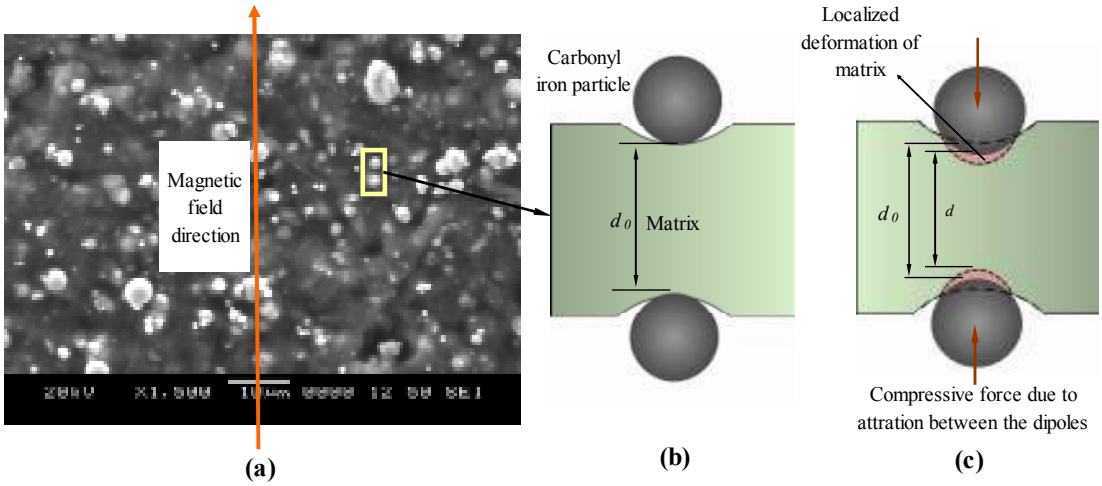

Figure 3.8. (a) Microstructure image of MRE sample. (b) Schematic representation of a MRE unit cell under non-magnetized state. (b) Unit cell of MRE under magnetized state representing the localized deformation of the matrix.

The differences in field-induced dynamic stiffness enhancement are associated with the variation in the energy interaction E between the dipoles, which is expressed as (Liao et al., 2012),

$$E = \frac{-1}{4\pi\mu_m\mu_0}\frac{4\zeta m^2}{d_0^3} \tag{3.12}$$

where, μ_0 is the permeability of vacuum, μ_m is the relative permeability of the elastomer matrix, d_0 is the separation distance of two adjacent particles, $\zeta = \sum_{k=0}^{k=\infty} 1/k^3 \approx 1.202$ and m is the magnetic dipole moment of each iron particle. As illustrated in the Figure 3.8c, the magnetic force of attraction between the fillers vary the separation distance between the dipoles which is expressed as (Guo et al,. 2014),

$$d = d_0(1 - \varepsilon_{matrix}) \tag{3.13}$$

where, ε_{matrix} is the localized compressive in the matrix. The compressive force exerted due to the field-induced interaction between the fillers increases the ε_{matrix}. Subsequently, the energy of interaction between the dipoles is increased by reducing the separation distance, which in turn enhances the localized stiffness of the matrix (Martinelli and Augusto 2005; Fukushi et al. 2013). At a lower magnetic field, the variation in ε_{matrix} is dominated by the magnetic force of attraction. However, at a higher magnetic field, the field-induced variation in ε_{matrix} is diminished due to the contribution of matrix resistance force resulting from the localized stiffness enhancements. As a consequence, the field-induced interactions are effected, which imparts a saturation behavior to MRE above 0.3 T. These findings are in a good agreement with the field-induced saturation characteristics reported in past studies (Chen et al. 2008a, 2008b; Jian-Feng and Gong, 2008).

3.5.1 Energy dissipation

Vibration isolation characteristics of a material depend on its ability to dissipate energy. Figure 3.9 represents the variations in energy dissipation of MRE under different magnetic field and frequency. Energy dissipation recorded at 6 Hz and 0 T is 0.052 mN-m and the corresponding values at 0.4 T is 0.080 mN-m with a total enhancement of 0.028 mN-m. The field-induced enhancement in energy dissipation is consistent with the increase in frequency. At 80 Hz excitation frequency, varying the magnetic field from 0 T to 0.4 T, energy dissipation is increased by 0.0292 mN-m.

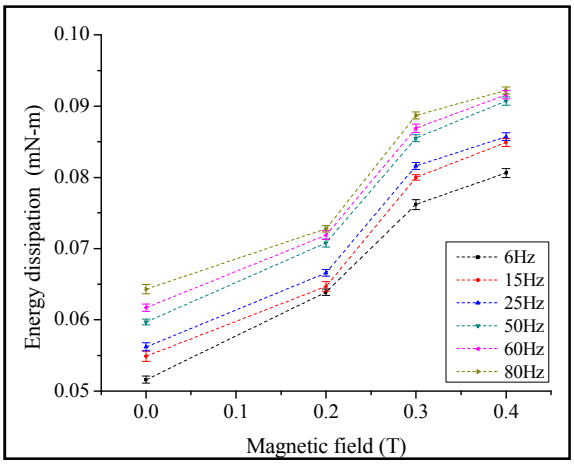

Figure 3.9. Variation in magnetic field dependent energy dissipation of MRE at different frequencies.

The energy dissipation (D) in MRE under dynamic loading condition includes the contributions from energy dissipation of the matrix (D_m), energy dissipation of the particles (D_p), energy dissipation due to friction at matrix-filler interface (D_{pm}) and energy dissipation due to ferromagnetic filler-filler interactions (D_{pp}). The mathematical relations between D and its constituents are (Ju et al., 2012;Fan et al, 2011; Chen et al.,2008b),

$$D = D_m + D_p + D_{pm} + D_{pp} \tag{3.14}$$

The energy dissipation due to the intrinsic characteristics of micron-sized filler particles is minimum compared to the other effects (Ju et al., 2012). Therefore, the modified equation for D by excluding the effect of D_p is,

$$D = D_{pp} + D_m + D_{pm} \tag{3.15}$$

The D_{pp} refers to the energy dissipation due to relative slippage between the particles. Contribution of D_{pp} on the energy dissipation in a filled elastomer is significant at larger content of filler reinforcements (Yang et al., 2012). For an increase in filler content, the scope for filler-filler interactions are high due to more number of particles. As evident from the microstructure image shown in Figure 3.8a, major contribution to D_{pp} in MRE arises from the agglomeration of CIP. The CIP particles are clustered at the sites of agglomeration and surrounded by polymer matrix. These fillers experience a relative slippage under non-magnetized state. However, in the presence of a magnetic field, relative motion between the fillers is inhibited as the particles are bound together. Consequently, the effect of D_{pp} on the overall energy dissipation of MRE is diminished.

The D_m represents the intrinsic damping in the polymer matrix of MRE (Yang et al., 2012). The D_m originates due to the polymer chain friction at the molecular level of a matrix (Fay et al.,1991). This phenomenon is associated with the interaction between the adjacent polymer chains during the coordinated movement under harmonic shear loading (Tsai et al., 2003; Tsai et al., 2007). The mechanism of chain friction is modified under magnetized and non-magnetized state of MRE, which is attributed to the field-induced interactions between the fillers.

The matrix-filler interface friction energy dissipation (D_{pm}) depends on the interaction between the particles and matrix at the interface (Yang et al., 2012). The

interface friction in MRE results from the relative motion between the matrix and filler under dynamic loading. In a weakly bonded interface, the D_{pm} is more pronounced (Ge et al., 2013; Li and Sun 2011; Chen et al. 2008a; Jian-Feng and Gong, 2008) due to the unstable chemical crosslink between the matrix and filler. The microstructure image of the tested MRE sample (Figure 3.2a) is similar to a weakly bonded interface reported in past studies (Chen et al., 2008a; Qiao, et al., 2012) and its contribution on D_{pm} is expressed mathematically as (Chen et al., 2008b; Jian-Feng and Gong, 2008),

$$D_{pm} = nFs \tag{3.16}$$

where, F is the sliding friction force between the particle and the matrix, n is the number of interfaces and s is the relative displacement at the interface.

The frictional force at the interface is expressed as a function of normal force N and the friction factor μ as (Chen et al., 2008b),

$$F = n\mu N \tag{3.17}$$

The expression for the frictional energy dissipation D_{pm} in terms of normal force N is,

$$D_{pm} = n\mu Ns \tag{3.18}$$

The normal force at the interface is a function of magnetic field, which causes the variation in interface friction energy dissipation. Under non-magnetized state, the normal force is constant. With an increase in magnetic filed, the normal force is enhanced, which intensifies the interface interaction and promotes the friction energy dissipation.

Contributions of $D_{m,}$ D_{pm} and D_{pp} on D differ under magnetized and non-magnetized state. The modified expression for energy dissipation in MRE under magnetized state is expressed as,

$$D = D_m + D_{pm} \tag{3.19}$$

Cumulative contribution of D_m and D_{pm} is enhanced with the increase in the magnetic field. For the magnetic field strength between 0 T to 0.3 T, the variations in field-induced energy dissipation are pronounced. Meanwhile, these enhancements are not significant as the magnetic field strength is increased from 0.3 T to 0.4 T. This variation can be attributed to the effect of field-induced localized compression, which influences the enhancements in D_m and D_{pm} under the magnetized state of MRE.

3.5.2 Loss factor

Figure 3.10 represents the variation in the loss factor of MRE with the magnetic field and frequency. The loss factor decreases with the increase in frequency, which is attributed to the dominance of real part of the complex stiffness over the imaginary part (Osman and Atallah, 2006; Yurkeli et al., 2000). As evident from Figure 3.10, MRE exhibits a unique trend in loss factor variation with respect to the magnetic field. Between 0 T to 0.3 T, the loss factor is decreased, while it exhibits an increasing trend for varying the magnetic field strength from 0.3 T to 0.4 T. This unique nature of loss factor variation is assessed from the variations in the equivalent viscous damping (C) and real part of the stiffness (K').

For a SDOF system, the loss factor η is given by (Ungar and Kerwin, 1962),

$$\eta = \frac{C\omega}{K'} \tag{3.20}$$

where, C and K' are the equivalent viscous damping capacity and stiffness of the MRE respectively and ω is the angular frequency of excitation. Figure 3.11 represent the variations in C and K' with respect to the magnetic field. The equivalent viscous

damping C of MRE is estimated from equation (3.11) and the stiffness component, K' is evaluated from the resultant dynamic stiffness.

The K' and C of MRE is sensitive to the variations in frequency and magnetic field. The dependency of C on the frequency is more pronounced compared to the K'. For the excitation frequencies up to 50 Hz, the variation in C is more articulated, which indicates the dominance of viscous effect (Payne, 1966; Deshpande et al,. 2010). However, the contribution of viscous component is diminished for the frequencies above 50 Hz, signifying the dominance of elastic component (Osman and Atallah, 2006;Jong, 2005).

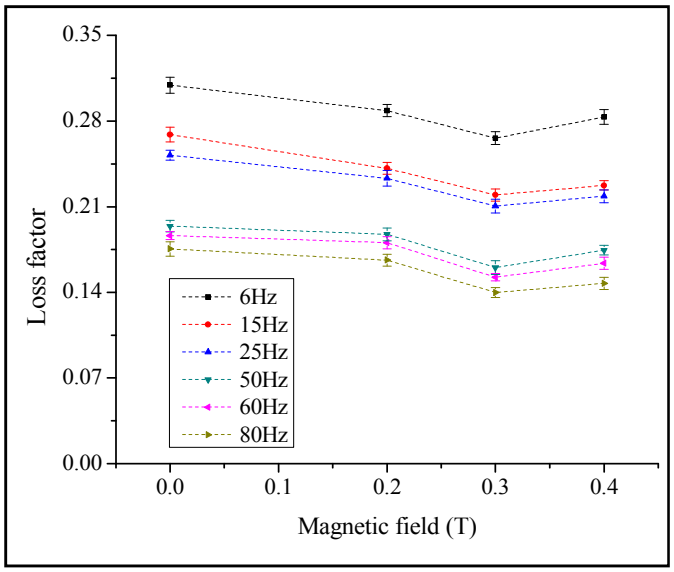

Figure 3.10. Variation of magnetic field dependent loss factor observed at different frequencies

The modified expression for the loss factor by incorporating the field-induced changes in C and K' is expressed as,

$$\eta = \frac{(C_{ref} + \Delta C_{incr})\omega}{(K'_{ref} + \Delta K'_{incr})} \tag{3.21}$$

where, C_{ref} and K'_{ref} are the corresponding equivalent viscous damping and stiffness measured at reference magnetic field. The incremental change in C and K' with the

increase in magnetic field is denoted as ΔC_{incr} and $\Delta K'_{incr}$ respectively. The incremental change represents the difference corresponding to the value measured at the next higher incremental magnetic field relative to the value registered for reference magnetic field. For example, the C value measured at 0.3 T is taken as reference to evaluate the incremental change between 0.3 T to 0.4 T.

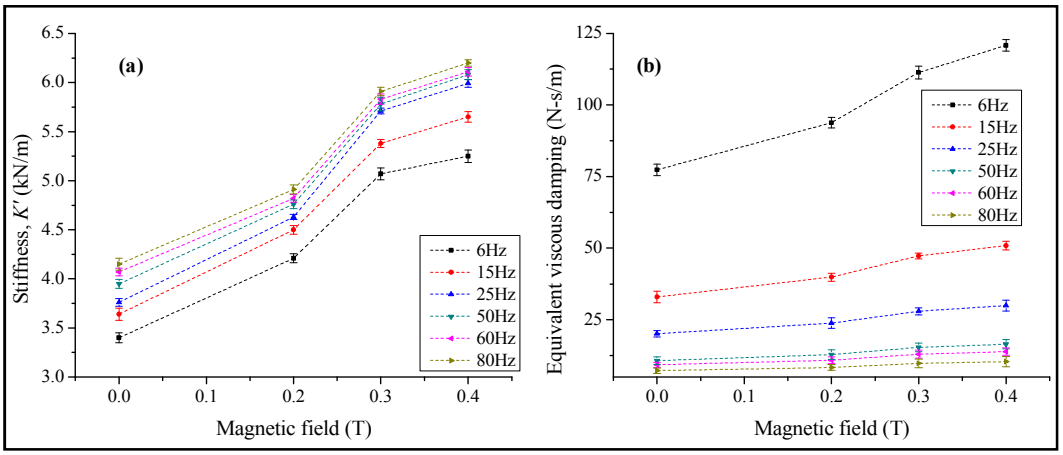

Figure 3.11. (a) Magnetic field and frequency dependent stiffness variation of MRE. (b) Magnetic field and frequency dependent equivalent viscous damping variation of MRE.

The magnetic field dependent variation in ΔC_{incr} and $\Delta K'_{incr}$ are represented in Figure 3.12. As evident from the graph, enhancements in ΔC_{incr} and ΔK_{incr} are pronounced for the increase in magnetic field between 0 T - 0.3 T. The variations in ΔC_{incr} and ΔK_{incr} are minimum for the magnetic field in the range of 0.3 T- 0.4 T. Meanwhile, the field-induced variation in ΔK_{incr} is pronounced over ΔC_{incr} variation for the magnetic field below 0.3 T. For an increase in magnetic field from 0.3 T to 0.4 T, the ΔC_{incr} increase is more pronounced compared to the enhancement in ΔK_{incr}. As a consequence, the loss factor exhibits an increasing and decreasing trend with the variations in magnetic field.

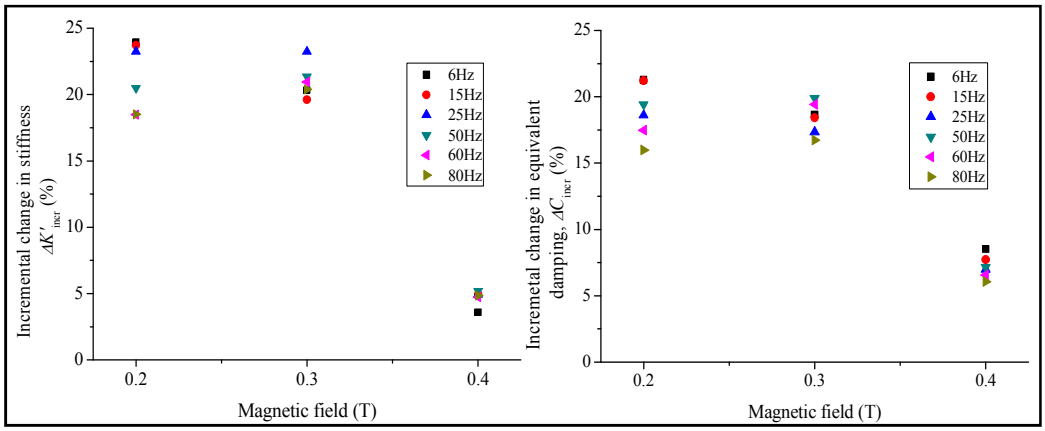

Figure 3.12. (a) Magnetic field induced incremental change in Stiffness. (b) Magnetic field induced incremental change in equivalent viscous damping.

3.6 Summary

In this chapter, the concept of dynamic blocked transfer stiffness method and its theoretical formulations were presented. An experimental test setup was developed as per the dynamic blocked transfer stiffness method to characterize the frequency and magnetic field dependent properties of MRE. The viscoelastic properties were estimated from the force-displacement hysteresis loops. Results of the study revealed that the properties of MRE were sensitive to the variations in magnetic field and frequency but the effect of magnetic field was more pronounced. The dynamic stiffness of MRE was enhanced with the increase in frequency and the magnetic field. However, the energy dissipation ability of MRE was decreased with the increase in frequency and it exhibited a positive trend with the variations in magnetic field. As a consequence, the loss factor displayed a field dependent increase and decreasing trend, which confirmed that the loss factor of MRE cannot be controlled independently under the magnetic field.

CHAPTER 4

EXPERIMETAL INVESTIGATION OF THE LINEAR VISCOELASTIC LIMIT AND AMPLITUDE DEPENDENT CHARACTERISCTICS OF MAGNETPORHEOLOGICAL ELASTOMER

4.1 Introduction

Preliminary dynamic viscoelastic property measurement studies revealed the magnetic field and frequency sensitive characteristics of MRE. Apart from these factors, the input strain is also an important aspect due to the existence of matrix-filler interface. As discussed in chapter 2, the properties of a viscoelastic material are categorized as linear and nonlinear with respect to the critical strain. Under linear regime, viscoelastic modeling approaches based on theory of linear viscoelasticity are used to model the material behavior. These modeling approaches are effective in representing the viscoelastic behavior within the critical strain. However, beyond the critical strain, linear viscoelastic models fail to predict the material behavior as the storage and loss modulus transform into a strain dependent quantities. Moreover, the input strain coupled with the frequency and magnetic field dependency influences the linear viscoelastic behavior of MRE. Consequently, control strategies developed based on the assumption of linear viscoelasticity fail to represent the material behavior in nonlinear region, which in turn affects the performance of a MRE device

The critical strain could not be interpreted as the point where the dynamic stiffness/ modulus transform from a strain independent to strain dependent quantity. In general, a 10% deviation from the strain independent modulus is contemplated as the critical strain as the material still retains the linearity. Therefore, it is important to have a critical assessment of the properties of MRE in the transition region. Present

chapter is focused on evaluating the effect of frequency and magnetic field on the critical strain of MRE. Above studies are extended to evaluate the influence of frequency and magnetic field on the strain dependent characteristics in the transition region. An overview of the present study is listed below.

1. Characterizing the Linear viscoelastic (LVE) limit of MRE through forced vibration test and assess its dependency on frequency and the magnetic field
2. Experimentally investigate the influence of strain on the field-induced characteristics of MRE.

4.2 Methodology

LVE limit of MRE is characterized from the forced vibration tests performed according to the testing standard ISO 10846-1:2008 discussed in chapter 3. MRE test sample is idealized as a Kelvin-Voigt spring with stiffness K and damping C (Figure 4.1). The resultant stiffness is denoted by K^*.

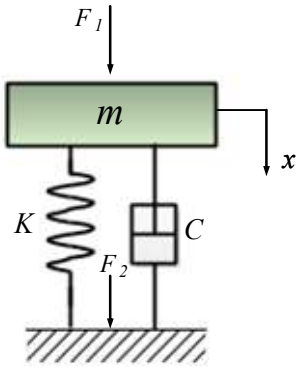

Figure 4.1. SDOF representation of forced vibration test setup

According to the standard, dynamic drive point stiffness estimates the stiffness with respect to the force at the input end. Estimated stiffness from the drive point approach is affected by the inertial mass of the system, which induces terminal nonlinearity to the measurement at higher frequencies (Nadeau and Champoux, 2000). On the contrary, the blocked transfer stiffness, which is based on the blocked force

measurement, overcomes the weakness of drive point stiffness approach (Ooi et al., 2011).

With respect to the Figure 4.1, the dynamic blocked transfer stiffness is given by,

$$K^* = \frac{F_2(t)}{x(t)} = \frac{Kx(t) + C\dot{x}(t)}{x(t)} \tag{4.1}$$

Rearranging the terms in equation (4.1), the force-displacement relations with respect to the blocked transfer stiffness is given by,

$$F_2(t) = K^* x(t) \tag{4.2}$$

The linear and nonlinear behavior of viscoelastic material is distinguished from the response under harmonic excitation. In linear viscoelastic region, for the imposed harmonic excitation, the response force at the blocked end will be sinusoidal but lags by a phase angle δ.

$$\left.\begin{aligned} x(t) &= x_0 \sin \omega t \\ F_2(t) &= F_0 \sin(\omega t + \delta) = Kx_0 \sin \omega t + C\omega x_0 \cos \omega t \end{aligned}\right\} \tag{4.3}$$

However, the non-linear response of the material for the imposed harmonic input cannot be represented by a single harmonic function rather it is described as Fourier series of odd harmonics (Tariq et al., 1998; Gong et al., 2012a).

$$\left.\begin{aligned} x(t) &= x_0 \sin \omega t \\ F_2(t) &= \sum_{n=1,3,5,..\ \text{odd}}^{N} F_n \sin(n\omega t + \delta_n) \end{aligned}\right\} \tag{4.4}$$

where, F_n and δ_n are the amplitude and phase angles of the odd harmonics respectively.

A distinction between the linear and nonlinear response in a viscoelastic material is depicted in Figure 4.2. The force and displacement signal under the linear region is represented in Figure 4.2a and 4.2b. Corresponding signals under the

nonlinear region are represented in Figure 4.2e and 4.2f. The frequency-domain representation of the force signal under the linear and nonlinear regime is illustrated in Figure 4.2c and 4.2g respectively. By eliminating the parameter *t*, the viscoelastic response is represented in the form of a force-displacement hysteresis loop. In linear viscoelastic region, the hysteresis loop will be a proper ellipse (Figure 4.2d). The contribution from high-order harmonics gives rise to a non-elliptical shape of the hysteresis loop, which represents the nonlinear viscoelastic behavior (Figure 4.2h).

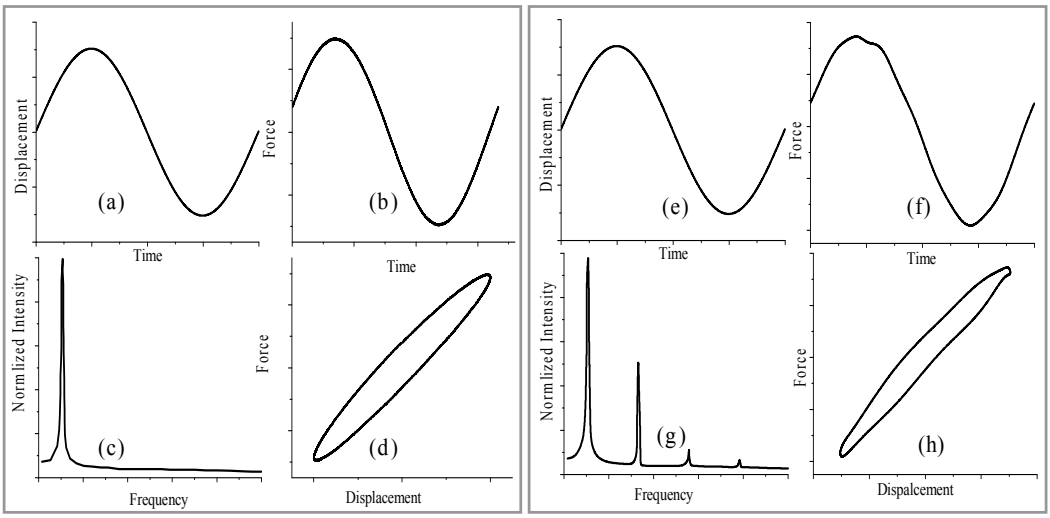

Figure 4.2. (a) Input displacement, (b) Output response force, (c) Frequency domain representation of response force and (d) hysteresis plot corresponding to linear response of a viscoelastic material. (e) Input displacement, (f) Output response force (g) Frequency domain representation of response force and (h) hysteresis plot corresponding to nonlinear response of a viscoelastic material.

4.3 Characterization of LVE limit and amplitude dependent properties of MRE

The LVE limit characterization was performed on a MRE sample comprising of 27% by volume CIP. Test sample preparation and its characterization were carried as per the procedures discussed in section 3.3. LVE limit is evaluated at different frequencies (6 Hz, 8 Hz, 10 Hz, 12 Hz, 14 Hz, 16 Hz, 18 Hz, 20Hz and 24 Hz) and magnetic fields (0 T, 0.2 T, 0.3 T and 0.4 T) based on the saturation characteristics

revealed from the preliminary studies. The LVE limit of MRE was monitored from the distortion in the shape of the hysteresis plot with the increase in the input strain. Experiments were performed under constant frequency and magnetic field by varying the input strain until a distortion in the shape of the hysteresis loop is observed. The strain amplitude corresponding to the deviation in the regular elliptical shaped hysteresis loop was interpreted as the LVE limit. To ensure the consistency and accuracy in the measured LVE limit, the procedure discussed in section 3.3 are implemented.

The LVE limit characterization experiments were extended to evaluate the strain dependent characteristics of MRE. These tests were performed at fixed strain amplitudes corresponding to different frequencies and magnetic field strength. The deviations in the slope of the hysteresis loop were monitored to assess the strain dependent response and its influence on the field-induced characteristics of MRE.

4.4 Results and discussion

4.4.1 LVE limit of MRE

The force-displacement hysteresis loop of MRE under magnetized and non-magnetized state is represented in Figure 4.3-4.5. As visualized from the graph, the shape of the curve is a proper ellipse at lower strain levels, and it distorts as the strain exceeds the LVE limit. The limiting strain corresponding to the transition from linear to nonlinear viscoelastic behavior is termed as the critical strain.

Frequency and magnetic field dependent variation in the critical strain is depicted in Figure 4.6. The critical strain exhibits a strong dependency on the magnetic field. With the increase in the magnetic field, the transition from linear to nonlinear behavior occurs at lower strain levels. Corresponding to 6 Hz and 0 T

magnetic field, the critical strain is 5.17% and increasing the magnetic field to 0.2 T, the critical strain is decreased to 4.67% with a reduction of 9.6%. Further increasing the magnetic field to 0.4 T, 19% reduction in critical strain is noticed. The field dependency of the critical strain is consistent with the frequency as it exhibits a reduction of 20.3% for varying the magnetic field from 0 T to 0.4 T at 16 Hz. From Figure 4.4, it is also noticed that the influence of frequency on critical strain is not as pronounced as compared to the magnetic field.

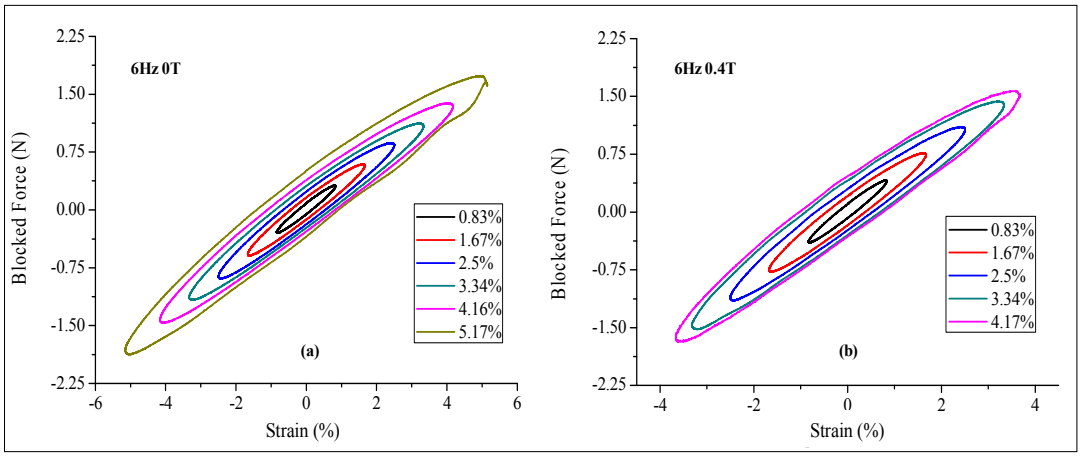

Figure 4.3 (a-b) Hysteresis plots representing the transition from linear to nonlinear response of MRE at 0T and 0.4 T corresponding to 6 Hz.

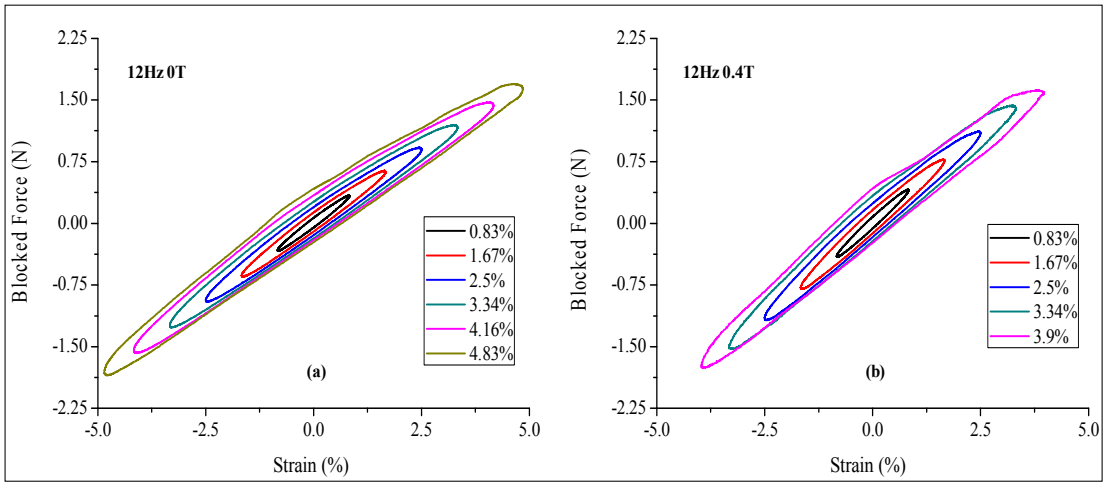

Figure 4.4 Hysteresis plots representing the transition from linear to nonlinear response of MRE at 0T and 0.4 T corresponding to 12 Hz.

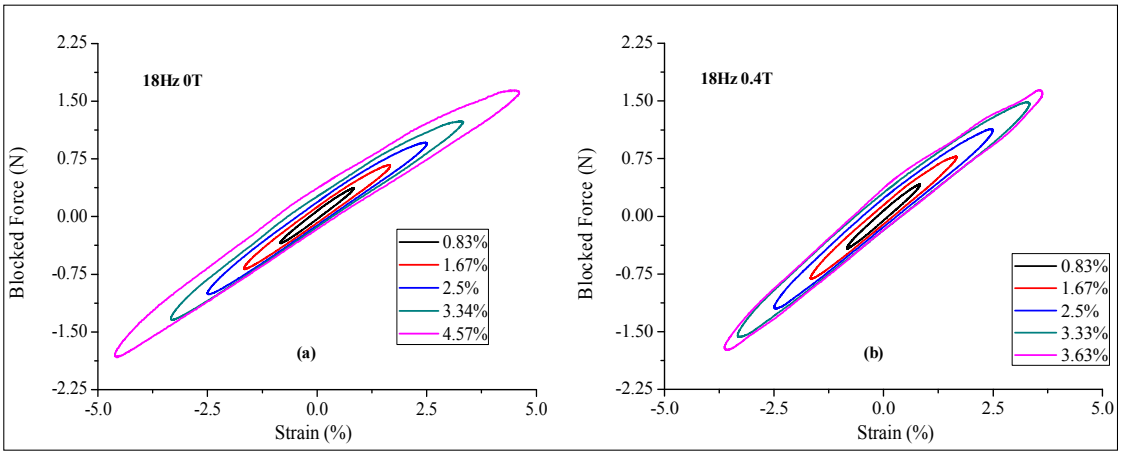

Figure 4.5 Hysteresis plots representing the transition from linear to nonlinear response of MRE at 0 T and 0.4 T corresponding to 18 Hz.

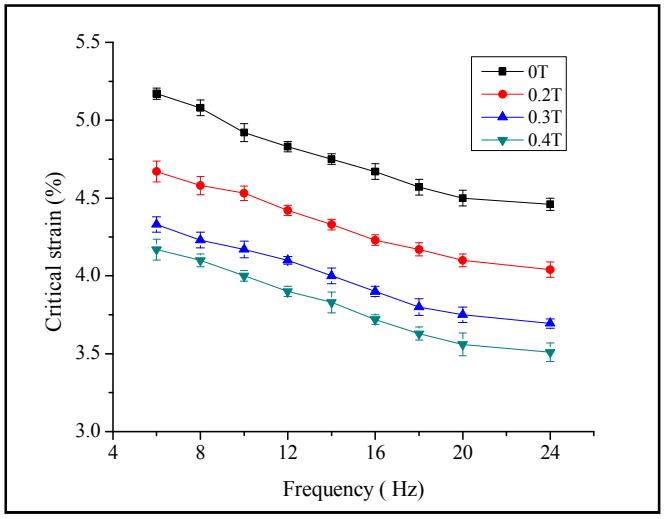

Figure 4.6. Variation in critical strain with respect to the frequency observed at different magnetic fields.

The transition from linear to nonlinear viscoelastic behavior in MRE is attributed to the mechanisms of interface interactions between the matrix and the filler (Funt, 1998; Ge et al., 2013; Wang, et al., 2006). Under harmonic displacement, MRE deforms as the strain is transferred from the matrix to the filler (Ge et al., 2012; Fan et al., 2011). The mechanism of strain transfer depends on the type of interface existing between the matrix and filler. A strongly bonded interface is effective in transferring the strain, but a weakly bonded interface dissipates the energy at the interface (Yang et al., 2012). The microstructure image of MRE (Figure 3.8a) confirms that the

interface is dominated by weak matrix-filler interactions (Chen et al., 2008b), which are characterized by the unstable chemical crosslinks (Gauthiera et al., 2004). The nonlinear viscoelastic behavior in MRE comes into light when these bonds break under the imposed strain. At smaller strains, the matrix-filler bonds are intact, which results in a strain independent response of MRE. As the strain is increased, de-bonding at the interface occurs, which decreases the number of intact bonds (Lion A and Kardelky, 2004). Further increase in strain results in the slippage at the interface due to the breakage of intact bonds. As a consequence frictional energy dissipation increases, which induces additional harmonics and results in nonlinear response of MRE (Stacer et al., 1990; Gil-Negrete et al., 2006).

Under magnetized state, MRE attains smart properties as the fillers readily interact. These interactions are affected under the applied strain. Consequently, LVE limit of MRE is modified due to the variations in the frictional energy dissipation. The frictional energy dissipation can be estimated from the equivalent viscous damping of MRE (Song et al., 2009) as it includes the dominant contribution from the matrix-filler interface friction (Ju et al., 2012; Fan et al., 2011; Chen et al., 2008a). Moreover, the equivalent viscous damping can solely represent the energy dissipation due to friction at the matrix-filler interface under constant strain and constant frequency. Figure 4.7 represents frequency and magnetic field dependent variation in the equivalent viscous damping corresponding to 2.5% strain. Equivalent viscous damping exhibits a positive trend with an increase in magnetic field, which signifies the enhancements in matrix-filler interface friction. As a consequence, nonlinearity (Stacer et al., 1990) occurs at lower strain levels compared to the non-magnetized state of MRE.

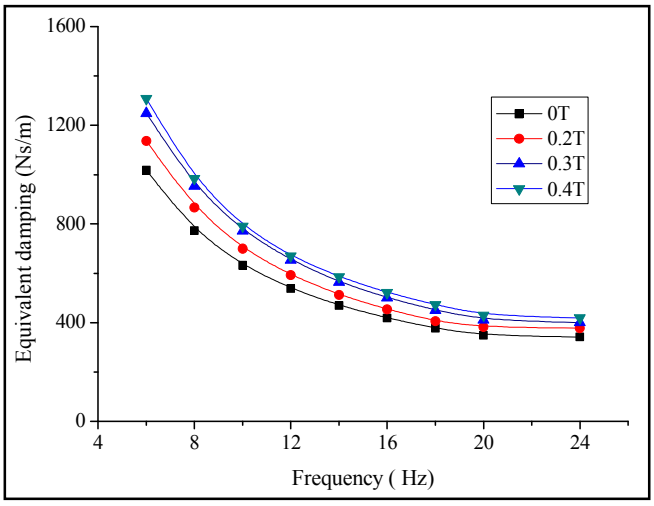

Figure 4.7. Frequency and magnetic field-induced variation in equivalent viscous damping in MRE corresponding to 2.5% strain.

Present investigation also revealed the influence of frequency on the LVE limit. Similar observations were reported by many researchers on the frequency dependent variation of LVE limit in a filled elastomer (Wang and Robertson, 2005; Ren and Krishnamoorti 2003; Lion A and Kardelky, 2004; Luo et al., 2010). This phenomenon can be attributed to the increased energy input due to the breakage and reformation of bonds at the interface (Wang and Robertson, 2005; Glenn, 1968). With the increase in frequency, time available for the reformation of bonds will reduce, and it results in the appearance of nonlinear response at lower strain levels.

4.4.2 Strain dependent properties of MRE

The influence of frequency and magnetic field on the strain dependent behavior of MRE is evaluated from the change in slope of the force-displacement hysteresis loops. Figure 4.8-4.11 shows the hysteresis loops corresponding to the frequencies 8, 12, 16 and 20 Hz observed at 0 T and 0.4 T. As evident from the graph, the strain dependent characteristics exist under passive and active state of MRE.

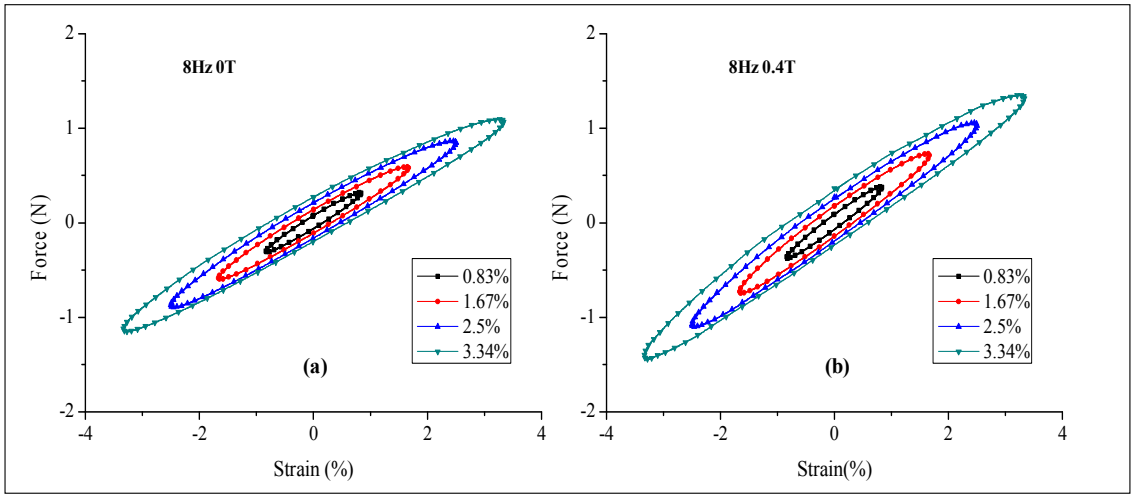

Figure 4.8 (a-b) Hysteresis loops corresponding to 8 Hz evaluated at different strain levels.

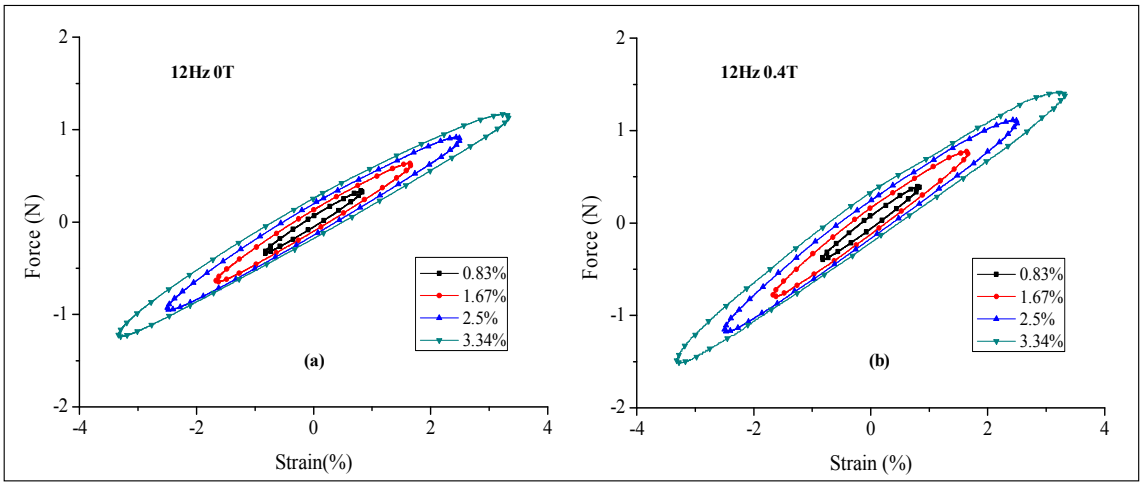

Figure 4.9 (a-d) Hysteresis loops corresponding to 12 Hz evaluated at different strain levels.

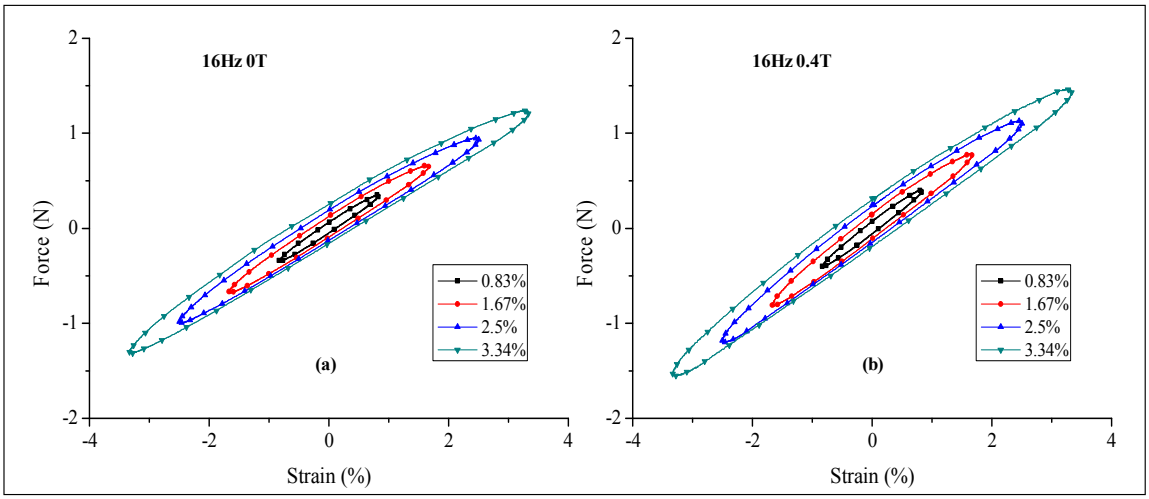

Figure 4.10 (a-d) Hysteresis loops corresponding to 16 Hz evaluated at different strain levels.

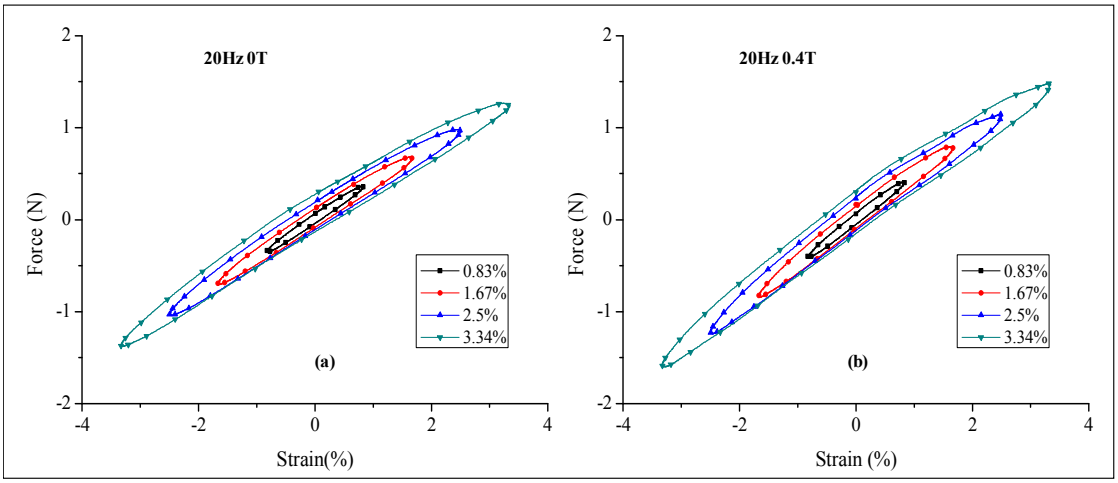

Figure 4.11 (a-d) Hysteresis loops corresponding to 20 Hz evaluated at different strain levels.

Strain dependency is visible in the form of reduction in the dynamic stiffness or modulus when a material is cyclically deformed (Yurkeli et al., 2000; Glenn,1963; Ren and Krishnamoorti, 2003; Stacer et al., 1990). The strain dependent characteristic in MRE is associated with the attributes of a filled elastomer possessed by it, which is referred to as Payne effect (Payne, 1962). On the molecular level, strain dependency is envisioned as the filler-structure model or matrix-filler bonding and debonding model, also referred to as bound rubber model (Ramier et al., 2006; Chazeau et al., 2000;Funt,1988). In a filler-structure model, interactions between the filler-filler are the dominant factor for the strain dependency. The stiffness reduction with an increase in strain is associated with the reversible breakdown and recovery process of filler aggregate structure (Payne, 1962; Heinrich and Vigilis 1995; Garnier et al., 2013).

In a bound rubber model, interaction between the filler and the matrix at the bound rubber is the prominent factor responsible for the strain dependent characteristics (Stelandre et al., 2003; Stacer et al., 1990; Gauthier et al., 2004). The bound rubber is represented as a thin layer of elastomer around the filler particle,

which is surrounded by the bulk polymer. Bound rubber is harder than the bulk rubber, and it has less molecular mobility due to the supplementary crosslinks at the filler surface (Funt, 1988; Kalfus and Jancar, 2007; Chazeau et al., 2000). The difference in the hardness results in a stress concentration at matrix-filler interface under the imposed strain. This initiates the bonding and debonding process of the bound rubber at the interface. Consequently, the total number of intact bonds is reduced, which decreases the stiffness of the filled elastomer (Lion, and Kardelky, 2004).

The filler-structure model is well adopted to describe the strain dependency in the elastomers filled with nano-sized fillers (Jong, 2005;Osman and Atallah., 2006; Suzuki et al., 2005). However, a bound rubber model interprets the strain dependency in elastomers filled with micron-sized fillers (Stelandre et al., 2003; Stacer et al.,1990) and nano-sized fillers (Leopoldes et al 2002; Chen and Xu, 2011). The bound rubber model can be extended to describe the strain dependency in MRE as the microstructure images shown in Figure 3.8 suggest the uniform distribution of the micron-sized particles. Moreover, the formation of network of agglomerations is not evident, which rules out the relevancy of the filler-network model for MRE. The applicability of matrix-filler bonding and debonding models is further justified from the studies by Zhang et al. (2007) which has proven the existence of bound rubber in MRE.

The strain dependent characteristics of MRE have an influence on the interaction between the fillers under magnetized state. Affects of strain are analyzed from the reduction in the stiffness of MRE as the input strain is varied. The stiffness reduction is expressed as,

$$\text{Stiffness reduction} = K_L - K_H \quad (4.5)$$

where, K_L corresponds to the dynamic stiffness registered for the lower strain level, and K_H represents the dynamic stiffness at higher strain. Table 4.1 lists the stiffness reduction measured by varying the strain from 0.83% to 3.34% at different frequency and magnetic fields.

Table 4.1. Amplitude dependent stiffness reduction in kN/m of MRE by increasing the strain from 0.83% to 3.34% at different frequency and magnetic field.

Magnetic field (T)	Frequency (Hz)								
	6	**8**	**10**	**12**	**14**	**16**	**18**	**20**	**24**
0	0.711 ± 0.014	0.708 ± 0.015	0.693 ± 0.011	0.688 ± 0.010	0.676 ± 0.014	0.664 ± 0.012	0.661 ± 0.010	0.657 ± 0.013	0.648 ± 0.011
0.2	0.673 ± 0.013	0.660 ± 0.011	0.650 ± 0.010	0.643 ± 0.016	0.638 ± 0.013	0.630 ± 0.011	0.625 ± 0.013	0.612 ± 0.015	0.605 ± 0.015
0.3	0.646 ± 0.011	0.637 ± 0.013	0.635 ± 0.012	0.628 ± 0.013	0.617 ± 0.013	0.610 ± 0.013	0.605 ± 0.010	0.600 ± 0.012	0.594 ± 0.010
0.4	0.630 ± 0.012	0.623 ± 0.010	0.620 ± 0.011	0.611 ± 0.012	0.604 ± 0.012	0.596 ± 0.015	0.584 ± 0.012	0.580 ± 0.012	0.575 ± 0.012

Stiffness reduction values listed in the table 4.1 suggest that, magnetic field has a significant influence on the strain dependent properties of MRE. The strain dependent stiffness reduction is pronounced under non-magnetized state, and it diminishes as the magnetic field is increased. The field-induced stiffness reduction is unaffected by the increase in frequency. Stiffness reduction observed at 0 T and 6 Hz is 0.711 N/mm. Correspondingly, at 0.4 T a stiffness reduction of 0.630 N/mm is observed with a total decrement of 11.65%. Under similar conditions, increasing frequency to 20 Hz, the corresponding reduction is 11.85%.

The difference in strain dependent characteristic of MRE under magnetized and non-magnetized state is attributed to field-induced compressive force exerted by the fillers on the entrapped rubber (Possinger et al., 2014). The compressive force has a significant influence on the enhancement in the dynamic stiffness of MRE by

modifying the interface interactions between the matrix and the fillers (Cho and Youn, 2006; Wollscheid, 2014). This phenomenon can be interpreted by adapting the bound rubber model proposed by Zhang (Zhang et al., 2007). The bound rubber model (4.12 c) is a schematic representation of the microstructure images of filler shown in Figure 4.12a and 4.12b. As depicted in Figure 4.12d, the strain dependency in MRE is illustrated on a section of the bound rubber with the supplementary crosslinks at the interface (Stacer et al.,1990; Qiao et al., 2012). In the absence of magnetic field, the bonding and deboning process initiated due to the input strain reduces the total number of intact bonds (Figure 4.12e). Subsequently, it reduces the overall dynamic stiffness of MRE.

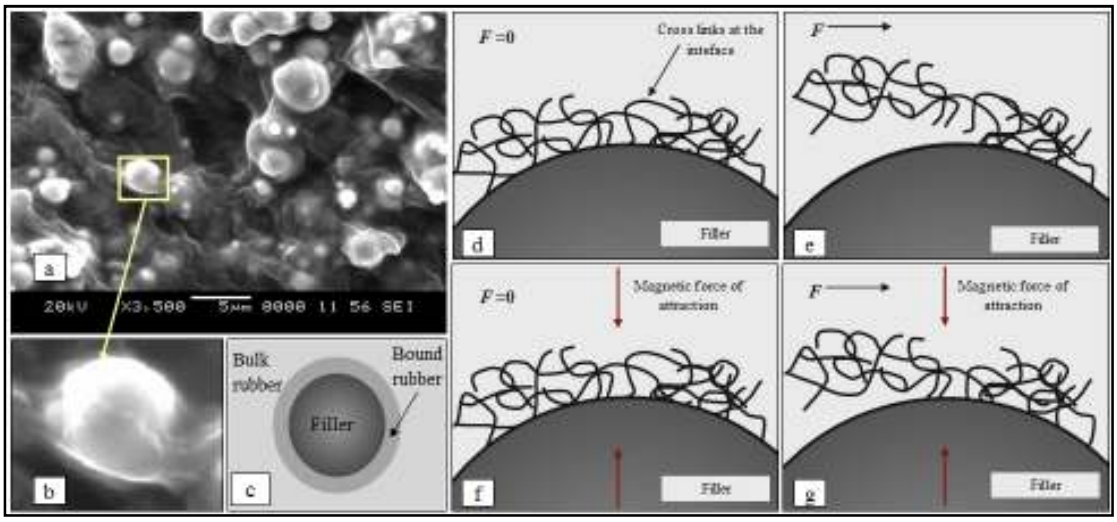

Figure 4.12. (a-b) Microstructure image of MRE sample. (b) Bound rubber around the ferromagnetic filler. (b) Schematic representation of bound rubber.(d-e) Chemical crosslinks at the bound rubber under non-magnetized state corresponding to undeformed and deformed state of MRE. (f-g) Chemical crosslinks at the bound rubber under magnetized state corresponding to un-deformed and deformed state of MRE.

Under magnetized state, the mechanism responsible for the strain dependency differs due to the field-induced interaction between the fillers. As represented in Figure 4.12f, the magnetic force brings the neighboring particles closer, which in turn transfers the force to the entrapped rubber. As a consequence, a resistance force is

experienced against the bonding and debonding process at the bound rubber, which creates an unfavorable condition for the breakage of bonds. This process results in the retaining of more intact bonds at the bound rubber under magnetized state compared to the non-magnetized state of MRE (4.12g). Subsequently, it leads to the variations in strain dependent characteristics of MRE under magnetized and non-magnetized state.

4.5 Summary

The Assessment of LVE limit and characterization of amplitude dependent characteristic of MRE is a crucial factor to transcend MRE from laboratory to the actual application prospectus. In this chapter, the influences of magnetic field and frequency on the amplitude dependent characteristics of MRE were discussed. The properties of MRE were evaluated as per the dynamic blocked stiffness method discussed in the chapter 3. The transition from linear to nonlinear viscoelastic behavior was assessed from the deviation in the regular elliptical shape of the hysteresis loops obtained from the blocked force measurement. The results indicated that the LVE limit of MRE was sensitive to the frequency and the magnetic field. The magnetic field had a greater influence on the transition behavior as it modified the interface interaction between the matrix and the filler.

The amplitude dependent characteristics of MRE were evaluated from the variation in the slope of the hysteresis loop. Like any other conventional viscoelastic material, MRE exhibited the Payne effect as the displacement amplitude was increased. The variation in the amplitude dependency was evaluated from the disparity in the stiffness registered between two different strain levels. These results indicated that within the tested strain levels, the reduction in stiffness was more

pronounced under non-magnetized state than the magnetized state. The mechanism associated with the deviation in strain characteristic of MRE was interpreted by adopting bound rubber model.

CHAPTER 5

EXPERIMENTAL INVESTIGATION OF DYNAMIC COMPRESSION PROPERTIES OF MRE

5.1 Introduction

In chapters 3 and 4, the dynamic viscoelastic properties of MRE are evaluated under shear loading as it represents the volume preserving deformation state. The results of shear test cannot be extended to model the compression stiffness, as the properties of MRE are sensitive to the loading status. Moreover, the compressive load simulates the realistic loading conditions of polymer composites and in this configuration it exhibits a larger load bearing capacity.

A review of past literatures indicates that there is a considerable amount of works reported on the shear properties of MRE, but few studies have addressed the properties under compression (Gordaninejad et al., 2012; Padalka et al., 2010; Kaillo et al., 2007). Koo et al. (2010) proposed a phenomenological model to represent the dynamic compression characteristics of MRE. Liao et al. (2012) investigated the field sensitive compressive characteristics in terms of variation in normal force. These researchers have enlightened the compressive characteristics of MRE. But, the results from above stated literatures cannot be used for the present work as the properties of MRE are unique. Moreover, these properties vary significantly with the combination of matrix and filler and also with the operating parameters.

In the present work, dynamic compression tests are performed as per blocked transfer stiffness method to evaluate the compressive stiffness of MRE. Experiments are performed at frequencies ranging from 8 Hz-24 Hz under different magnetic field and strain amplitudes. The effects of these parameters on the dynamic stiffness and

damping are calculated from the force–displacement hysteresis loop. The test results are used to develop a mathematical relation for the translation stiffness of MRE based on phenomenological modeling approaches.

5.2 Experimental studies

5.2.1 Experimental set up

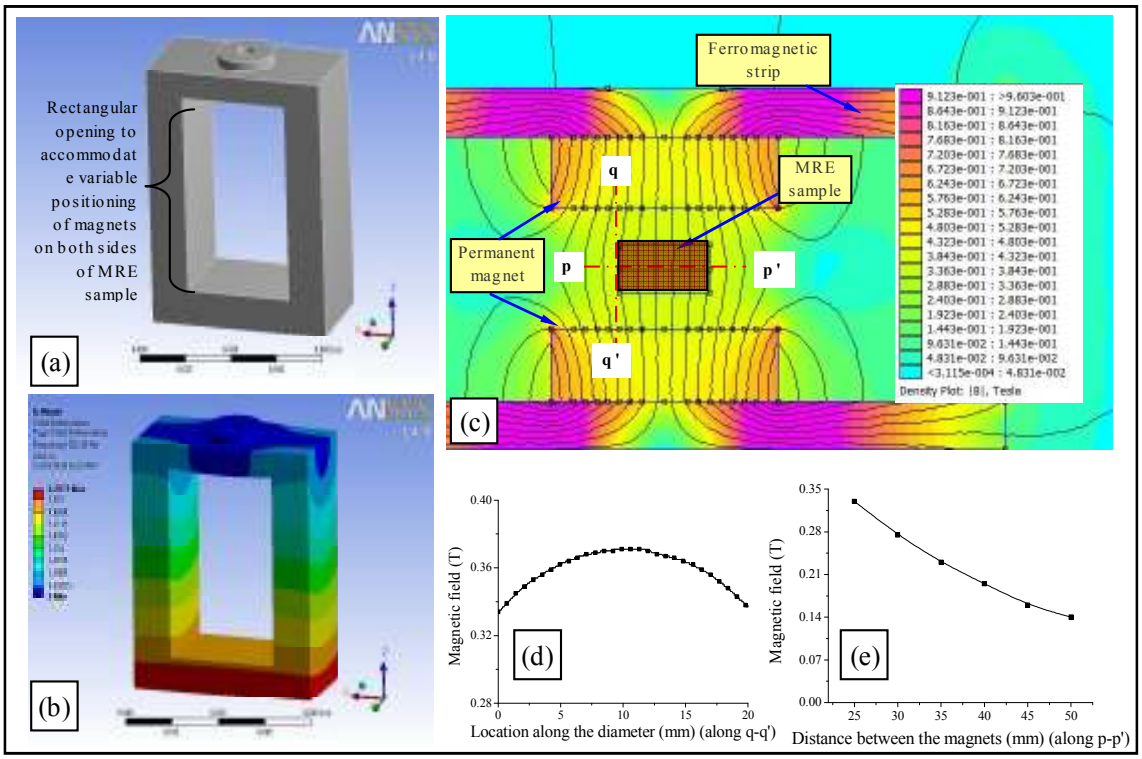

Figure 5.1 (a) 3D image of the test fixture for dynamic compression test. (b). Mode shape of test fixture corresponding to the fundamental frequency. (c) Contour plots of the magnetic field. (d) Magnetic field variation along the along the diameter of the MRE sample. (e) Magnetic field variation along the distance between the magnets.

Experiments were performed on a cylindrical shaped MRE (27 % by volume CIP and 73 % by volume RTV silicone matrix) sample with dimensions 10 mm high and 19 mm in diameter (Koo et al., 2010). The samples were prepared as per the procedure described in chapter 3. The measurement of field-induced compressive characteristics of MRE is challenging as the direction of deformation and the magnetic field are in the same direction. A customized fixture was designed with a rectangular opening to

accommodate the permanent magnets on either side of MRE. Figure 5.1a shows the 3D image of the test fixture. Modal analysis of the test fixture was performed in Ansys (ver 14) to assess the influence of its deformation on the measured properties of MRE. The results shown in Figure 5.1b indicated that the fundamental frequency of the test fixture is around 354.14 Hz, which is not likely to have an influence on the stiffness values up to 24 Hz.

The field dependent properties of MRE were tested by employing a pair of rare-earth neodymium permanent magnets (type: NdFeB 32, coercivity: 883310 A/m, and relative permeability: 1.045). A special type of test rig was designed to alter the distance between the magnets to vary the magnetic field. Magnetic flux at the opposite end of the permanent magnet was blocked by a ferromagnetic strip to enhance the magnetic field over the region occupied by MRE. Finite-Element Element Method Magnetics (FEMM) simulations were performed to analyze the magnetic field variations across the diameter (Figure 5.1c; along p-p') and along the region separated by two magnets (Figure 5.1c; along q-q'). As depicted in Figure 5.1d, variation in magnetic field from the centre to edges was within 10%. The distribution of magnetic field between the magnets at the edges of MRE was decreased with the increase in distance (Figure 5.1e). For a minimum possible separation distance of 30 mm, FEMM simulations showed 6% deviation with the actual measured values (0.27 T at the edges of sample along the line p-p').

The schematic representation and the actual image of dynamic compression property measurement experimental setup are shown in Figure 5.2a and 5.2b. Compressive properties of MRE were tested by the steady-state harmonic excitation from an electrodynamic shaker. The harmonic signals of different frequencies were

generated by a NI PXI-5412 function generator and fed to the electrodynamic shaker through a power amplifier system. Force at the blocked end was measured by a force transducer (KISTLER, type 9712). To minimize the effect of rocking motion, two identical accelerometers (KISTLER, K-shear) were used (Thompson, 1998). The sensed signals from accelerometer and force transducer were acquired through NI PXI-4496 data-acquisition system.

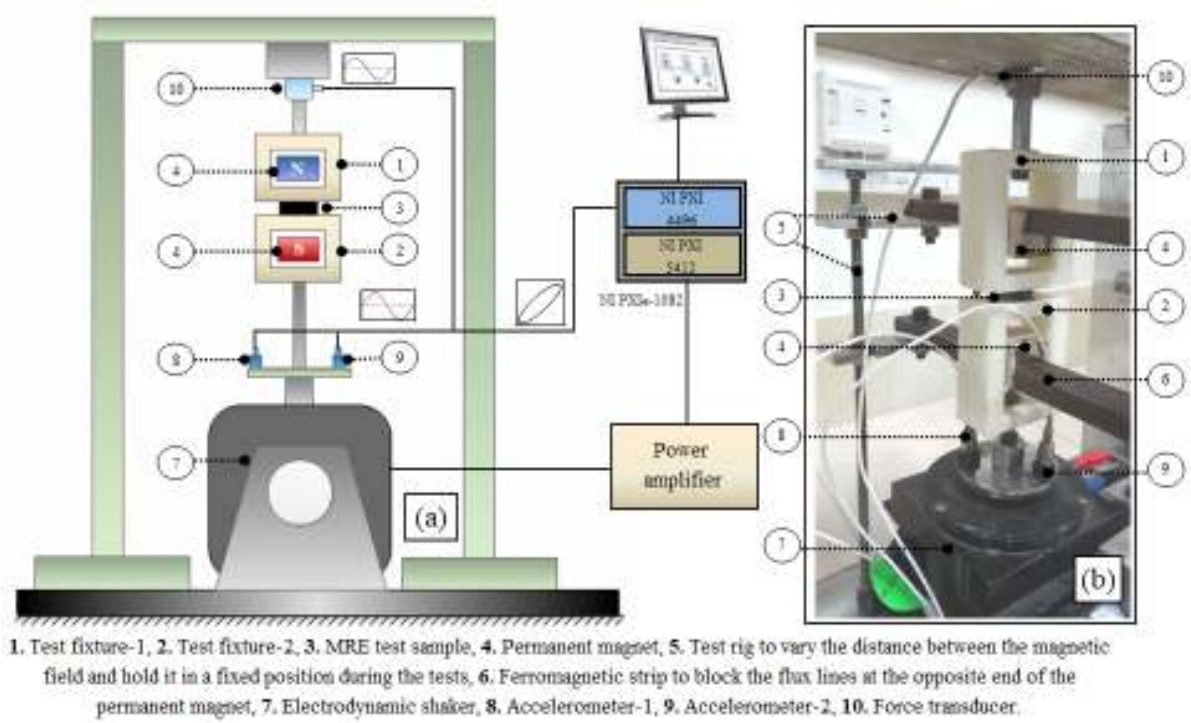

1. Test fixture-1, 2. Test fixture-2, 3. MRE test sample, 4. Permanent magnet, 5. Test rig to vary the distance between the magnetic field and hold it in a fixed position during the tests, 6. Ferromagnetic strip to block the flux lines at the opposite end of the permanent magnet, 7. Electrodynamic shaker, 8. Accelerometer-1, 9. Accelerometer-2, 10. Force transducer.

Figure 5.2. (a) Schematic representation of dynamic property measurement experimental setup. (b) Actual image of the dynamic compression property measurement apparatus.

Experiments were performed at frequencies: 8 Hz, 10 Hz, 12 Hz, 14 Hz, 16 Hz, 18 Hz, 20 Hz and 24 Hz. Influence of magnetic field was evaluated by carrying out the viscoelastic property measurement studies at different magnetic field strengths (0 T, 0.1 T, 0.2 T and 0.27 T). The frequency and magnetic field dependent properties were measured at constant strain amplitude of 0.25%. The amplitude dependent properties of MRE were evaluated at 0.5%, 1.0% and 1.5% strain. To alleviate the

effects of deformation history and stress softening on the measured viscoelastic properties, procedures discussed in the chapter 3 were implemented.

5.3 Results and discussion

Force-displacement hysteresis plots evaluated at different magnetic fields (0 T, 0.1 T, 0.2 T and 0. 27 T) corresponding to 8 Hz, 12 Hz, 16 Hz and 20 Hz are depicted in Figure 5.3a-5.3d. The slope and area of the hysteresis loop vary with the magnetic field and excitation frequency. Field-induced variation in the hysteresis behavior of MRE is associated with the interaction between the magnetically active fillers. The frequency dependency in MRE is attributed to the viscoelastic behavior, which it inherited from the elastomer matrix.

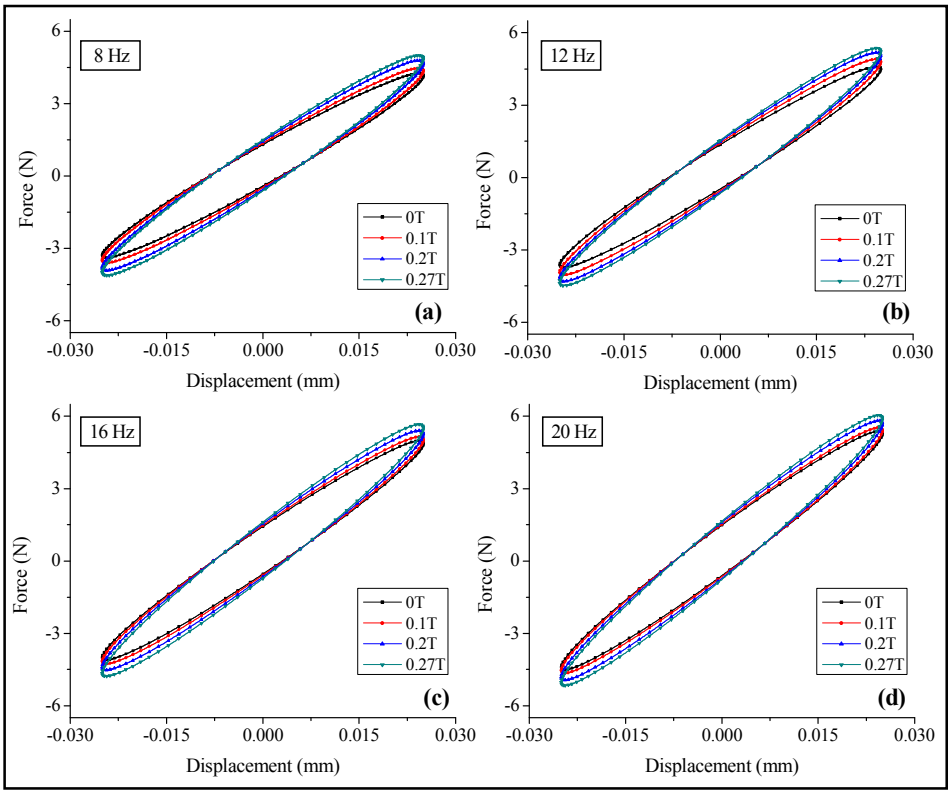

Figure 5.3. (a-d) Magnetic field dependent variation in hysteresis loop for 8 Hz, 12 Hz, 16 Hz and 20 Hz

As depicted in Figure 5.4a and 5.4b, the variation in magnetic field and frequency dependent viscoelastic properties of MRE is expressed in terms of dynamic

stiffness (K^*) and equivalent viscous damping (C). The K^* of MRE enhance with an increase in frequency, which signifies the frequency dependent stiffening behavior (Osman and Atallah, 2006). Influence of frequency on the field-induced enhancement in K^* is not pronounced. Corresponding to 8 Hz, K^* is increased by 29.6 N/mm by varying the magnetic field from 0 T-0.27 T. Similarly at 24 Hz, the field-induced enhancement in K^* is 25.63 N/mm. However, the C of MRE is decreased with an increase in frequency, indicating the reduction in damping characteristics (Hu et al., 2015). Enhancement of C with an increase in the magnetic field is sensitive to the excitation frequency. For the input frequency of 8 Hz, the C of MRE is increased by 0.688 Ns/mm as the magnetic field is varied from 0 T-0.27 T. The corresponding enhancement in C at 24 Hz is 0.192 Ns/mm.

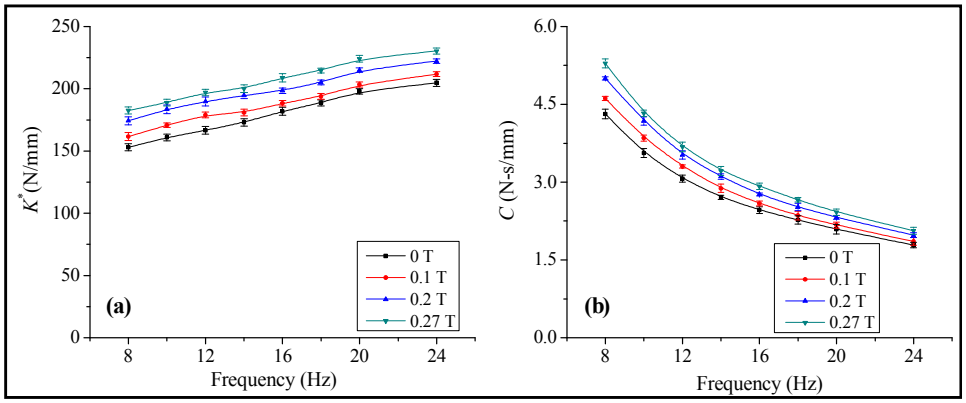

Figure 5.4 Magnetic field and frequency dependent variation in K^* and C of MRE

The amplitude dependent compression behavior of MRE is evaluated by varying the amplitude of harmonic excitation at constant frequency and magnetic field. Figure 5.5(a-d) represents the amplitude dependent hysteresis behavior of MRE corresponding to 8 Hz and 16 Hz. As evident from the graph, with an increase in amplitude, the slope of the hysteresis loop decreases and the area of the hysteresis loop increases. This indicates the phenomenon of Payne effect as discussed in chapter 4.

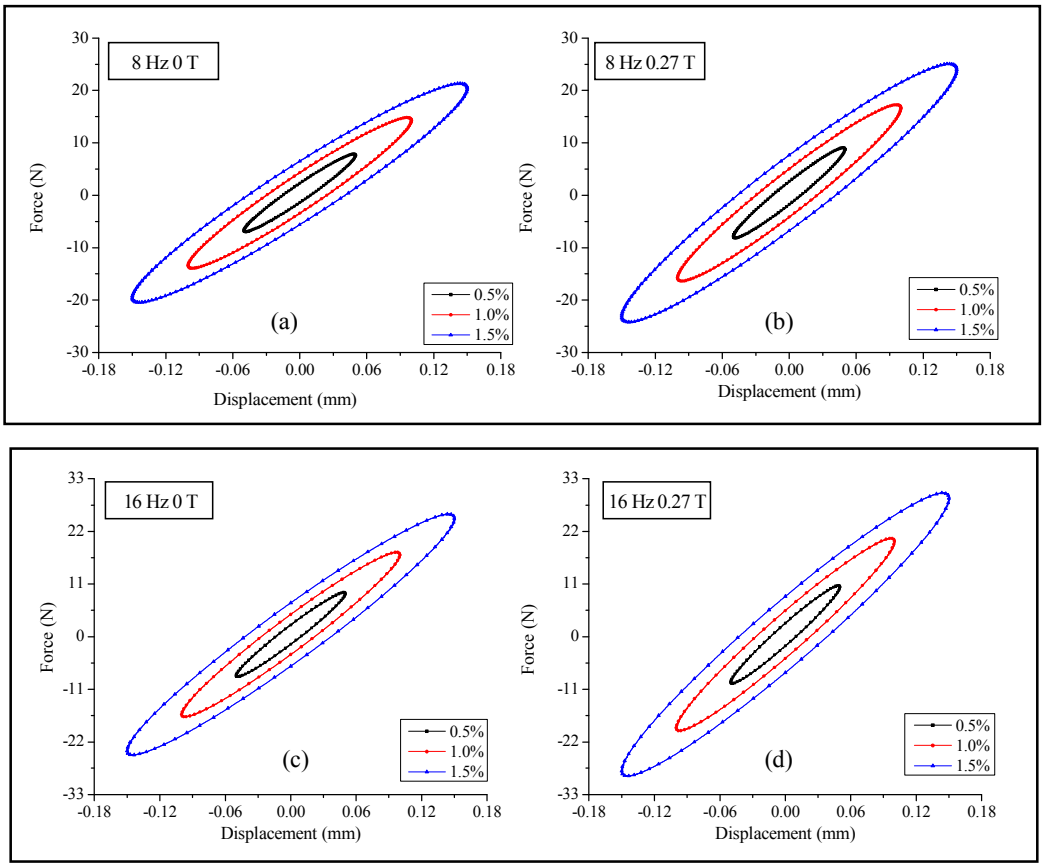

Figure 5.5 Amplitude dependent variation in hysteresis loop corresponding to 8 Hz and 16 Hz at 0 T and 0.4 T magnetic field.

The dynamic test results revealed the existence of magnetic field, frequency and the strain dependent viscoelastic properties of MRE under compression mode. In order to describe these effects simultaneously, a mathematical formulation of the material behavior is essential. The material modeling approaches simplify the material property characterization studies by eliminating the costlier and time consuming data collection processes.

5.4 Summary

In this chapter, the dynamic properties of MRE were experimentally evaluated to develop a mathematical representation of the compression properties of MRE. The dynamic blocked transfer stiffness method was adopted to evaluate the viscoelastic

properties. MRE test sample was attached to a special type of fixture and pair of permanent magnets was used to provide the testing magnetic field. Modal characteristics of the fixture was studied to assess the effect of fixture compliance on the measured properties of MRE and the FEMM analysis was carried out to evaluate the field variation in the region occupied by MRE. The results revealed that like shear mode, the properties of MRE under compression are also sensitive to the magnetic field, frequency and input strain.

CHAPTER 6

VISCOELASTIC MODELLING OF FREQUENCY AND MAGNETIC FIELD INDUCED PROPERTIES OF MAGNETPORHEOLOGICAL ELASTOMER

6.1 Introduction

Material behavior of MRE is represented by adopting the phenomenological modeling approaches based on viscoelastic constitutive relations. These models are developed within the framework of a spring and a dashpot, which can simultaneously describe the magnetic field and frequency dependent behavior. As discussed in chapter 2, the type of modeling elements has a significant influence on the predictive accuracy over a broad-band frequency. Both integer and fractional order based models can effectively predict the behavior over wide frequencies, but the fractional order based models require lesser parameters.

In this chapter, modeling approaches to describe the field-induced compressive properties of MRE for the frequency range from 8 Hz to 24 Hz are presented. Two types of modeling techniques namely, integer and fractional derivative order are proposed. Integer order based model comprises of two Maxwell elements with six parameters, and fractional order model includes a total of five parameters. MATLAB optimization tool box is used to obtain the parameters of these models. An equally spaced frequency interval of 4 Hz, 8 Hz and 16 Hz is chosen to evaluate the ability of the models in predicting the broad-band viscoelastic behavior. The parameters at the intermediate frequencies are described by an interpolation function, which is used to evaluate the ability of the model in reproducing the experimental results.

6.2 Viscoelastic material modeling

A general relationship between the force and displacement in a viscoelastic material under the harmonic loading is expressed as (Özkaya and Nordin, 2006),

$$F = f\left(x, \frac{dx}{dt}\right) \tag{6.1}$$

Above equation states that, the force F in a viscoelastic material is not only a function of input displacement, but also depends on the displacement rate dx/dt ; where, t is the time.

6.2.1 Modeling components for viscoelastic behavior

This section deals with the basic viscoelastic modeling elements used to portray the viscoelastic material behavior. The physical representation and the fundamental equations describing these modeling components are briefly discussed and its response under a harmonic loading is also addressed.

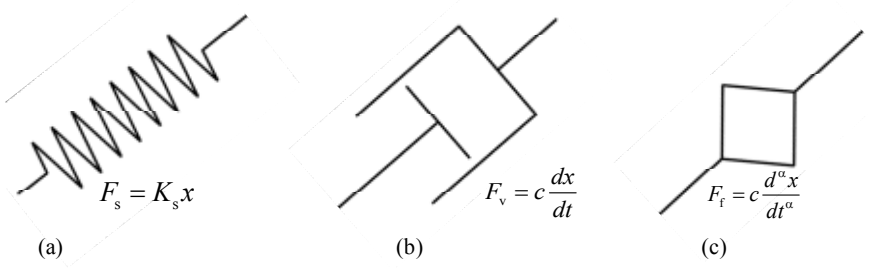

Figure 6.1. MRE viscoelastic behavior modeling components (a) Spring element. (b) Dashpot element. (c) Spring-pot element

6.2.1.1 Elastic spring

The spring element (Figure 6.1a) represents the basic modeling element which constitutes the elastic part of a viscoelastic model. It describes the instantaneous recovery of the deformation upon removing the external load (Berg, 1997).

The relation between the input displacement and the elastic force F_s is given by,

$$F_s = K_s x \tag{6.2}$$

The relationship between force amplitude F_{s0} and harmonic displacement, $x=x_0e^{i\omega t}$, in a spring element of stiffness K_s is represented as,

$$F_{s0} = K_s x_0 \tag{6.3}$$

where, x_0, ω and t are displacement amplitude, excitation frequency and time respectively.

6.2.1.2 Viscous dashpot

The dissipative behavior in a viscoelastic material is represented by a linear viscous dashpot shown in Figure 6.1b. The viscous force F_v developed by a dashpot does not depend on the displacement rather it is a function of the rate of deformation (Berg, 1997). In the mathematical form, dissipative force experienced by a viscous dashpot is given by,

$$F_v = c\dot{x} \tag{6.4}$$

For a harmonic displacement excitation $x=x_0e^{i\omega t}$, a delay exists between the force and displacement in a dashpot, which represents the phase difference. This result in an elliptical shaped force-displacement plot, and the corresponding amplitude of viscous force F_{v0} is given by,

$$F_{v0} = ic\omega x_0 \tag{6.5}$$

6.2.1.3 Spring-pot

Spring-pot element is a modified form of the dashpot element, where the viscoelastic constitutive relations are described as a fractional time derivatives rather than the regular integer order derivative (Bagley and Torvik, 1983; Makris and Constantinou, 1991). The mathematical form of force-displacement relation in a spring-pot element is given by (Berg and Kari, 2003),

$$F_f = c\frac{d^\alpha x}{dt^\alpha} \tag{6.6}$$

where, F_f is the force acting on the spring pot, c and α are the parameters of the fractional model. The derivative d^α/dt^α denotes a fractional time derivative of the order α. The spring-pot element is effective in approximating the damping characteristics of a viscoelastic material, which is neither linearly dependent on frequency nor frequency independent (Hu et al., 2011b). The spring-pot concept can be conceived by an interpolation between a purely viscous and a purely elastic behavior, which occupies the intermediate range with a fractional order between zero and one.

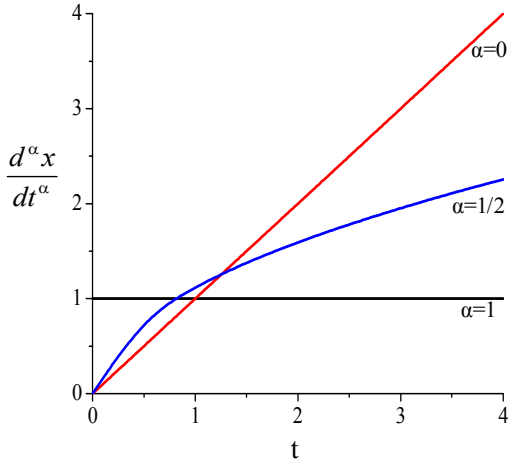

Figure 6.2. Comparison between the derivatives of the order 0, 0.5 and 1.

Compared to an integer order, the fractional order derivative offers a wide range to model the continuous variation in the rate of change of viscoelastic behavior. Figure 6.2 shows a comparison between the variation of first derivative and a half derivative. The fractional order derivative falls between the closest integer order derivatives which allows a smoother variation to monitor the damping characteristics (Shahsavari and Ulm, 2009).

6.2.2 Empirical models of viscoelasticity

The ideal elastic and viscous behavior of a material is represented by spring and dashpot respectively. Correspondingly, a combination of these elements yields

different viscoelastic relations that could be employed to simulate the viscoelastic behavior of materials. The structure of basic viscoelastic models and the response under complex loading are briefly discussed below.

6.2.2.1 Kelvin–Voigt Model

The simple empirical model obtained by the parallel arrangement of a spring and a dashpot is called Kelvin-Voigt model (Riande et al., 2000). This configuration results in a same deformation in both elements as shown in Figure 6.3. Total force, F_{KV} applied to the entire system is the sum of the forces in spring and dashpot (Özkaya and Nordin, 1998).

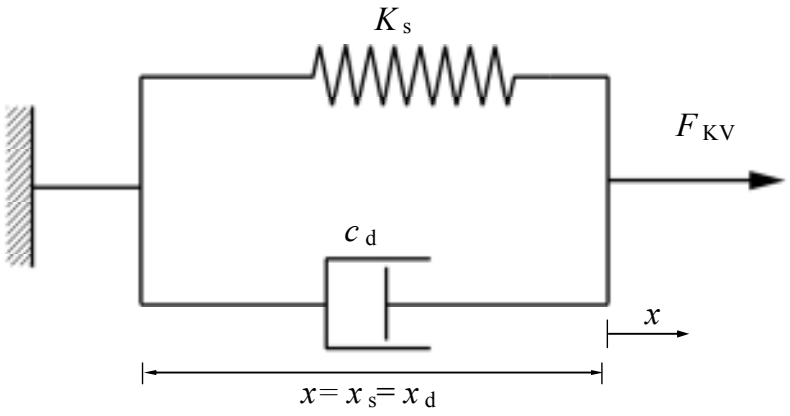

Figure 6.3. Kelvin-Voigt model

The governing equation of the Kelvin-Voigt model is given by,

$$F_{\mathrm{KV}}(t) = K_s x(t) + c_d \frac{dx(t)}{dt} \tag{6.7}$$

where, K_s is the stiffness of the spring element and c_d is the damping constant of the dashpot. The response of the Kelvin-Voigt model under harmonic displacement is expressed in terms of the complex stiffness K_{KV}^* as,

$$K_{\mathrm{KV}}^* = \frac{F_{KV}}{x(t)} = K + ic\omega \tag{6.8}$$

6.2.2.2 Maxwell Model

The arrangement of spring and dashpot in a series configuration results in an empirical relation referred to as Maxwell model (Riande et al., 2000). As represented in Figure 6.4, under quasi-static deformation, by neglecting the inertial effects, the force experienced by the both elements is same (Özkaya and Nordin, 1998).

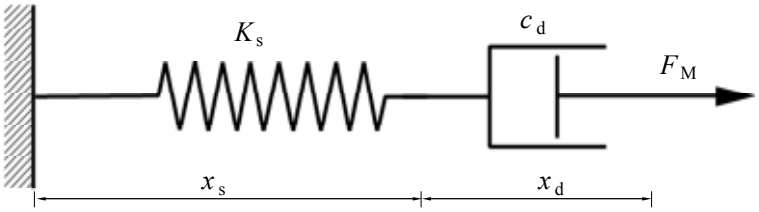

Figure 6.4. Maxwell Model

The resulting deformation is the sum of the deformations in spring and the dashpot. The force (F_M) and displacement relation in a Maxwell model are expressed as,

$$\frac{dx(t)}{dt} = \frac{1}{K_s}\frac{dF_M(t)}{dt} + \frac{F_M}{c_d} \tag{6.9}$$

where, K_s is the stiffness of the spring element and c_d is the damping constant.

The complex stiffness K_M^* of the system under harmonic loading is given by,

$$K_M^* = \frac{F_M}{x(t)} = \frac{i\omega c_d K_s}{K_s + i\omega c_d} \tag{6.10}$$

$$K_M^* = \frac{\omega^2 c_d^2 K_s}{K_s^2 + \omega^2 c_d^2} + i\frac{\omega c_d K_s^2}{K_s^2 + \omega^2 c_d^2} \tag{6.11}$$

6.2.3 Standard Linear Solid Models (SLS)

The Kelvin–Voigt and Maxwell are the basic viscoelastic models constructed by connecting spring and dashpot in parallel and series configurations respectively. However, these models are not effective in representing the viscoelastic behavior of a real engineering material. To some extent, these deficiencies can be overcome by arranging a spring in series with the Kelvin-Voigt unit or placing a spring parallel

with the Maxwell, which is referred to as Poynting-Thomson and Zener form of SLS respectively (Riande et al., 2000; Özkaya and Nordin, 1998).

6.2.3.1 Zener model

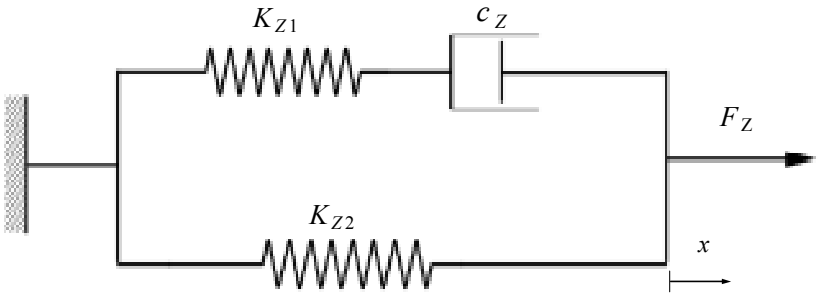

Figure 6.5. Standard Linear Solid model - Zener model

Zener model is a three parameter SLS comprising of a Maxwell element in parallel with a spring element (Lakes, 2009). As depicted in Figure 6.5, this arrangement results in the same deformation in Maxwell and the spring element. The governing equation which defines the force-displacement relation is given by,

$$c_Z \frac{dF_z(t)}{dt} + K_{Z2}F_z(t) = c_Z\left(K_{Z1} + K_{Z2}\right)\frac{dx(t)}{dt} + K_{Z1}K_{Z2}x(t) \tag{6.12}$$

Where, F_z is the net force acting on the model, K_{Z1} and K_{Z2} are the spring elements and c_Z is the viscous damping coefficient.

The complex stiffness K_Z^* of the Zener model under harmonic loading is given by,

$$K_Z^* = \frac{K_{Z1}^2K_{Z2} + \left(K_{Z1} + K_{Z2}\right)\omega^2c_Z^2}{K_{Z1}^2 + \omega^2c_Z^2} + i\frac{\omega c_Z K_{Z1}^2}{K_{Z1}^2 + \omega^2c_Z^2} \tag{6.13}$$

6.2.3.2 Poynting Thomsons model

The modified version of Zener model is the Poynting-Thomson (PT) model (Riande et al., 2000). This model comprises of a Kelvin-Voigt unit in series with a spring element (Figure 6.6). Total load acting on the spring element is same as that of Maxwell element. The governing differential equation of the system is obtained from the resultant deformation in the system, which is the sum of the deformation in the

spring element and Kelvin-Voigt unit. The force-displacement relation in a PT model is expressed as,

$$(K_{P1} + K_{P2})F(t) + c_P \frac{dF_{PT}(t)}{dt} + = K_{P1}K_{P2}x(t) + K_{P1}c_P \frac{dx(t)}{dt} \tag{6.14}$$

Where, F_{PT} is the net force acting on the model, K_{P1} and K_{P2} are the spring elements and c_P is the viscous damping coefficient.

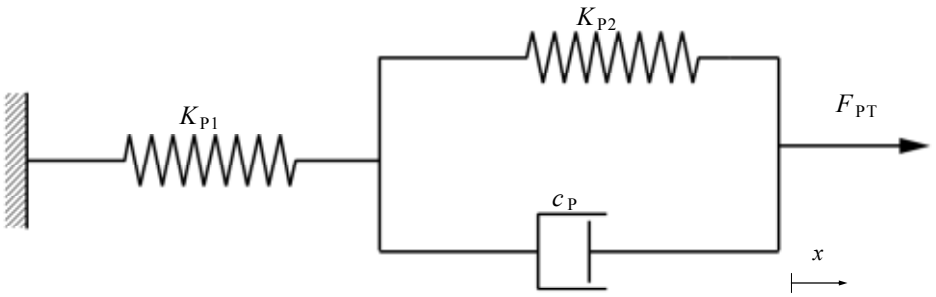

Figure 6.6. Standard Linear Solid model - Poynting Thomson

The complex stiffness K_P^* of the PT model under harmonic loading is given by,

$$K_P^* = \frac{K_{P1}K_{P2}\left(K_{P1} + K_{P2}\right) + K_{P1}\omega^2 {c_P}^2}{\left(K_{P1} + K_{P2}\right)^2 + \omega^2 {c_P}^2} + i\frac{\left(K_{P1} + K_{P2}\right)K_{P1}\omega c_P - K_{P1}K_{P2}\omega c_P}{\left(K_{P1} + K_{P2}\right)^2 + \omega^2 {c_P}^2} \tag{6.15}$$

6.3 Proposed models for MRE

The viscoelastic behavior of MRE is modeled by employing the basic viscoelastic relations discussed in section 6.2. Combination of these elements coupled with the field-induced characteristics yield different configurations of MRE models. In the proposed study, material models based on integer order and fractional order viscoelastic constitutive relations are developed. The integer order based model is referred to as 2-Maxwell model and the fractional order model is termed as fractional Maxwell model. The 2-Maxwell model compromises of a total of six parameters. Damping characteristic in the model is addressed by two Maxwell elements connected in parallel. An elastic spring and a magnetic spring element are connected in parallel

with the Maxwell elements to incorporate elastic and magnetic characteristics. The fractional Maxwell model of MRE comprises of a fractional Maxwell element connected in parallel with spring and magnetic element. The fractional Maxwell element describes the damping characteristics. Stiffness and field sensitive characteristics are addressed by elastic and magnetic springs respectively.

6.3.1 2-Maxwell element model

The configuration of 2-Maxwell MRE model is represented in the Figure 6.7. This model comprises of a total of six parameters K_{sm}, K_1, c_1, K_2, c_2 and K_B. Parameter K_{sm} represents the stiffness of the spring element, which simulates the elastic behavior of the model. The coefficients of Maxwell element are denoted by K_1, c_1, K_2, c_2 and parameter K_B represents the field sensitive characteristics.

Proposed MRE model is one dimensional, and its response depends on the contribution of elastic spring force (F_e), viscous force (F_v) and magnetic force (F_m) (Berg et al., 1997; Chen and Jerrams, 2011). Cumulative contribution of these forces yield the total force F_{2m} as,

$$F_{2m} = F_e + F_v + F_m \tag{6.16}$$

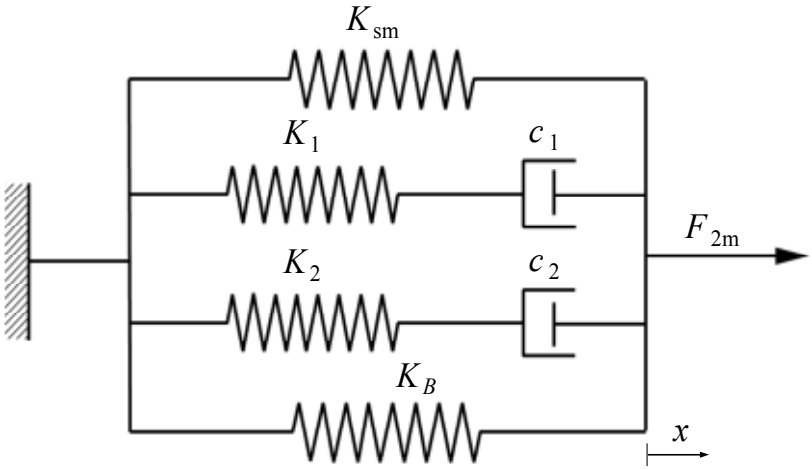

Figure 6.7. 2-Maxwell MRE model.

6.3.1.1 Elastic force

Elastic force in MRE is due to the stiffness of the polymer matrix. The elastic force associated with the stiffness K_{sm}, for the input harmonic displacement x is given by,

$$F_s = K_{sm} x \tag{6.17}$$

6.3.1.2 Viscous force

Rate dependent characteristics are incorporated in the model by the Maxwell elements. The parallel arrangement with the elastic spring results in the same deformation in Maxwell elements. Mathematical expression for the total viscous force (F_v) due to Maxwell elements (Lijun et al., 2010) is,

$$F_v = \left(\begin{array}{l} \left(\dfrac{K_1 (\omega c_1)^2}{(K_1)^2 + (\omega c_1)^2} + \dfrac{K_2 (\omega c_2)^2}{(K_2)^2 + (\omega c_2)^2} \right) + \\ i \left(\dfrac{\omega c_1 (K_1)^2}{(K_1)^2 + (\omega c_1)^2} + \dfrac{\omega c_2 (K_2)^2}{(K_2)^2 + (\omega c_2)^2} \right) \end{array} \right) x \tag{6.18}$$

6.3.1.3 Magnetic force

The field-induced diploe interactions between the ferromagnetic fillers impart field sensitive characteristics to MRE. These attributes are incorporated to the model by the inclusion of dipole interaction between the adjacent particles in a chain (Jolly et al., 1996). A schematic representation of a pair of fillers in MRE unit cell is shown in Figure 6.8. Under magnetic field, these particles are approximated as magnetic dipoles with a dipole moment m (Dong et al., 2012).

According to magnetic dipole theories, the interaction energy between two magnetic dipoles $\vec{m}_1$ and $\vec{m}_2$ separated by a distance $\vec{r}$ is as follows (Furst and Gast, 2000),

$$U = \frac{1}{4\pi r^3 \mu_1 \mu_0} \left[(\vec{m}_1 \cdot \vec{m}_2) - 3 (\hat{r} \cdot \vec{m}_1)(\hat{r} \cdot \vec{m}_2) \right] \tag{6.19}$$

where, μ_0 is the permeability of vacuum, μ_1 is the relative permeability of the elastomer matrix.

Simplified expression for interaction energy between any two dipoles of equal strength *m* and for the direction of deformation along the applied magnetic field (θ=0) is,

$$U = \frac{-m^2}{2\pi r^3 \mu_1 \mu_0} \tag{6.20}$$

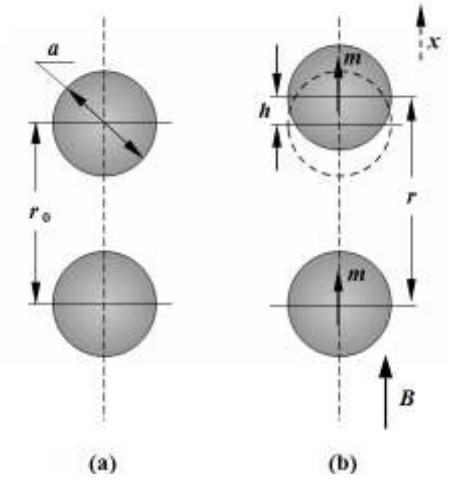

Figure 6.8. (a) Geometry of two particles of diameter *a* within a particle chain. (b) Magnetic interaction between two particles approximated as dipole moments m shared with respect to one another.

The dipole moment acquired by each ferromagnetic filler under the influence of magnetic field is (Spaldin, 2011),

$$m = \mu_0 VM \tag{6.21}$$

where, *V* is the volume of the iron particles, and *M* is the saturation magnetization. The relation between the magnetic induction *B* and magnetization *M* is (Spaldin, 2011),

$$M = DB \tag{6.22}$$

where, $D = \chi/(\mu_0(1+\chi)$ and χ is the susceptibility of the iron particles.

The deformation h, in a MRE unit cell (Figure 6.8b) is (Liao et al., 2012),

$$h = r - r_0 \tag{6.23}$$

The magnetic force of interaction between the fillers under an external deformation in a unit cell is expressed as (Shen et al., 2004; Liao et al., 2012),

$$F = -\frac{dU}{dh} = -\frac{dU}{dr}\ \frac{dr}{dh} \tag{6.24}$$

Upon simplification, the magnetic field-induced force between two fillers is expressed as,

$$F = \frac{3m^2}{2\pi r^4 \mu_1 \mu_0} \tag{6.25}$$

The total contribution of magnetic force, F_{m} in MRE is calculated by including the interactions between n number of particles (Shen et al., 2004; Jolly et al., 1996) is,

$$F_{\mathrm{m}} = \frac{\phi V_t 3m^2}{2\pi r^4 \mu_1 \mu_0 V} \tag{6.26}$$

where, ϕ is the percentage by volume of CIP and V_{t} is the volume of MRE sample. From equation 6.21 and 6.22 , the relation between the magnetic force F_{m} and the magnetic induction B is expressed as,

$$F_{\mathrm{m}} = K_{\mathrm{B}} B^2 \tag{6.27}$$

where, $K_{\mathrm{B}} = \dfrac{\phi V_t^3 \mu_0 V D^2}{2\pi r^4 \mu_1}$

6.3.1.4 Total force

In the linear viscoelastic regime, the elastic, viscous and magnetic forces are superimposed according to equation (6.16) to give the total force in the model. Contribution of these forces on total force $F_{2\mathrm{m}}$ is expressed as (Berg et al.,1997),

$$F_{2\mathrm{m}} = \left(K_{\mathrm{sm}} x + \left(\frac{K_1 (\omega c_1)^2}{(K_1)^2 + (\omega c_1)^2} + \frac{K_2 (\omega c_2)^2}{(K_2)^2 + (\omega c_2)^2} \right) x + K_{\mathrm{B}} B^2 \right) + i \left(\left(\frac{\omega c_1 (K_1)^2}{(K_1)^2 + (\omega c_1)^2} + \frac{\omega c_2 (K_2)^2}{(K_2)^2 + (\omega c_2)^2} \right) x \right) \tag{6.28}$$

The ratio of force and the input displacement yields the dynamic stiffness of the 2-Maxwell model $K_{2\mathrm{m}}^*$ as (Berg et al., 1997; Nadeau and Champoux, 2000),

$$K_{2\mathrm{m}}^* = \frac{F_{2\mathrm{m}}}{x} = K_{2\mathrm{m}}^{'} + iK_{2\mathrm{m}}^{''} \tag{6.29}$$

The steady state force-displacement response of the 2-Maxwell model for an input the harmonic displacement of $x=x_0 e^{i\omega t}$ is given by,

$$F_{2\mathrm{m}} = \left| K_{2\mathrm{m}}^* \right| x_0 e^{i(\omega t + \delta_{\mathrm{m}})} \tag{6.30}$$

where, δ_{m} is the phase difference between the force and the displacement, which is expressed as,

$$\delta_{\mathrm{m}} = \tan^{-1} \left(\frac{\left(\left(\frac{\omega c_1 (K_1)^2}{(K_1)^2 + (\omega c_1)^2} + \frac{\omega c_2 (K_2)^2}{(K_2)^2 + (\omega c_2)^2} \right) \right)}{\left(K_{\mathrm{sm}} + \left(\frac{K_1 (\omega c_1)^2}{(K_1)^2 + (\omega c_1)^2} + \frac{K_2 (\omega c_2)^2}{(K_2)^2 + (\omega c_2)^2} \right) + \frac{K_{\mathrm{B}} B^2}{x_0} \right)} \right) \tag{6.31}$$

6.3.2 Fractional Maxwell model

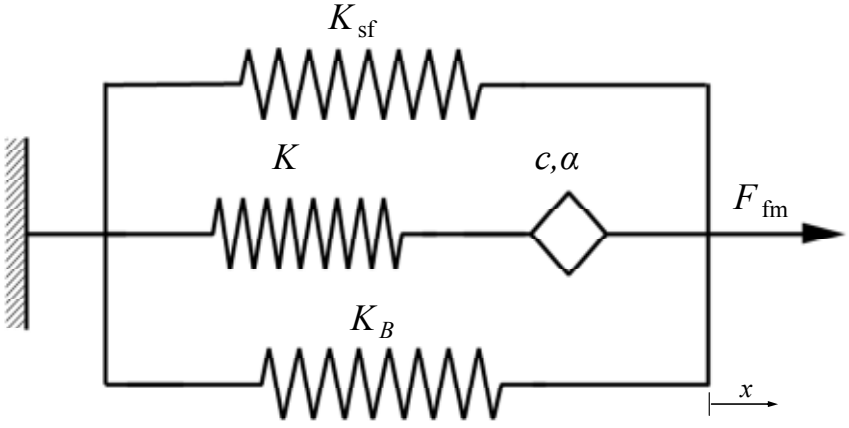

Figure 6.9. Fractional Maxwell MRE model

The fractional derivative based MRE model is represented in the Figure 6.9. This model comprises of a total of five parameters. The parameter K_{sf} represents the stiffness of the spring element and the field sensitive characteristic of the model is represented by parameter K_B. Stiffness of fractional Maxwell chain is denoted by K and the parameters c and α are the coefficients of fractional dashpot.

The superposition of elastic force, viscous force and the magnetic forces gives the total force F_{fm} as,

$$F_{fm} = F_e + F_{fv} + F_m \tag{6.32}$$

where, F_e, F_{fv} and F_m are the elastic, viscous and magnetic force respectively. The elastic and magnetic forces in the model are similar to the forces discussed in section 6.3.1.

Viscous force is derived from the force-displacement relations in a fractional Maxwell element. This element comprises of a spring and Scott–Blair dashpot connected in series (Xu and Chen, 2013; Lewandowski and Chorazyczewski, 2010). This configuration results in an equal force in spring and the spring-pot element. The total deformation of fractional Maxwell chain is the sum of deformation in the spring-pot and the elastic spring.

Force-displacement relations in spring and spring-pot of a fractional Maxwell chain is expressed as (Xu and Chen, 2013; Lewandowski and Chorazyczewski, 2010),

$$F_{fs} = Kx_{fs}(t),\ F_v = c\frac{d^{\alpha}x_{fv}(t)}{dt^{\alpha}} (0 \le \alpha \le 1) \tag{6.33}$$

$$x(t) = x_{fs}(t) + x_{fv}(t),\quad F_{fv} = F_{fs} = F_v \tag{6.34}$$

where, F and x denotes the force and displacements respectively. The subscript fs represent the spring and subscript v denotes the dashpot.

The differential equation relating the force, F_{fv} and displacement in a fractional Maxwell element is,

$$F_{fv}(t)+\frac{c}{K}\frac{d^{\alpha}}{dt^{\alpha}}\left(F_{fv}(t)\right)=c\frac{d^{\alpha}}{dt^{\alpha}}\left(x(t)\right) \tag{6.35}$$

Under linear regime, harmonic input displacement $x=x_0e^{i\omega t}$ results in an output harmonic force with a phase difference.

The complex modulus of the equation is derived by transforming time domain equation into the frequency domain by using the relation (Bagley and Torvik, 1983),

$$F\left[\frac{d^{\alpha_i}}{dt^{\alpha_i}}x(t)\right]=(i\omega)^{\alpha}x(t) \tag{6.36}$$

The relation between force and displacement of a fractional Maxwell chain in the frequency domain is,

$$\left(F_{fv}(t)\right)=\frac{Kc(i\omega)^{\alpha}\left(x(t)\right)}{\left(K+c(i\omega)^{\alpha}\right)} \tag{6.37}$$

After introducing the relation $i^{\alpha}=\cos(\alpha\pi/2)+i\sin(\alpha\pi/2)$, the modified form of force displacement relation is,

$$F_{fv}=\left(\begin{array}{l}\dfrac{Kc\omega^{\alpha}\left(c\omega^{\alpha}+K\cos\,\alpha\pi/2\right)}{(K)^2+(c\omega^{\alpha})^2+2c\omega^{\alpha}K\cos\,\alpha\pi/2}+\\ i\dfrac{K^2c\omega^{\alpha}\sin\alpha\pi/2}{(K)^2+(c\omega^{\alpha})^2+2c\omega^{\alpha}K\cos\,\alpha\pi/2}\end{array}\right)x \tag{6.38}$$

6.3.2.1 Total force response of fractional Maxwell model

Using equation 6.32, the expression for total force is given by,

$$F_{\mathrm{fm}} = \left(K_{\mathrm{sf}} x + \left(\frac{Kc\omega^{\alpha}\left(c\omega^{\alpha} + K\cos\,\alpha\pi/2\right)}{(K)^2 + (c\omega^{\alpha})^2 + 2c\omega^{\alpha}K\cos\,\alpha\pi/2} \right) x + K_{\mathrm{B}}B^2 \right) + i\left(\left(\frac{K^2 c\omega^{\alpha}\sin\alpha\pi/2}{(K)^2 + (c\omega^{\alpha})^2 + 2c\omega^{\alpha}K\cos\,\alpha\pi/2} \right) x \right) \tag{6.39}$$

The dynamic stiffness K_{fm}^{*} of the fractional Maxwell model is given by the ratio of total force to the displacement is,

$$K_{\mathrm{fm}}^{*} = K_{\mathrm{fm}}^{'} + iK_{\mathrm{fm}}^{''} = \frac{F_{\mathrm{fm}}}{x} \tag{6.40}$$

The steady-state force-displacement response of fractional Maxwell model for the harmonic strain $x=x_0e^{i\omega t}$ is given by,

$$F_{\mathrm{fm}} = \left| K_{\mathrm{fm}}^{*} \right| x_0 e^{i(\omega t + \delta_{\mathrm{f}})} \tag{6.41}$$

where, δ_{f} is the phase difference between the force and the displacement, which is given by,

$$\delta_{\mathrm{f}} = \tan^{-1}\left(\frac{\left(\left(\frac{K^2 c\omega^{\alpha}\sin\alpha\pi/2}{(K)^2 + (c\omega^{\alpha})^2 + 2c\omega^{\alpha}K\cos\,\alpha\pi/2} \right) \right)}{\left(K_{\mathrm{sf}} + \left(\frac{Kc\omega^{\alpha}\left(c\omega^{\alpha} + K\cos\,\alpha\pi/2\right)}{(K)^2 + (c\omega^{\alpha})^2 + 2c\omega^{\alpha}K\cos\,\alpha\pi/2} \right) + \frac{K_{\mathrm{B}}B^2}{x_0} \right)} \right) \tag{6.42}$$

6.4 Parameter identification

The performances of the proposed models are evaluated based on the accuracy in reproducing the experimental results. The parameters of each model are identified by minimizing the least square error between the measured and the predicted force from the dynamic model as represented in Figure 6.10 (Li et al., 2010b). The objective function, which optimizes the parameters of 2-Maxwell and fractional Maxwell MRE model are given by,

$$J_{2M} = \sum_{i=1}^{N} \left(Fm_{2m}(i) - F_e(i) \right)^2 \tag{6.43}$$

$$J_{FM} = \sum_{i=1}^{N} \left(Fm_{fm}(i) - F_e(i) \right)^2 \tag{6.44}$$

where, J_{2M} and J_{FM} are the objective functions for 2-Maxwell and fractional Maxwell model respectively, and N is the number of different experimental data of one loop. F_{2m} and F_{fm} are the compression forces given by equations 6.30 and equation 6.41 respectively and F_e represents the experimentally measured force response.

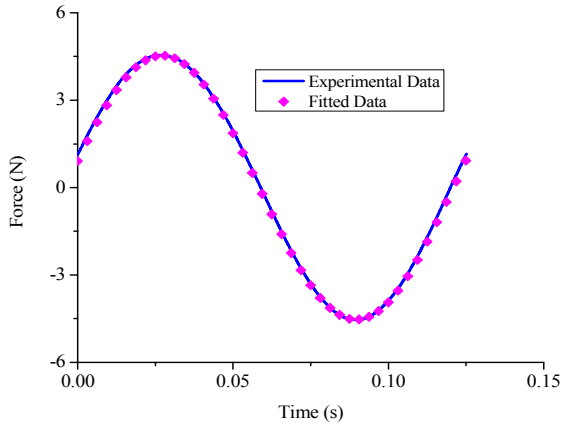

Figure 6.10. Force vs time graph showing the experimentally and fitted force values.

The proposed modeling approach aims at developing a generalized mathematical relation to portray the magnetic field (from 0 T - 0.27 T) and the frequency (between 8 Hz -24 Hz) dependent properties of MRE. A comparison is made between the 2-Maxwell and fractional Maxwell model by generalizing the variation of parameters with respect to frequency and magnetic field. The ability of the model to capture the viscoelastic behavior over a broader frequency spectrum is evaluated using three different sets of input data referred to as 2 point, 3 point and 5 point. The details of input data are listed in Table 6.1.

Two types of interpolating functions are chosen; linear and quadratic in magnetic field (B) and frequency (f). Selection of an interpolating function is based on

the variation of a particular parameter with respect to B and f. The generalized expression representing the variation of a parameter is given by,

$$Y = a_0 + a_1 B + a_2 f + a_3 B^2 + a_4 f^2 + a_5 B f \quad (6.45)$$

where, Y is the parameter of the model and a_0, a_1, a_2, a_3, a_4 and a_5 are the coefficients of generalized expression. The details of the interpolation function and the procedure to estimate the parameters of target frequency for 2-Maxwell and fractional Maxwell model are discussed in the following section.

Table 6.1. Input frequency and the target frequency

Modeling approach	Input frequency data	Input frequency	Target frequency
2-Maxwell and fractional Maxwell	2 Point	8Hz and 24 Hz	10 Hz, 12 Hz, 14 Hz,16 Hz and 20 Hz
	3 Point	8 Hz, 16 Hz and 24 Hz	10 Hz, 12 Hz, 14 Hz and 20 Hz
	5 Point	8 Hz, 12 Hz, 16 Hz, 20 Hz and 24 Hz	10 Hz, 14 Hz and 18 Hz

6.4.1 Parameters of 2-Maxwell MRE model

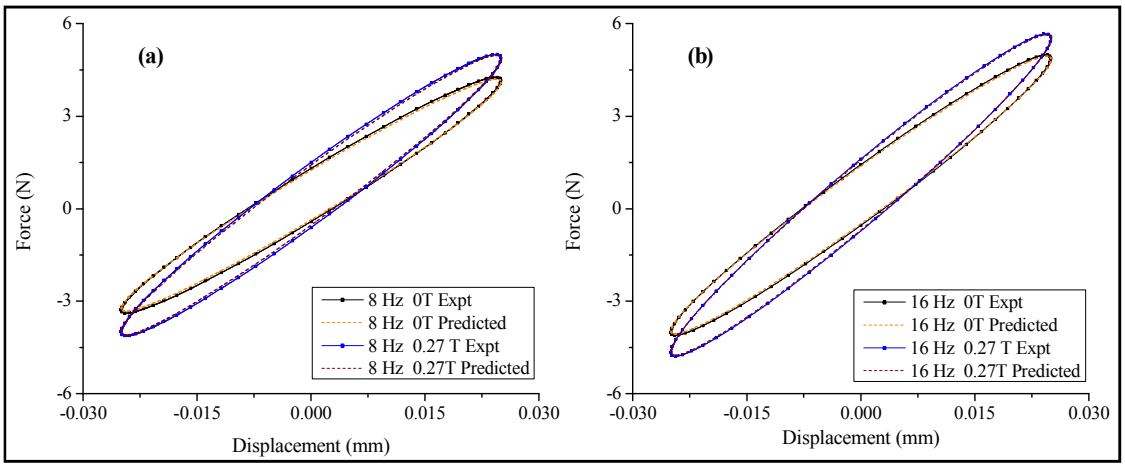

Figure 6.11. (a-b) Force-displacement hysteresis loops corresponding to experimental and fitted data for 8 Hz and 16 Hz at 0 T and 0.27 T.

Parameters of 2-Maxwell MRE model determined by minimizing the errors in equation 6.43 are listed in the table 6.2. Figure 6.11 shows a comparison between the

experimental results and the fitted data with optimized parameters corresponding to 8 Hz and 16 Hz evaluated at 0 T and 0.27 T.

The parameters of 2-Maxwell model are sensitive to B and f, and its variation in 3D space with respect 2 point, 3 point and 5 point input are depicted in Figure 6.12 - 6.14 (a-f). These variations are described by an interpolation function according to the equation 6.45. For 2 point input, all parameters are described by a 2D linear interpolation function (first 3 terms of equation 6.45). Corresponding to 3 point and 5 point input, the parameters K_2 and c_1 are expressed by 2D quadratic interpolation (all terms of equation 6.45). Remaining parameters of the model are predicted by a 2D linear interpolation. The coefficients of generalized expression for the parameters of 2-Maxwell model with 2 point, 3 point and 5 point input are listed in table 6.3-6.5 respectively.

Table 6.2. Optimized parameters of 2-Maxwell model

Frequency (Hz)	Magnetic field (T)	K_{sm} (N/mm)	K_1 (N/mm)	K_2 (N/mm)	c_1 (N-s/mm)	c_2 (N-s/mm)	K_B (N /T^2)
8	0	104.499	28.801	41.300	0.971	0.886	0.000
	0.1	114.046	37.519	36.107	1.034	0.819	1.602
	0.2	117.923	46.182	33.316	1.143	0.793	2.658
	0.27	122.589	52.675	32.293	1.259	0.752	3.511
12	0	106.923	35.263	44.072	0.922	0.752	0.000
	0.1	116.941	42.811	40.298	0.934	0.702	2.010
	0.2	123.458	49.840	37.444	0.985	0.666	2.851
	0.27	124.693	54.209	35.292	1.050	0.512	3.801
16	0	111.671	41.381	47.179	0.839	0.700	0.000
	0.1	118.567	46.117	43.612	0.851	0.591	2.231
	0.2	125.040	51.720	41.011	0.882	0.504	3.210
	0.27	127.890	57.595	39.055	0.903	0.481	4.102
20	0	120.064	45.130	50.119	0.774	0.589	0.000
	0.1	124.878	49.572	47.099	0.800	0.526	2.450
	0.2	126.651	56.402	43.037	0.822	0.462	3.730
	0.27	132.275	61.054	41.010	0.791	0.423	4.504
24	0	125.311	45.459	52.850	0.682	0.502	0.000
	0.1	129.639	50.090	49.219	0.720	0.423	2.750
	0.2	132.348	56.846	45.698	0.758	0.350	3.990
	0.27	137.651	61.891	43.329	0.739	0.283	5.010

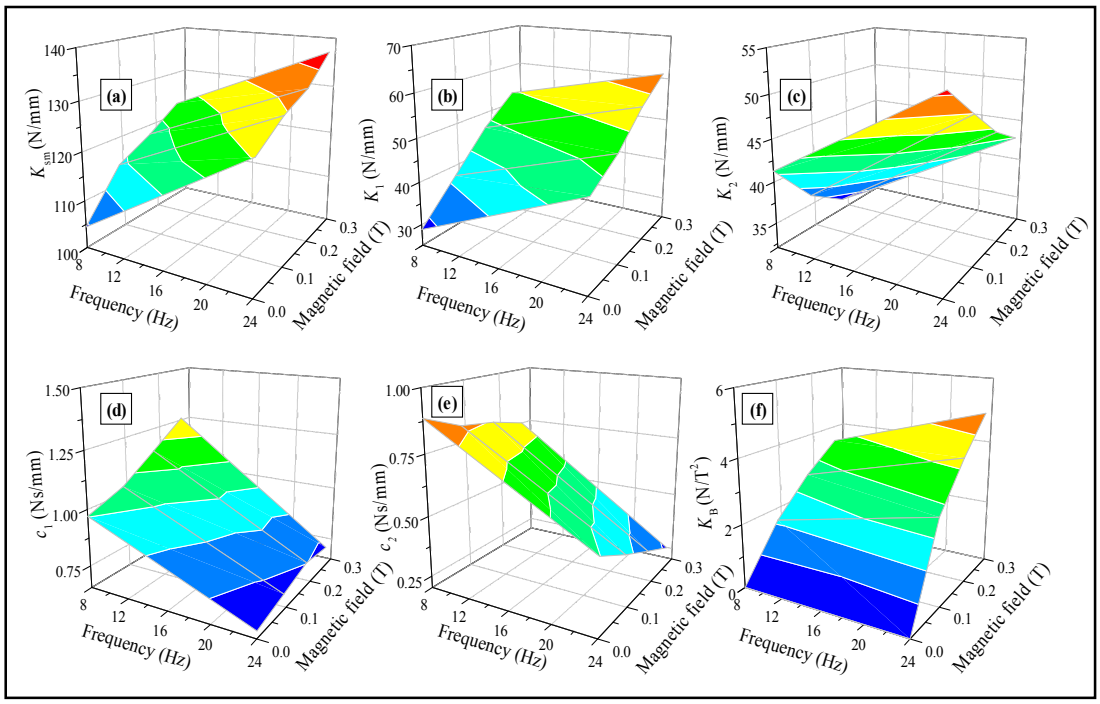

Figure 6.12. Variation in the parameters of 2-Maxwell model with respect to *B* and *f* corresponding to 2 point input.

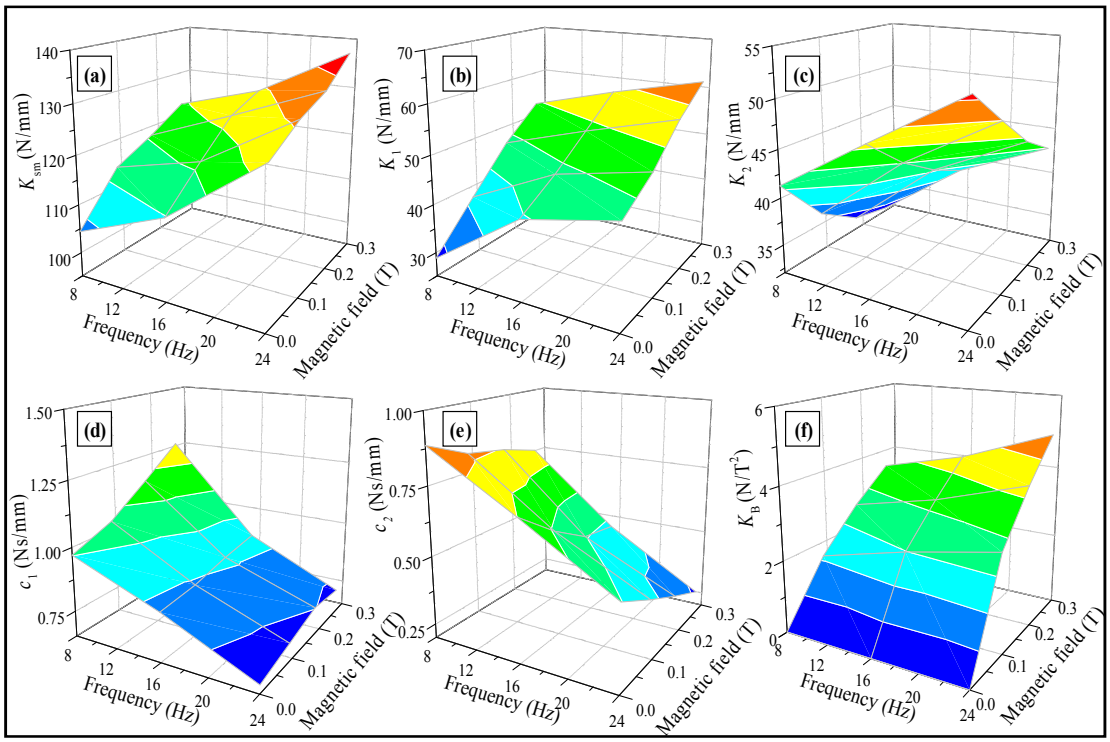

Figure 6.13. (a-f) Variation in the parameters of 2-Maxwell model with respect to *B* and *f* corresponding to 3 point input.

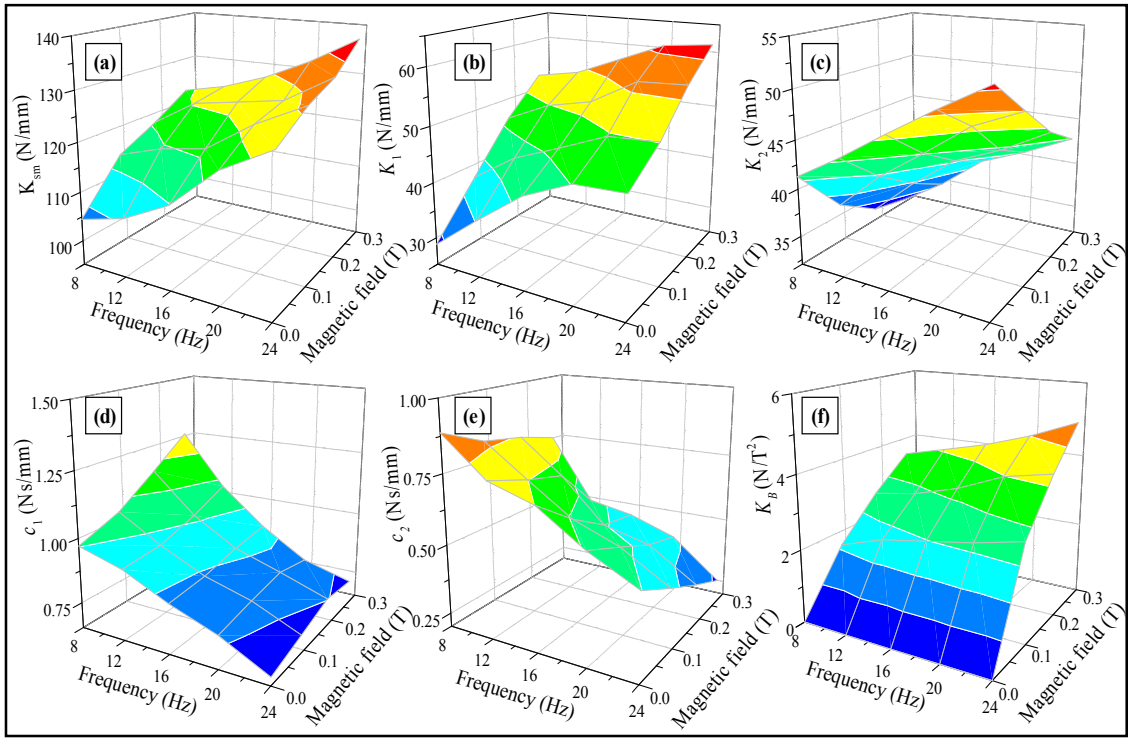

Figure 6.14. (a-f) Variation in the parameters of 2-Maxwell model with respect to *B* and *f* corresponding to 5 point input

Table 6.3. Coefficients of generalized expression for the parameters of 2-Maxwell model for 2 point input.

Parameters	a_0	a_1	a_2	a_3	a_4	a_5
K_{sm}	99.18741	54.37383	1.02956	—	—	—
K_1	24.92996	75.74306	0.76734	—	—	—
K_2	34.38625	-34.3869	0.75124	—	—	—
c_1	1.2016	0.65726	-0.02357	—	—	—
c_2	1.11073	-0.64396	-0.02642	—	—	—
K_B	-0.64658	15.46004	0.06237	—	—	—

Table 6.4. Coefficients of generalized expression for the parameters of 2-Maxwell model for 3 point input.

Parameters	a_0	a_1	a_2	a_3	a_4	a_5
K_{sm}	98.14141	56.66785	1.02956	—	—	—
K_1	26.21626	70.58656	0.76734	—	—	—
K_2	31.58371	-49.95827	1.24756	72.46932	-0.01484	-0.15769
c_1	1.2385	1.35538	-0.03853	0.05978	0.0006919	-0.05318
c_2	1.10813	-0.70425	-0.02642	—	—	—
K_B	-0.63271	15.22521	0.06237	—	—	—

Table 6.5. Coefficients of generalized expression for the parameters of 2-Maxwell model with 5 point input.

Parameters	a_0	a_1	a_2	a_3	a_4	a_5
K_{sm}	98.25195	55.83037	1.02274	––	––	––
K_1	26.43065	68.6786	0.8061	––	––	––
K_2	31.73275	-46.3173	1.20078	59.62521	-0.01324	-0.18708
c_1	1.2393	1.265	-0.03689	0.00624	0.0006478	-0.05259
c_2	1.08376	-0.71505	-0.02509	––	––	––
K_B	-0.62482	15.1395	0.062527	––	––	––

6.4.2 Parameters of fractional Maxwell MRE model

The optimized parameters of fractional Maxwell model are listed in table 6.6. Variations of these parameters with respect to B and f for 2 point, 3 point and 5 point inputs are represented in Figure 6.15-6.17. A linear interpolation function is chosen to estimate all the parameters of the model which is represented by the first three terms of equation 6.45. The corresponding coefficients of the interpolating function with different groups of input frequency are represented in table 6.7-6.9.

Table 6.6. Optimized parameters of fractional Maxwell model

Frequency (Hz)	**Magnetic field (T)**	K_{sf} **(N/mm)**	K **(N/mm)**	c **(N-s$^{\alpha}$/mm)**	α	K_B **(N /T^2)**
8	0	77.365	150.145	16.937	0.532	0.000
	0.1	87.784	160.040	15.855	0.541	1.512
	0.2	95.175	171.491	14.916	0.552	2.569
	0.27	96.695	180.954	13.639	0.559	4.012
12	0	83.051	159.194	15.672	0.535	0.000
	0.1	93.704	167.486	14.583	0.548	1.786
	0.2	97.498	175.596	14.230	0.558	3.199
	0.27	101.667	184.402	12.598	0.563	4.158
16	0	89.591	168.051	14.821	0.543	0.000
	0.1	97.092	173.079	13.399	0.551	2.305
	0.2	101.595	178.578	12.448	0.566	3.420
	0.27	105.133	187.710	11.613	0.573	4.655
20	0	97.644	175.331	13.619	0.553	0.000
	0.1	104.150	178.415	12.517	0.559	2.624
	0.2	105.220	183.617	11.650	0.572	3.946
	0.27	109.193	193.033	10.755	0.579	5.191
24	0	101.290	178.308	12.619	0.559	0.000
	0.1	107.031	182.045	11.852	0.561	3.103
	0.2	109.840	185.896	10.482	0.577	4.212
	0.27	113.240	195.174	9.513	0.583	5.522

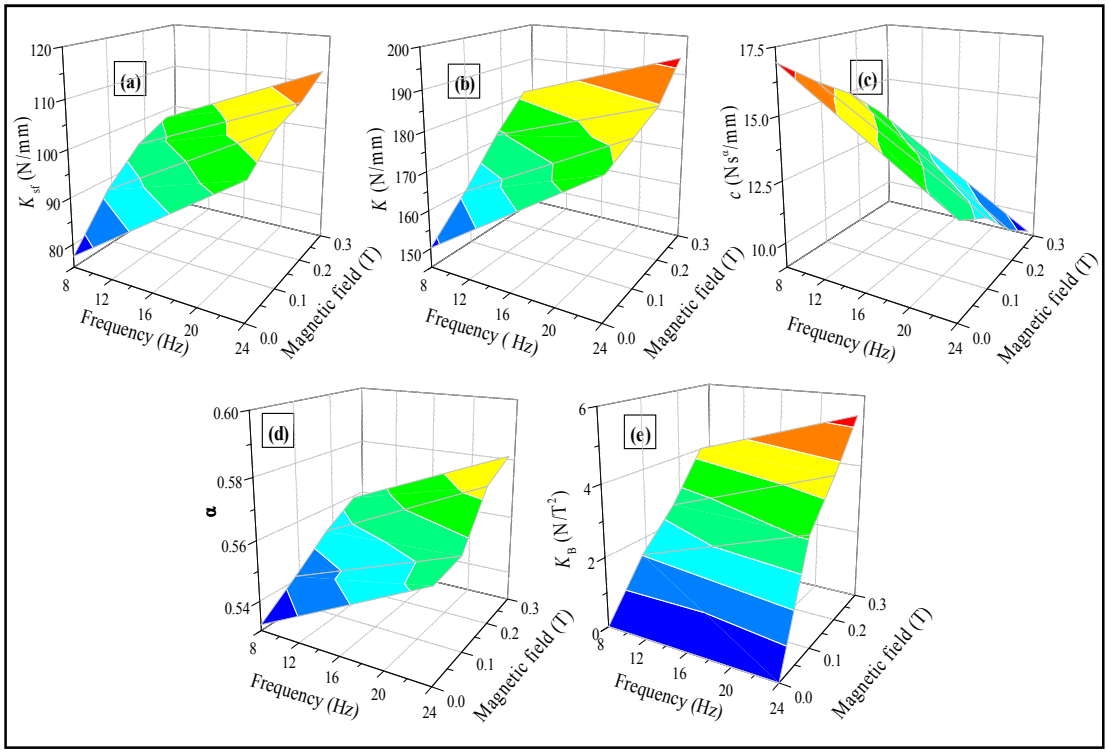

Figure 6.15 Variation in the parameters of fractional Maxwell model with respect to *B* and *f* corresponding to 2 point input

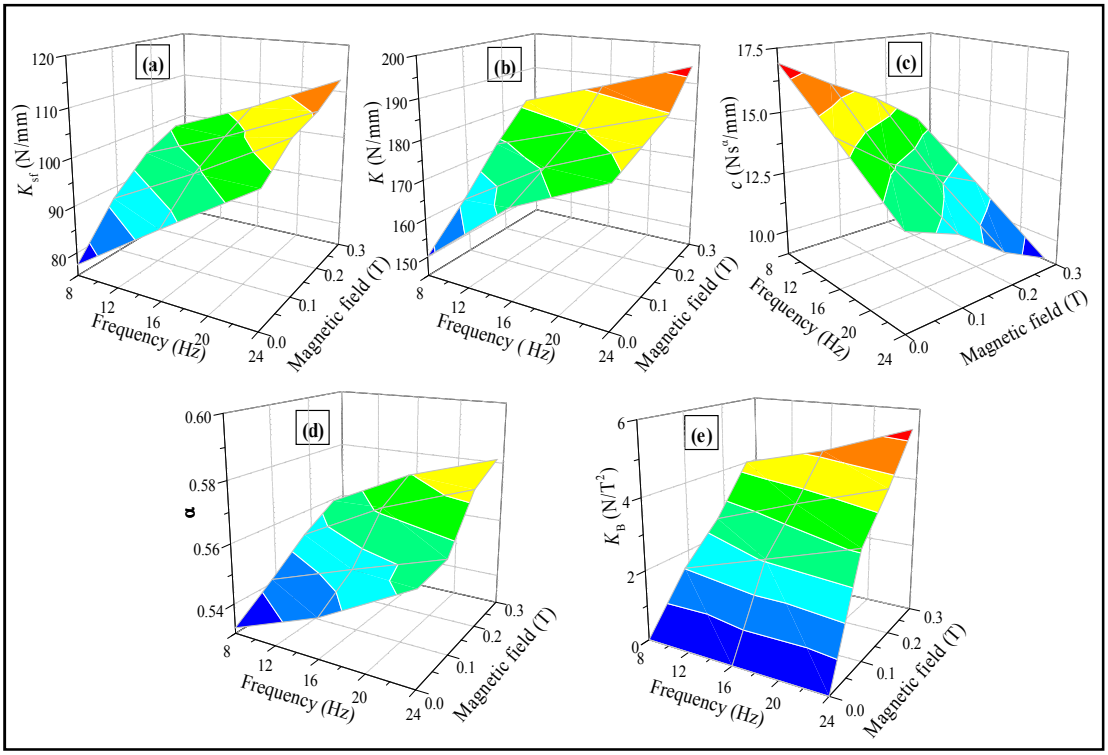

Figure 6.16. Variation in the parameters of fractional Maxwell model with respect to *B* and *f* corresponding to 3 point input.

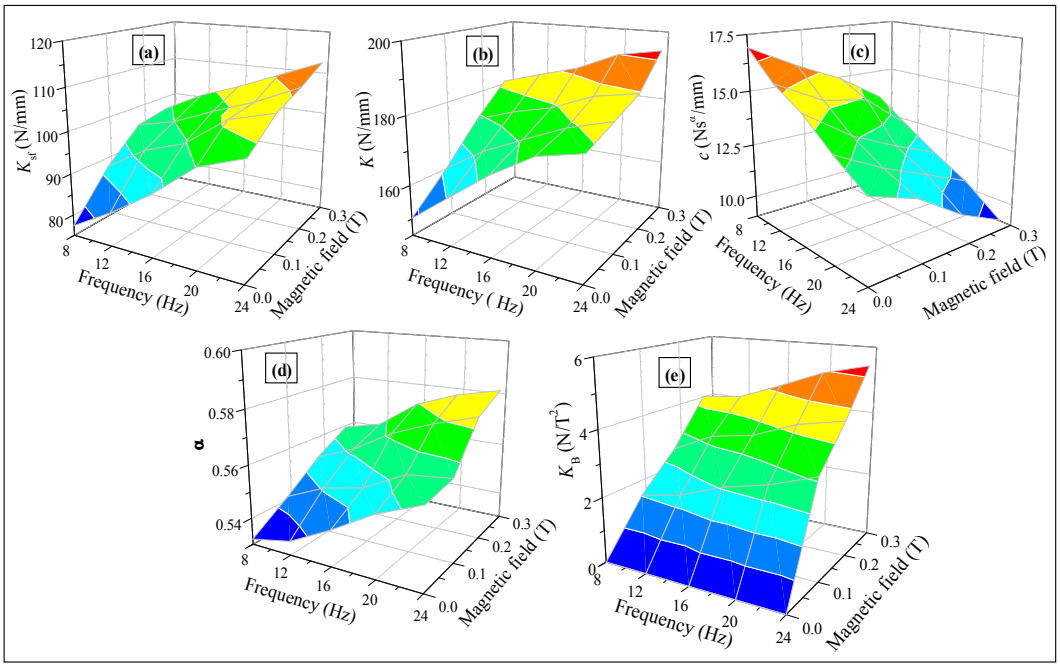

Figure 6.17. Variation in the parameters of fractional Maxwell model with respect to B and f corresponding to 5 point input.

Table 6.7. Coefficients of generalized expression for the parameters of fractional Maxwell model for 2 point input.

Parameters	a_0	a_1	a_2	a_3	a_4	a_5
K_{sf}	72.22541	59.62078	1.14132	—	—	—
K	143.9341	87.95998	1.23112	—	—	—
c	19.06108	-11.95743	-0.26376	—	—	—
a	0.52077	0.09884	0.00149	—	—	—
K_B	-0.87746	17.09385	0.07413	—	—	—

Table 6.8. Coefficients of generalized expression for the parameters of fractional Maxwell model for 3 point input.

Parameters	a_0	a_1	a_2	a_3	a_4	a_5
K_{sf}	72.2301	58.70052	1.14132	—	—	—
K	145.11788	82.51943	1.23112	—	—	—
c	18.99971	-11.88883	-0.26376	—	—	—
a	0.52016	0.10488	0.00149	—	—	—
K_B	-0.826925	16.98081	0.07413	—	—	—

Table 6.9. Coefficients of generalized expression for the parameters of fractional Maxwell model for 5 point input.

Parameters	a_0	a_1	a_2	a_3	a_4	a_5
K_{sf}	72.27689	55.67294	1.18158	—	—	—
K	145.35189	81.07555	1.25813	—	—	—
c	18.95023	-11.36262	-0.26439	—	—	—
a	0.5192	0.10392	0.00157	—	—	—
K_B	-0.89888	17.02925	0.07567	—	—	—

6.5 Comparison between the experimental and model estimated stiffness

A comparison between the stiffness K' and K'' estimated by the models and from the experiments are presented in Figure 6.18-6.21. Predicted K' by both the modeling approaches with 2 point, 3 point and 5 point input are in a good agreement with the experimental results. However, the K'' estimated by the 2-Maxwell and fractional Maxwell model are not as accurate as the predicted values of K'. Moreover, the K'' estimated by the 2-Maxwell and fractional Maxwell model differs as the frequency interval is varied. For both models, variations in the K'' predicted with 3 point and 5 point are not significant. But, the deviation in the predicted K'' values are pronounced corresponding to the 2 point input.

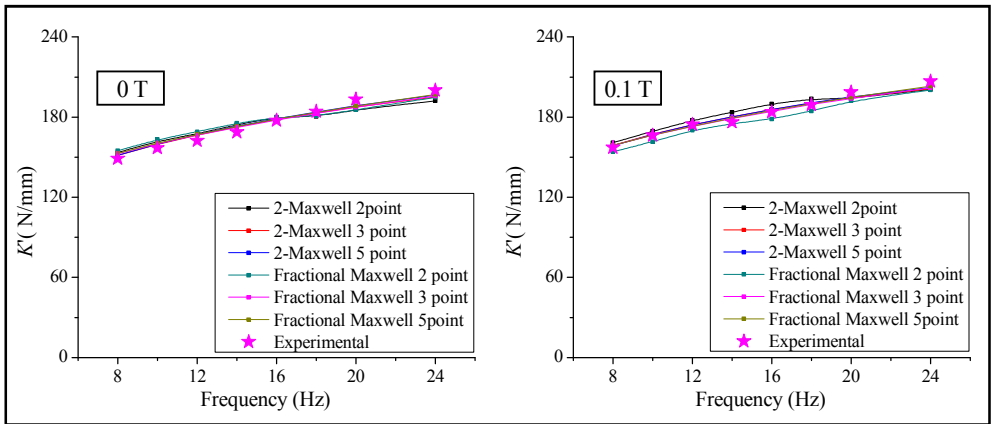

Figure 6.18. (a-f) Comparison between the experimental and predicated K' by 2-Maxwell and fractional Maxwell model with different set of input at 0 T and 0.1 T.

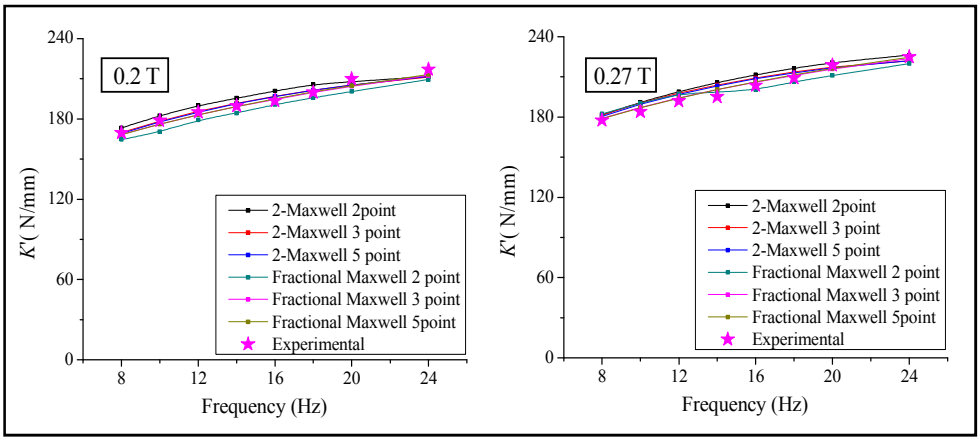

Figure 6.19. (a-f) Comparison between the experimental and predicated K' by 2-Maxwell and fractional Maxwell model with different set of input at 0.2 T and 0.27 T.

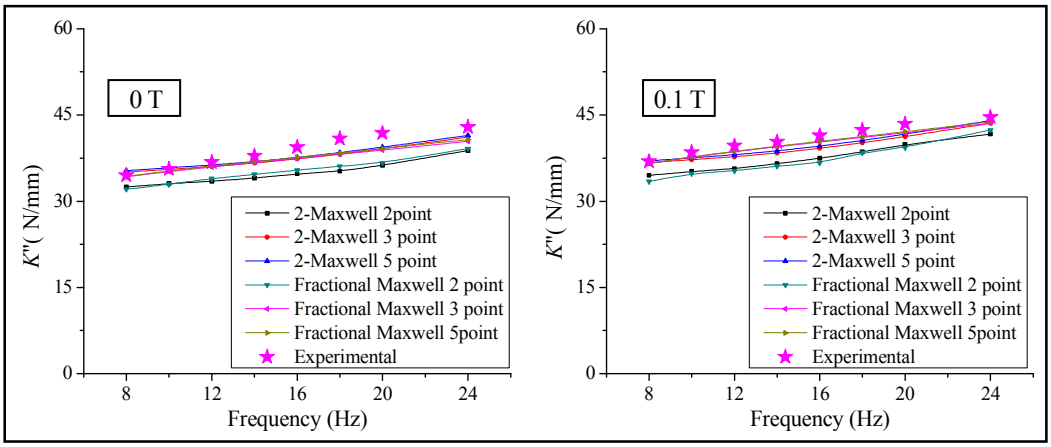

Figure 6.20. (a-f) Comparison between the experimental and predicated *K″* by 2-Maxwell and fractional Maxwell model with different set of input at 0 T and 0.1 T.

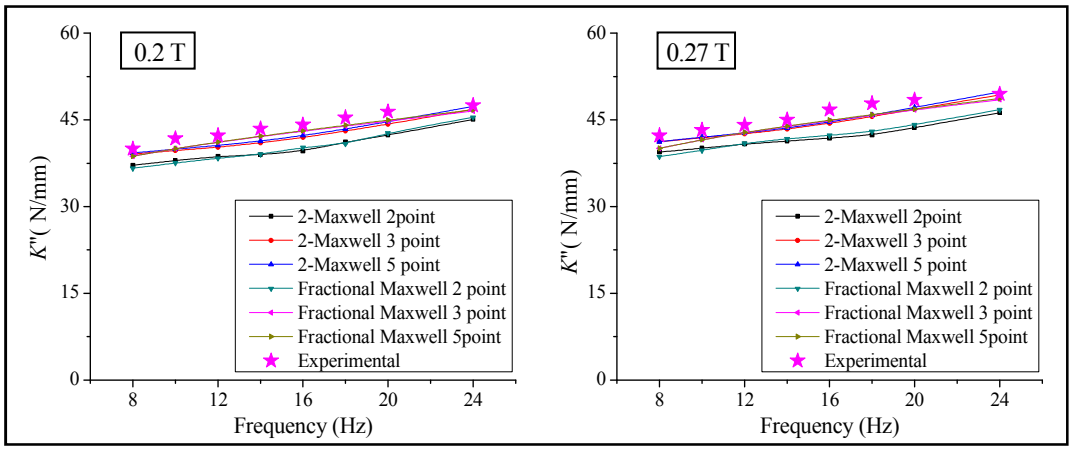

Figure 6.21. (a-f) Comparison between the experimental and predicated *K″* by 2-Maxwell and fractional Maxwell model with different set of input at 0.2 T and 0.27 T.

Maximum error in estimating stiffness (*K′* and *K*") by both modeling approaches with the different sets of input data are listed in Table 6.10- 6.11. These values indicate that 2-Maxwell and fractional Maxwell models are effective in predicting *K*' with a minimum error. It is also noticed that, even with 2 point input, both models are accurate in predicting the *K*' with an accuracy more than 94.5%. Corresponding accuracies for 3 point and 5 point input are 95.45% and 95. 84%. Accordingly, fractional Maxwell model with 2 point, 3 point and 5 point input predicts the *K*' with accuracies greater than 96.4%, 97.22% and 97.18%.

The maximum error in estimating the *K*" by 2-Maxwell model and fractional Maxwell with 2 point input is more than 10%. But, with 5 point input, the accuracy in predicting *K*" by both models are maximum. In addition, by varying the input from 5 point to 3 point, the improvement in the accuracies of predicted *K*" are not significant. This implies that the stiffness values predicted by fractional Maxwell and 2-Maxwell models are unaffected by varying the frequency interval from 4 Hz to 8 Hz.

Table 6.10 Maximum percentage error in estimating *K*' and *K*" by 2-Maxwell and fractional Maxwell with 3 point input.

Model	Magnetic field	*K*'			*K*″		
		2 Point	3 Point	5 Point	2 Point	3 Point	5 Point
2-Maxwell	0T	4.08	3	2.74	13.93	6.64	6.15
	0.1T	4.13	3.02	3.24	10.01	5.32	4.42
	0.2T	3.81	2.68	2.5	10.41	5.65	4.93
	0.27T	5.49	4.55	4.16	11.34	5.01	4.52
Fractional-Maxwell	0T	4.15	3.16	2.83	12.49	7.06	6.46
	0.1T	3.33	2.41	2.02	11.53	3.58	3.12
	0.2T	4.68	2.69	2.39	10.24	4.24	4.18
	0.27T	3.61	2.78	2.82	10.17	5.21	5.21

The 2-Maxwell and fractional Maxwell with 3 point input could portray the frequency and magnetic field dependent properties with a reasonable accuracy. Stiffness *K*' estimated by these models are in good agreement with the experimental results but there exists a difference among the estimated *K*." A comparison between the percentage error in estimating *K*" for 2-Maxwell 3 point and fractional Maxwell 3 point corresponding to 0 T to 0.27 T are shown in Figure 6.22.

As visualized from the graph, the predictive accuracy is relatively better with fractional Maxwell than the 2-Maxwell model. Corresponding to 14 Hz, the error in estimating *K*" by 2-Maxwell model with 3 point input is 3.48%, 5.03%, 5.99% and 3.69% for 0 T, 0.1 T, 0.2 T and 0.27 T respectively. The corresponding errors for fractional Maxwell 3 point input are 3.25%, 2.15%, 3.3% and 2.6%. These variations

depend on two aspects. Firstly, the process of objective function minimization and second, the number parameters in a model.

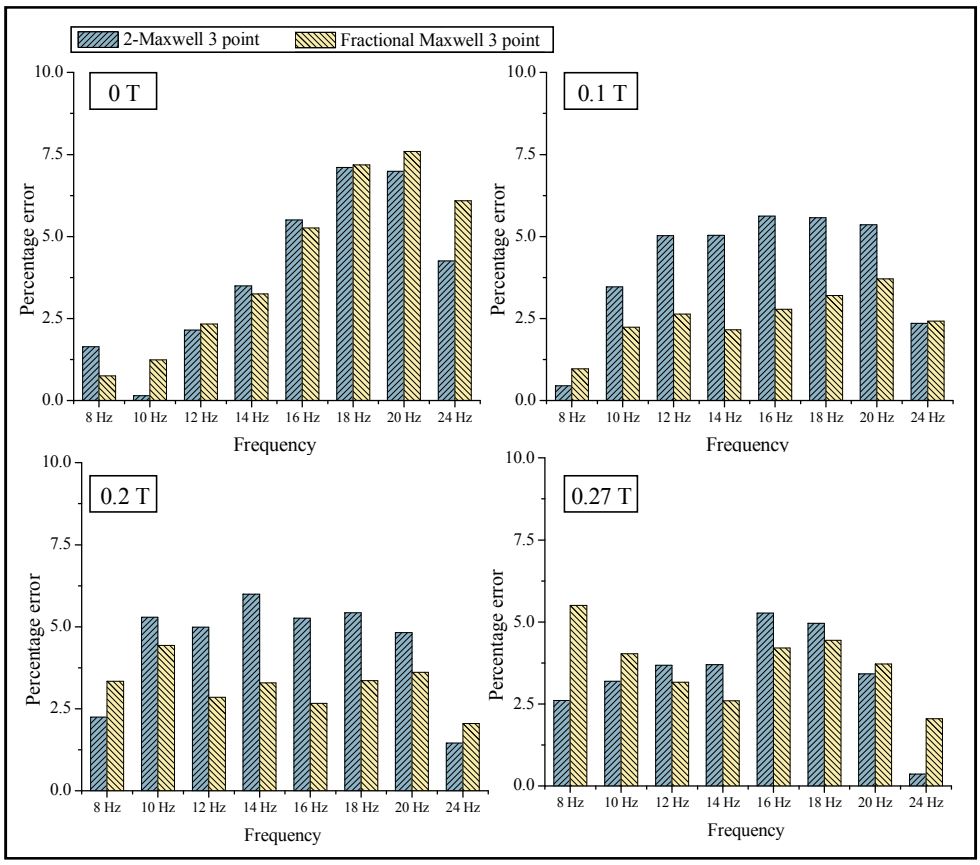

Figure 6.22.Percentage error in estimating *K*" by 2 Maxwell and Fractional Maxwell model at 0 T,0.1 T, 0.2 T and 0.27 T.

The hysteresis loop obtained from the optimized parameter (Figure 6.11) is not an exact representation of the experimental hysteresis loop. As a consequence, a difference exists between the *K*" obtained from the experiments and computed from the optimized parameters.. Subsequently, this error is reflected on the predicted *K*" by the model as it maps the results obtained from the optimized parameters.

The accuracies in reproducing *K*" obtained from the optimized parameters by 2-Maxwell are 94.66%, 97.6%, 96.69% and 97.17% corresponding to 0 T, 0.1 T, 0.2 T and 0.27 T respectively. Accordingly, the accuracies of fractional Maxwell model are 95.91%, 97.86%, 97.26% and 98.79%. Relatively better prediction by the

fractional Maxwell model is attributed to the lesser number of parameters. With a reduced number of parameters, the possibility of propagation of error during the estimation of parameters by an interpolating function is lowered (Figliola and Beasley, 1995). Subsequently, this error is reflected in estimated stiffness values corresponding to the target frequencies while representing it in the generalized form.

In addition, the stiffness parameters K_{sm} and K_{sf} represent the elastic characteristics of 2-Maxwell and fractional Maxwell respectively. As evident from the parameters listed in table 6.2 and table 6.6, the numerical value of K_{sm} is larger than K_{sf}. This signifies that, the real part of the stiffness in fractional Maxwell model depends on the elements of fractional Maxwell chain (K, c, α). Meanwhile, the imaginary part of the stiffness is also a function of these parameters. This interdependency of fractional Maxwell chain on K' and K'' is beneficial as it can facilitate in choosing a better interpolating function to improve the predictive accuracy of the model.

Furthermore, an ideal model should be able to represent the material behavior in a simple form over wide frequency range. Among the proposed models, variations of two out of six parameters in 2-Maxwell model are governed by a 2D quadratic interpolation function. On the contrary, all the parameters of fractional Maxwell model are represented by 2D linear function in B and f. The linear correlation between the operating parameters is more advantageous than the quadratic as it offers simple control algorithms to realize MRE based semi-active devises (Wang and Tang, 2008). Above results confirm that fractional Maxwell model with 3 point input is better compared to the integer order based model in terms of accuracy, simplicity and flexibility. By incorporating the amplitude dependent effects, the fractional Maxwell

model can be used to represent the frequency, magnetic field and strain dependent properties of MRE.

6.6 Summary

Two types of modeling approaches based on the integer and fractional order viscoelasticity were presented. The integer order based model comprised of six parameters, and the fractional order model included five parameters. These parameters were identified by minimizing the error between the responses from the model and the dynamic compression test results discussed in chapter 5. With respect to the optimized parameters, the ability of the model in reproducing the experimental results over the tested frequency range of 8 Hz to 24 Hz was assessed. The variations of the parameters with respect to magnetic field and frequency were simulated by selecting an interpolation function. A 2D quadratic and linear interpolation function was considered and based on the variation of a particular parameter, a suitable interpolation function was chosen. The accuracies of both the models were assessed with respect to the predicted response corresponding to 2 point, 3 point and 5 point input data, which represented the frequency interval of 4 Hz, 8 Hz and 16 Hz. From the response predicted by the model, it was confirmed that both modeling approaches were effective in portraying the experimentally predicted response with the 3 point input data. However, the fractional order based model was more versatile compared to the integer order based models. This modeling technique offered a greater accuracy, simplicity and flexibility in predicting the viscoelastic behavior of MRE.

CHAPTER 7

DEVELOPING A GENERALIZED EXPRESSION TO REPRESENT THE FREQUENCY, MAGNETIC FIELD AND STRAIN DEPENDENT PROPERTIES OF MAGNETPORHEOLOGICAL ELASTOMER

7.1 Introduction

The material modeling of MRE based on viscoelastic constitutive relations is effective in portraying the magnetic field and frequency dependent properties. But, these models are not efficient as the input amplitude is varied. As evident from chapter 4 and chapter 5, MRE exhibits a pronounced strain dependency like conventional filled rubbers. Therefore, the model should incorporate the amplitude dependent effects while representing in a mathematical form.

As discussed in chapter 2, the amplitude dependent effects can be included by adding the frictional or hysteresis characteristics to the model. But, in the present study, the fractional Maxwell model coupled with a stochastic linearized Bouc-Wen component is employed to represent the overall behavior of MRE. This approach is sufficient to describe the amplitude dependent characteristics, as the hysteresis loops (Figure 5.5) revealed that MRE does not show the strain stiffening or softening phenomenon (Yu et al., 2016). The parameters of the model are identified by minimizing the error between the experimental and the model predicted response. Based on these parameters, a generalized expression is developed to represent frequency, magnetic field and amplitude dependent effects simultaneously. The performance of this model is evaluated based on the ability to fit the experimental data, which is expressed in terms of fitness value.

7.2 Modeling magnetic field, frequency and amplitude dependent behaviour of MRE.

Nonlinear systems like Bouc-Wen hysteresis model (Ismail et al., 2009) are often used to describe the response of a material when subjected to high amplitudes of vibrations. In the proposed model, the amplitude dependent component is coupled with the frequency and magnetic field dependent response predicted by the fractional Maxwell model. By using the relation in equation 6.40, a generalized expression for the blocked force by including the viscoelastic and amplitude dependent effect is given by (Greco et al., 2001; Alkhatib, 2013),

$$\left(K_{\text{fm}}' + iK_{\text{fm}}''\right)x(\omega) + K_2 z(\omega) = F(\omega) \tag{7.1}$$

where K_{fm}' and K_{fm}'' are the real and imaginary part of the dynamic stiffness of fractional Maxwell model. The parameter K_2 represents the hysteretic component of the restoring force and z is a non-observable parameter described by a nonlinear equation, which is given by (Greco et al.,2001),

$$\dot{z} = A\dot{x} - \beta\left|\dot{x}\right|\left|z\right|^{n-1} z - \gamma\dot{x}\left|z\right|^{n} \tag{7.2}$$

where A, β, γ, n are parameters that describe the hysteresis loop. Each parameter of the above governing equations influences the hysteresis loops in different ways. This could be in the form of vertical intercept, amplitude, thickness or area under the graph (Yu et al., 2016).

It is difficult to solve the nonlinear Bouc-Wen system to obtain closed-form solutions for the differential equations. Hence, it is a common practice to linearize the system to obtain a frequency response function. The Bouc-Wen model can be modified in several ways to simplify the system and to make it computationally faster

for parameter estimation. The system can also be normalized to reduce the number of parameters without any compromise in rigorosity (Ismail et al., 2009; Ikhouane and Rodellar, 2007; Hurtado, and Barbat, 2000).

Deriving the frequency response function is vital to obtain the storage and the loss moduli of the elastomer. Although the parameter estimation can be accomplished using the nonlinear form of equation, it is not possible to obtain a transfer function for the differential equation. To overcome this limitation, a stochastic linearization which replaces the nonlinear hysteresis component by an equivalent linear model can be employed (Hurtado, and Barbat, 2000; Love et al., 2011; Marano, and Greco, 2003; Giaralis, and Spanos, 2013; Foliente et al., 1996). In the linearization technique, the linear model is obtained by taking the reference of nonlinear equation, which portrays the hysteretic loop is assumed as (Marano, and Greco, 2003),

$$\dot{z} = C_e \dot{x} + K_e z \tag{7.3}$$

where, C_e and K_e are the linearized parameters, which represent the stochastically equivalent damping and stiffness.

Frequency domain transform of the linearized equation is,

$$i\omega z(\omega) = iC_e \omega x(\omega) + k_e z(\omega) \tag{7.4}$$

The expression for $z(\omega)$ is simplified as,,

$$z(\omega) = \frac{i\omega C_e}{i\omega - k_e} x(\omega) \tag{7.5}$$

The modified form of blocked force F, with the inclusion of Bouc-Wen stiffness and damping parameters are given by,

$$F = \left(K_{\text{sf}} x + \left(\frac{Kc\omega^{\alpha}\left(c\omega^{\alpha} + K\cos\,\alpha\pi/2\right)}{(K_v)^2 + (c\omega^{\alpha})^2 + 2c\omega^{\alpha}K\cos\,\alpha\pi/2} \right) x + K_b B^2 + K_2 \left(\frac{C_e.\omega^2}{k_e^2 + \omega^2} \right) x \right) + i\left(\left(\frac{K^2 c\omega^{\alpha}\sin\alpha\pi/2}{(K_v)^2 + (c\omega^{\alpha})^2 + 2c\omega^{\alpha}K\cos\,\alpha\pi/2} \right) x + K_2 \left(\frac{C_e k_e.\omega}{k_e^2 + \omega^2} \right) x \right) \tag{7.6}$$

The expression for the complex form of dynamic stiffness K^* (= K_R+iK_i), of proposed model is given by,

$$K^* = \frac{F}{x} = \left(K_{\text{sf}} + \left(\frac{Kc\omega^{\alpha}\left(c\omega^{\alpha} + K\cos\,\alpha\pi/2\right)}{(K)^2 + (c\omega^{\alpha})^2 + 2c\omega^{\alpha}K\cos\,\alpha\pi/2} \right) + \frac{K_b B^2}{x_0} + K_2 \left(\frac{C_e.\omega^2}{k_e^2 + \omega^2} \right) \right) + i\left(\left(\frac{K^2 c\omega^{\alpha}\sin\alpha\pi/2}{(K)^2 + (c\omega^{\alpha})^2 + 2c\omega^{\alpha}K\cos\,\alpha\pi/2} \right) - K_2 \left(\frac{C_e k_e.\omega}{k_e^2 + \omega^2} \right) \right) \tag{7.7}$$

The dynamic stiffness comprises of a real part, denoted by K_R and an imaginary part of the stiffness represented by K_i.

Under steady-state, the force-displacement response of MRE for the harmonic input displacement, $x=x_0 e^{i\omega t}$ is given by,

$$F_{\text{fm}} = |K^*| x_0 e^{i(\omega t + \delta_{\text{f}})} \tag{7.8}$$

where, δ_{f} is the phase difference between the force and displacement,

$$\delta_{\text{f}} = \tan^{-1}\left(\frac{\left(\left(\frac{K^2 c\omega^{\alpha}\sin\alpha\pi/2}{(K)^2 + (c\omega^{\alpha})^2 + 2c\omega^{\alpha}K\cos\,\alpha\pi/2} \right) - K_2 \left(\frac{C_e k_e.\omega}{k_e^2 + \omega^2} \right) \right)}{\left(K_{\text{sf}} + \left(\frac{Kc\omega^{\alpha}\left(c\omega^{\alpha} + K\cos\,\alpha\pi/2\right)}{(K)^2 + (c\omega^{\alpha})^2 + 2c\omega^{\alpha}K\cos\,\alpha\pi/2} \right) + \frac{K_b B^2}{x_0} + K_2 \left(\frac{C_e.\omega^2}{k_e^2 + \omega^2} \right) \right)} \right) \tag{7.9}$$

and the magnitude of dynamic stiffness is given by,

$$|K^*| = \sqrt{\left(\left(K_{sf} + \left(\frac{Kc\omega^{\alpha}\left(c\omega^{\alpha} + K\cos\,\alpha\pi/2\right)}{(K)^2 + (c\omega^{\alpha})^2 + 2c\omega^{\alpha}K\cos\,\alpha\pi/2}\right) + \frac{K_b B^2}{x_0} + K_2\left(\frac{C_e.\omega^2}{k_e^2+\omega^2}\right)\right)\right)^2 + \left(\left(\frac{K^2 c\omega^{\alpha}\sin\alpha\pi/2}{(K)^2 + (c\omega^{\alpha})^2 + 2c\omega^{\alpha}K\cos\,\alpha\pi/2}\right) - K_2\left(\frac{C_e k_e.\omega}{k_e^2+\omega^2}\right)\right)^2} \quad (7.10)$$

7.3 Parameter estimation

A complete formulation of the viscoelastic material model of MRE is developed by using the experimental results discussed in the chapter 5. The developed model comprises of a total eight parameters, namely, K_s, K, c, α, K_B, K_2, C_e and K_e. The proposed model uses the experimental results as the input to estimate the parameters. Using these parameters, the real and imaginary part of the dynamic stiffness is computed. The parameter estimation process involves a nonlinear regression algorithm in order to minimize the error between the experimental and the model - predicted force for each set of experimental results. The expression for the objective function which optimizes the parameter of the model is given by (Eem et al., 2012; Norouzi et al., 2015),

$$J = \sum_{i=1}^{N}\sum_{j=1}^{M}\left(F(i,j) - F_e(i,j)\right)^2 \quad (7.11)$$

where, N and M are the number of different experimental data corresponding to the various loading conditions like, frequency and strain. The optimized parameters obtained for the different magnetic field (0 T, 0.1 T, 0.2 T and 0.27 T), frequency (8 Hz, 16 Hz and 24 Hz) and the stain amplitudes (0.05 mm, 0.1 mm and 0.15 mm) are listed in table 7.1-7.3.

Table 7.1. Optimized parameters of the model corresponding to 0.05 mm input displacement

Input variable	K_{sf} (N/mm)	K (N/mm)	c (N-s$^{\alpha}$ /mm)	α	K_B (N /T^2)	K_2 (N/mm)	C_e (N-s/mm)	K_e (N/mm)
8 Hz-0 T	92.00	322.56	9.842	0.5217	0.000	38.90	0.3980	208.79
8 Hz-0.1 T	97.97	364.45	9.749	0.5243	0.250	46.35	0.3459	202.52
8 Hz-0.2 T	104.36	376.08	9.703	0.5312	0.966	51.55	0.2917	190.29
8 Hz-0.27 T	111.26	409.08	9.631	0.5382	1.602	52.55	0.1997	185.29
16 Hz-0 T	100.91	328.07	9.162	0.5239	0.000	40.73	0.5458	199.51
16 Hz-0.1 T	109.10	374.24	8.990	0.5249	0.257	48.97	0.4001	191.49
16 Hz-0.2 T	116.46	388.92	8.921	0.5339	1.004	55.18	0.3946	188.72
16 Hz-0.27	121.76	425.92	8.781	0.5419	1.604	63.08	0.3796	182.72
24 Hz-0 T	103.31	340.14	8.510	0.5326	0.000	45.02	0.5787	188.02
24 Hz-0.1T	111.64	376.81	8.342	0.5349	0.269	56.60	0.4658	175.32
24 Hz- 0.2 T	120.61	400.47	8.316	0.5360	1.042	58.89	0.3969	160.08
24 Hz- 0.27 T	125.56	427.50	8.280	0.5422	1.803	65.78	0.3945	150.26

Table 7.2. Optimized parameters of the model corresponding to 0.1 mm input displacement

Input variable	K_{sf} (N/mm)	K (N/mm)	c (N-s$^{\alpha}$ /mm)	α	K_B (N /T^2)	K_2 (N/mm)	C_e (N-s/mm)	K_e (N/mm)
8 Hz-0 T	86.92	355.60	9.561	0.5291	0.000	39.25	0.3610	192.48
8 Hz-0.1 T	93.70	399.08	9.469	0.5333	0.248	48.43	0.2623	180.84
8 Hz-0.2 T	100.07	426.08	9.399	0.5423	0.948	54.43	0.2123	170.84
8 Hz-0.27 T	105.77	445.08	9.327	0.5523	1.548	58.84	0.1853	161.84
16 Hz-0 T	98.49	360.06	8.614	0.5308	0.000	47.51	0.4569	186.16
16 Hz-0.1 T	103.59	403.06	8.438	0.5368	0.245	55.51	0.3949	170.16
16 Hz-0.2 T	113.19	439.06	8.208	0.5458	0.998	58.51	0.3579	160.16
16 Hz-0.27	119.32	465.06	7.981	0.5568	1.980	68.51	0.3149	150.16
24 Hz-0 T	100.49	382.04	8.131	0.5338	0.000	54.15	0.4711	180.85
24 Hz-0.1T	108.49	407.04	7.931	0.5390	0.350	59.95	0.3991	162.85
24 Hz- 0.2 T	118.49	450.04	7.531	0.5490	0.990	65.95	0.3691	152.85
24 Hz- 0.27 T	121.99	470.04	7.231	0.5589	1.855	70.95	0.3591	142.85

Table 7.3. Optimized parameters of the model corresponding to 0.15 mm input displacement

Input variable	K_{sf} (N/mm)	K (N/mm)	c (N-s$^{\alpha}$ /mm)	α	K_B (N /T^2)	K_2 (N/mm)	C_e (N-s/mm)	K_e (N/mm)
8 Hz-0 T	81.72	380.60	9.361	0.5359	0.000	43.25	0.3110	182.48
8 Hz-0.1 T	87.52	417.60	9.311	0.5421	0.526	50.25	0.2510	173.48
8 Hz-0.2 T	95.52	425.60	9.211	0.5523	0.926	52.25	0.1871	167.48
8 Hz-0.27 T	102.12	450.60	9.161	0.5633	0.926	62.25	0.1569	153.48
16 Hz-0 T	92.25	390.06	8.298	0.5368	0.000	55.51	0.3619	175.16
16 Hz-0.1 T	100.25	424.06	8.138	0.5428	0.546	59.51	0.3219	165.16
16 Hz-0.2 T	109.45	445.06	7.898	0.5558	0.546	65.51	0.2725	155.16
16 Hz-0.27	116.25	475.06	7.798	0.5658	0.546	70.51	0.2425	146.16
24 Hz-0 T	94.49	405.04	8.031	0.5400	0.000	60.15	0.3951	170.85
24 Hz-0.1T	102.99	430.04	7.692	0.5480	0.243	64.15	0.3411	156.85
24 Hz- 0.2 T	113.69	456.04	7.292	0.5600	0.243	70.15	0.3011	140.85
24 Hz- 0.27 T	119.19	490.04	7.112	0.5680	0.243	80.15	0.2711	134.85

In total, 36 sets of compression test data were used to estimate the parameters of the model. From the parameters listed in table (table 7.1- 7.3), it is found that the parameters are sensitive to the change in magnetic field, frequency and the amplitude. These variations are represented in a mathematical form by using LINEST function (MS Excel). This function approximates a linear equation to simulate the simultaneous variations of the parameters with respect to frequency, magnetic field and strain. Assumed linear function is advantageous as it offers a simple mathematical formulation of MRE, which is easier to implement in MRE based semi active control strategies (Wang and Tang, 2008). A generalized form to represent these variations is expressed as,

$$d = d_1 A + d_2 B + d_3 f + d_4 \tag{7.12}$$

where, d is the parameter of the model. The coefficients of the expression are denoted by d_1, d_2, d_3 and d_4. Input frequency, amplitude and the magnetic field are denoted by f, B and A respectively. The coefficients of the generalized expression are listed in the table 7.4. Using above relations, the real and the imaginary part of the stiffness is calculated to evaluate the ability of the model in reproducing the experimental results.

Table 7.4. Coefficients of the generalized expression of the parameters of MRE model.

Parameters	d_1	d_2	d_3	d_4
K_{sf}	-82.93	79.803	0.94789	87.33
K	546.3	315.63	1.3685	287.6
c	-7.433	-1.7307	-0.10064	11.196
α	0.1874	0.08288	0.00040	0.5049
K_B	-0.4143	5.688	-0.01075	0.05644
K_2	91.65	66.31	0.7998	25.23
C_e	-1.1483	-0.5568	0.00823	0.40547
K_e	-250.93	-112.4	-1.3196	233.3

7.4 Results and discussion

Using the parameters estimated from the optimization process, a comparison is made between the experimental, and the model predicted hysteresis behavior. Figure 7.1 compares the force-displacement hysteresis loops at different magnetic field strengths. Correspondingly, a comparison between the force-displacement relations under different frequency and the input strain are represented in Figure 7.2 and Figure 7.3 respectively. From these graphs, it can be observed that the proposed model is able to predict the frequency, magnetic field and strain dependent characteristics of MRE. The area of hysteresis loops is increased by increasing the magnetic field, which is very well portrayed by the model. Additionally, with an increase in frequency, the stiffness of the MRE is enhanced, which is consistent even in the presence of the magnetic field. Moreover, the slopes of the main axis and the area of hysteresis loops vary with the increase in the input strain. This indicates that the proposed model is effective in portraying the Payne effect in MRE under magnetized and non-magnetized state.

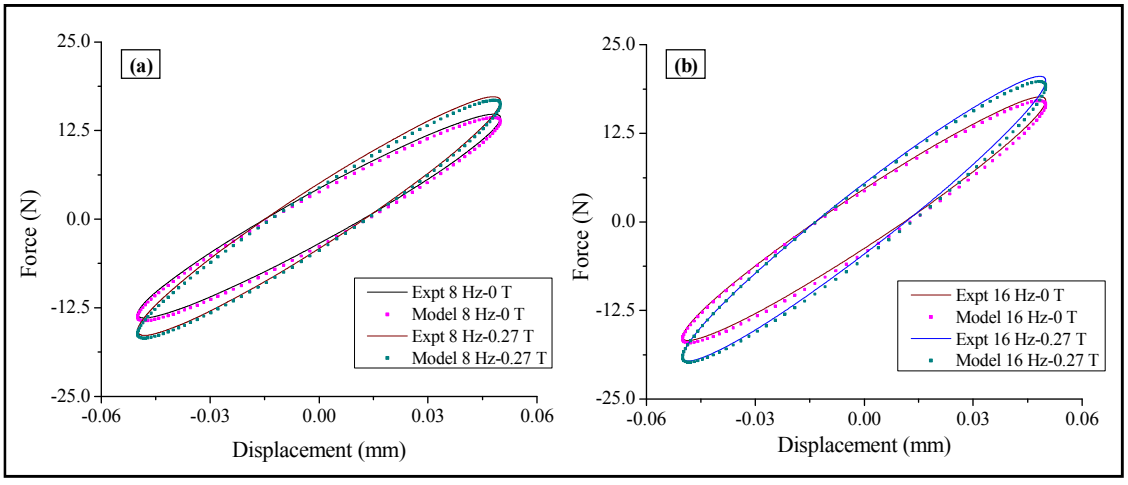

Figure 7.1. Force-displacement curves of the experimental data and proposed model for different magnetic field strength (a) 8 Hz (b) 16 Hz.

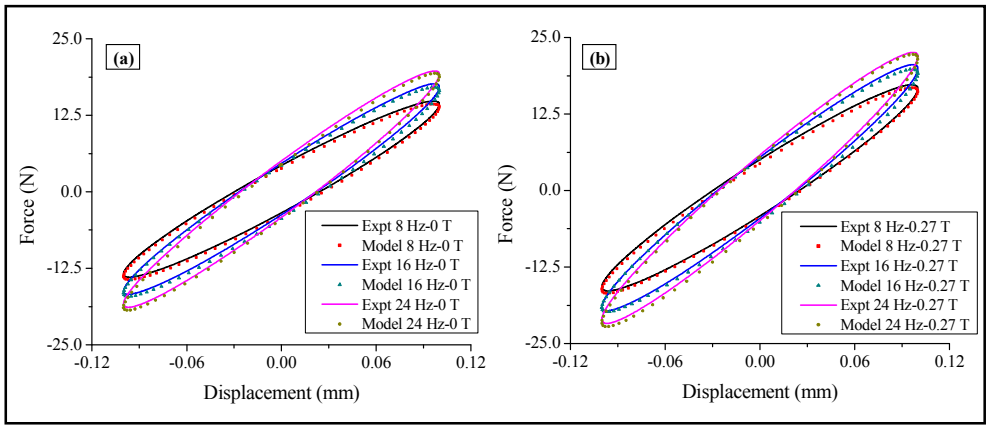

Figure 7.2. Force-displacement curves of the experimental data and proposed model for different frequencies (a) 0 T (b) 0.27 T

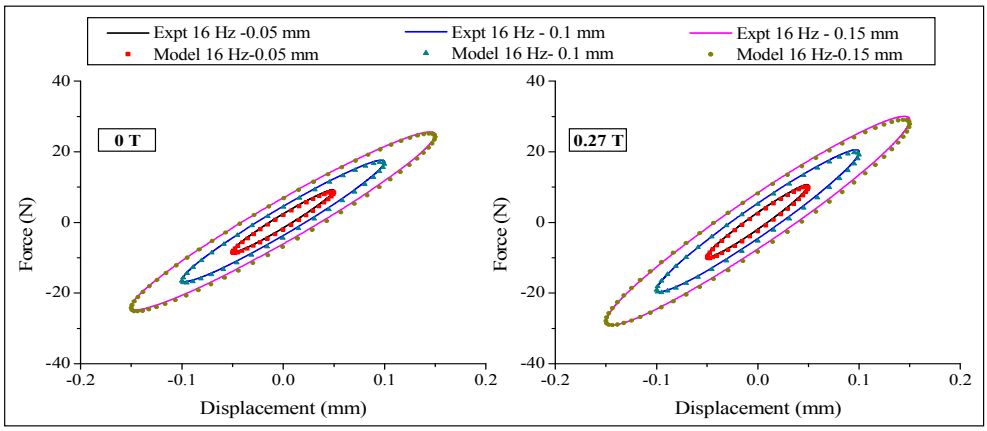

Figure 7.3. Force-displacement curves of the experimental data and proposed model for different input amplitude (a) 0 T (b) 0.27 T

The real and the imaginary part of the dynamic stiffness are computed using the equation 7.7. A comparison between the K_R and K_i evaluated from the experiments and predicted by the model at different amplitudes are presented in Figure 7.4-7.6. As evident from the graphs, by increasing the magnetic flux density, both K_R and K_i are increased. This behavior is observed for all the tested frequencies and the strain amplitudes. For example, at a strain of 1.5 % (0.15 mm) and frequency of 16 Hz, increasing the magnetic field from 0 T to 0.27 T, K_R is increased from 168.06 N/mm to 196.836 N/mm. The corresponding K_R estimated from the experiments is increased from 176.245 N/ mm to 204.822 N/ mm.

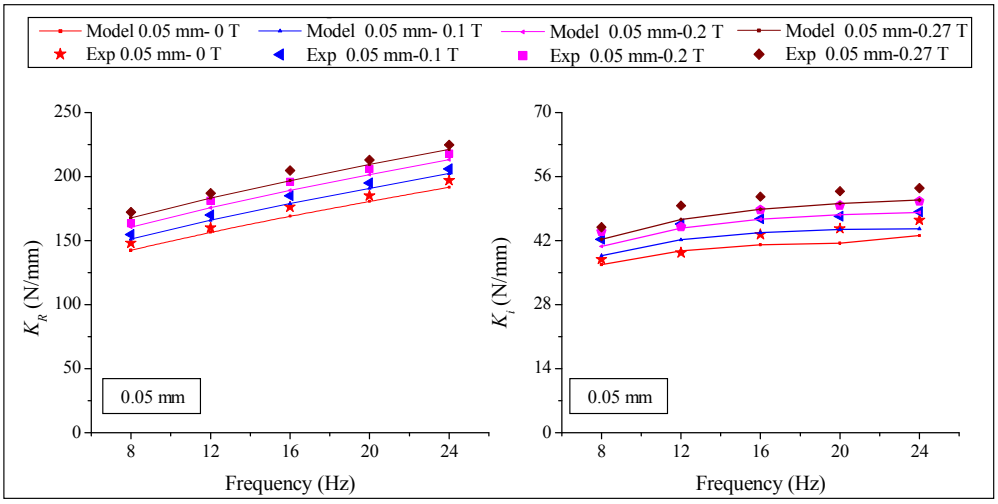

Figure 7.4. Comparison between the experimental data and model predicted K_R and K_i at different magnetic field corresponding to 0.05 mm input amplitude.

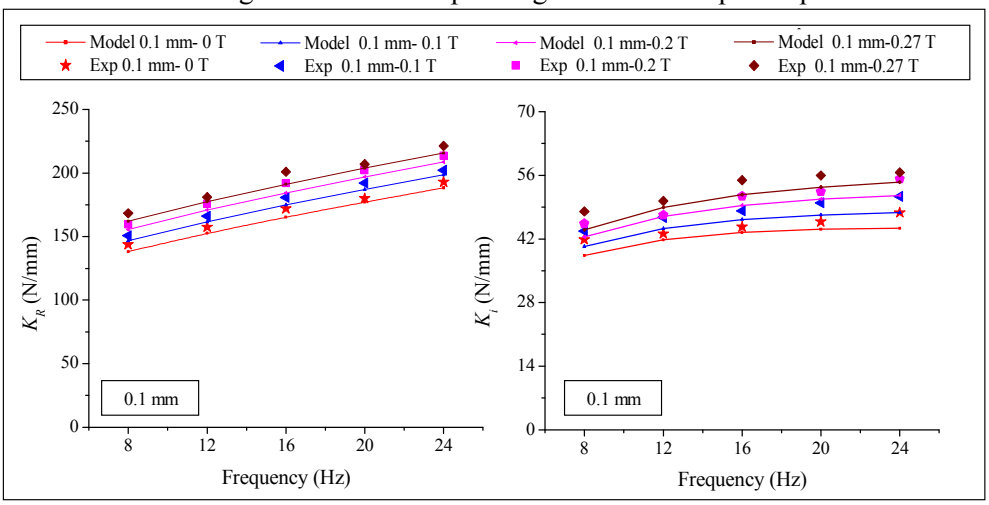

Figure 7.5. Comparison between the experimental data and model predicted K_R and K_i at different magnetic field corresponding to 0.1 mm input amplitude.

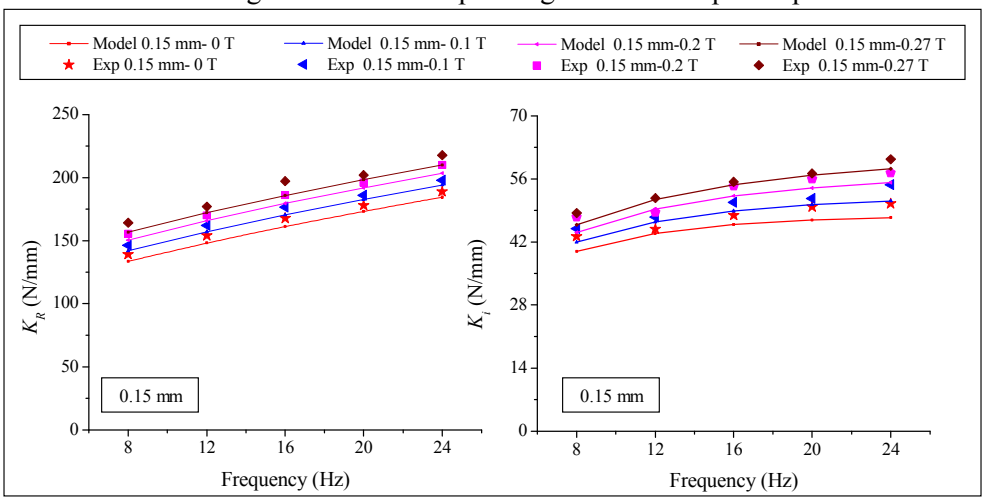

Figure 7.6. Comparison between the experimental data and model predicted K_R and K_i at different magnetic field corresponding to 0.15 mm input amplitude

From the graphs, it is observed that model predicted real part of the stiffness (K_R) is in good agreement with the experimental results. This proposed model is able to reproduce K_R with an accuracy of more than 94.3 %. However, the accuracy of predicted K_i by the model is relatively lower than the K_R. Moreover, this model is able to capture the experimentally determined K_i with an accuracy greater than 90.1 %. This disparity can be attributed to the variation in the damping characteristics of MRE, which is not exhibiting a linear variation with respect to the frequency. Moreover, as discussed in chapter 6, the parameter identification processes have a significant influence on the accuracy of the predicted stiffness values. The present model reproduces the K_i of the experimental results with an error of 9.9 %. However, the error in predicting the stiffness $K_{i,}$, with respect optimized parameter is less than 4.9%.

Apart from graphical analogy, the ability of the model in reproducing the experimental results is quantitatively investigated from the fitness value (Eem, et al. 2012; Norouzi et al., 2015). The fitness value represents the correlation between the force value predicted by the proposed model and the measured force from the experiments. This is calculated by the normalized root mean square function, and it is given by the equation,

$$\text{Fitness value } (\%) = \left[\frac{\text{norm}(F_P - F_E)}{\text{norm}(F_P - \text{mean}(F_E))} \right] \text{ x } 100 \qquad (7.13)$$

where, F_{P} is the predicted force and the F_{E} is the measured force from the experiments. The resulting fitness values are listed in table 7.5. In all the experimental cases, the values of the fitness are higher (more than 93.22%). This indicates that the proposed dynamic model of MRE can be effectively used to predict the frequency,

magnetic field and amplitude dependent dynamic compressive characteristics for the tested operating conditions.

Table 7.5. Fitness values of the MRE model.

Amplitude (mm)	Magnetic field (T)	Frequency (Hz)				
		8	12	16	20	24
0.05	0	93.22	97.22	95.55	94.9	94.02
	0.1	93.32	94.8	95.60	95.52	94.62
	0.2	95.19	97.8	94.34	96.4	95.04
	0.27	95.68	94.8	94.23	94.9	97.96
0.1	0	94.09	97.05	96.82	96.9	93.82
	0.1	94.68	95.2	96.58	95.89	95.58
	0.2	96.25	99.02	97.28	97.8	95.28
	0.27	93.75	98.21	97.31	96.54	97.31
0.15	0	94.01	97.5	96.51	96.15	97.01
	0.1	94.55	98.22	96.73	98.22	96.73
	0.2	93.95	99.15	96.51	97.3	97.21
	0.27	95.25	99.15	98.30	99.01	98.30

7.5 Summary

In this chapter, a mathematical relation to represent the frequency, magnetic field and amplitude dependent variation in the dynamic compressive behavior of MRE was presented. This model was an extension of the fractional order viscoelastic model coupled with the linearized Bouc-Wen component. The proposed model comprised of a total of eight parameters, which were obtained by minimizing the error in the objective function by a nonlinear regression algorithm. Variations of these parameters with respect to the operating conditions were generalized by the LINEST function. Performance of the model was evaluated based on its ability to map the experimental results. The results confirmed that the proposed model satisfactorily reproduced the experimental results under varying frequency, magnetic field and the displacement amplitude. The model could fit the experimental results with a fitness value of more than 93. 33%.

CHAPTER 8

SUMMARY AND CONCLUSIONS

8.1 Summary

The present work deals with the mathematical modeling of translation stiffness of MRE. The material modeling of MRE is a complex task as it exhibits the viscoelastic behavior, which is intermediate between an ideal solid and an ideal liquid. Under fixed processing conditions, the viscoelastic properties of MRE vary with the operating parameters like frequency, magnetic field, and the input strain. Additionally, these properties vary with the modes of operation and their inter conversion are unrealistic. This demands a huge amount of experimental data for effectively characterizing the properties of MRE. On the contrary, the modeling approach based on the viscoelastic constitutive relations simplifies the overall viscoelastic property characterization studies. But, this approach requires the experimental characterization data to obtain the parameters of the model. The ability of these models in representing the dynamic behavior over a wider range of frequencies differs with the modeling components considered. Moreover, the effectiveness of the model in describing the material behavior depends on the input strain, which controls the transition from linear to the nonlinear viscoelastic behavior. Therefore, in the proposed study, the influence of operating parameters on the viscoelastic properties of MRE is evaluated under volume preserving deformation state. Later, a material model is developed to represent the dynamic behavior of MRE in response to the varying operating conditions.

The viscoelastic properties of MRE are characterized by dynamic blocked transfer stiffness method. The properties of MRE are represented in terms of dynamic stiffness, and the loss factor is obtained from the force-displacement hysteresis loops. Preliminary tests are performed on MRE to study the influence of magnetic field and frequency on the viscoelastic properties of MRE. These tests revealed the existence of saturation limit for frequency and magnetic field dependent properties. Based on these findings, the dynamic property characterization studies are extended to assess the linear viscoelastic behavior of MRE and its dependency on the frequency and magnetic field. The amplitude dependency on the field-induced properties of MRE is also evaluated from the variation in the slope of the hysteresis loop. These results revealed that the amplitude is a critical parameter, which needs to be addressed while designing a MRE based devise.

The viscoelastic properties of MRE are modeled by adapting viscoelastic constitutive relations. Two modeling approaches, namely, integer order and fractional order derivative are considered. The integer order model is referred to as 2-Maxwell model, comprising of a total of six parameters. The fractional order model is referred to as fractional Maxwell model, which includes five parameters. Parameters of these models are obtained by minimizing the error between the response predicted by the model and the dynamic compression test data. To compare the predictive accuracy of the models in portraying the experimental results, an interpolation function is chosen. This interpolation polynomial generalizes the variation of each parameter with respect frequency and the magnetic field. The predicted stiffness values indicated that both the modeling approaches are effective in portraying the viscoelastic behavior of MRE but the fractional order model is more versatile. The fractional order based model

describes the broad-band frequency dependent viscoelastic behavior in a simple form with lesser number of parameters.

Based on the results of preliminary modeling studies, the fractional Maxwell model is extended to incorporate the amplitude dependent effects. The amplitude dependency is a critical factor for MRE as it leads to strain softening behavior, which cannot be predicted by the conventional viscoelastic modeling approaches. Moreover, the amplitude dependency, if not considered may lead to failure of control strategies of MRE device when it is exposed to varying levels of strain. The amplitude dependency is incorporated to the fractional Maxwell model by coupling the linearized Bouc-Wen element. The proposed model comprises of a total of eight parameters, which are identified from the objective function minimization approach by using 36 sets of experimental data. From the obtained model parameters, the variations with respect to the magnetic field, frequency and strain are generalized using a planar function. The performances of the model in reproducing the experimental results are evaluated at different frequency, magnetic field and input stain. These results showed that the model predicted response is in a good agreement with the experimental results, which is assessed in terms of fitness value.

8.2 Conclusions

From this research work following conclusion are made.

The dynamic viscoelastic properties of MRE are frequency and magnetic field dependent. The influence of magnetic field on the dynamic viscoelastic property is stronger compared to the frequency. These properties saturate with the magnetic field and the frequency. The saturation limit of tested MRE sample is around 50 Hz and 0.3 T magnetic field. The frequency has the least influence on the field-induced property

enhancements of MRE, but its influence on loss factor variations is significant. Under magnetized state, the loss factor cannot be controlled independently as it depends on the field-induced enhancement in stiffness and equivalent damping.

The LVE limit is a critical parameter which needs to be addressed while designing a MRE based isolator. The critical strain of MRE is a function of magnetic field and the excitation frequency, which depends on the interface interaction between the matrix and the filler. LVE limit of MRE is decreased with increasing the frequency or increasing the magnetic field. However, the influence of magnetic field on critical strain variation is more pronounced compared to the excitation frequency. The MRE sample characterized in the present work can be incorporated as a resilient element in a semi-active isolator device operating in the frequency ranges below 24 Hz. This device can exhibit a linear response up to a 3.54% strain under the magnetic field of 0.4T when the source of non-linearity is solely from the material response of MRE.

MRE exhibits Payne effect as the input strain amplitude is increased. The strain dependency is pronounced under non-magnetized state of MRE and it diminishes with the increase in the magnetic field. Moreover, the ability of MRE to transcend into an alternative to conventional elastomers depends on the understanding of its strain dependent characteristics under active as well as the passive state.

The viscoelastic material modeling approaches simplify the overall material characterization process of MRE. This semi-physical modeling approach is beneficial as it reduces the amount of experimental tests substantially and saves time and cost. The fractional order and integer order based models effectively portray the viscoelastic properties of MRE between 8 Hz-24 Hz by considering the experimental

response corresponding to 8 Hz, 16 Hz and 24 Hz. The accuracy of the viscoelastic model depends on its ability to reproduce the variation of experimentally evaluated damping characteristics (K'').

Predicted stiffness and damping characteristics of the model depend upon the effectiveness of the parameter optimization process in reproducing the experimental results. The difference arising from the parameter optimization process carried over during the interpolation process, and it reflected on the predictive accuracies of the viscoelastic model. The realistic assessment of the model performance is based upon its ability to map the results obtained from the optimized parameters.

Compared to 2 Maxwell model, the fractional Maxwell model is more versatile in describing the dynamic viscoelastic properties of MRE. Existence of a fractional order element in fractional Maxwell model simplifies the interpolation function to reproduce the frequency dependent viscoelastic behavior of MRE at intermediate frequencies. This modeling approach describes the viscoelastic behavior with fewer number parameters and thus abridges the process of objective function minimization without compromising the predictive accuracy. The fractional Maxwell model is more accurate than the 2-Maxwell model due to reduced error propagation. Moreover, the parameters of the fractional Maxwell chain in the fractional order model have a greater influence on the predicted K' and K''. This characteristic of fractional Maxwell is beneficial in identifying the critical parameter and representing it with a better interpolating function to improve the predictive accuracy.

The amplitude dependency in the transition region can be effectively represented by coupling the conventional viscoelastic model with the linearized Bouc-Wen element. This model efficiently portrays the frequency, magnetic field and

amplitude behavior of MRE. The proposed model effectively predicted the stiffness characteristics with accuracy more than 94.3% and the corresponding accuracy in predicting the damping characteristic is above 90.1%. This model is capable of fitting the experimental value with a fitness value of more than 93.22%. Moreover, the variation in the model parameters is represented by a planar function, which simplifies the control strategies to realize the MRE based device.

8.3 Impact of this study and direction for further research

In this study, the dynamic viscoelastic properties of MRE under different operating conditions like frequency, magnetic field and input strain are evaluated through dynamic blocked transfer stiffness method. This method offers a simple and economical approach for characterizing the properties of MRE. Present study has highlighted the significance of the operating parameters and the need for incorporating these aspects during the design stage of MRE based device. The present investigation also revealed the importance of LVE limit and its dependency on the operating condition. LVE limit of the MRE can be enhanced by modifying the interaction between the matrix and fillers. This can be achieved by the addition of an additive, which could be a scope for further work. Moreover, additives improve the properties of MRE and it also enables to have a better control over its stiffness and damping characteristics.

The material modeling of MRE by adopting viscoelastic modeling approach is an effective way to reduce the effort of performing the experimental based characterization studies. The material model based on fractional order viscoelasticity has better flexibility in predicting the properties than the integer order based model.

This modeling approach can be extended to model the dynamic behavior of a MRE based isolator or absorber devices to tune it over a wide frequency range.

The generalized expression for the translation stiffness represents the response of MRE under varying frequency, magnetic field and amplitude (under tested range). However, apart from these factors, the thickness of MRE is also an important parameter. As the thickness is increased, the magnetic flux distribution varies. As a result, the field sensitive properties are altered. Moreover, under the operating environment, MRE is also subjected to the static preload. This preloaded state alters the distance between particles, which in turn affect the field sensitive properties. Therefore, incorporating the geometry and the preload effects in the mathematical representation of MRE is an important aspect which can be a scope for future work.

To realize a beam on MRE on a boundary support, the rotational stiffness of MRE needs to be modeled. To represent these characteristics mathematically, the approaches followed for dynamic compression characteristics need to be performed. Using the mathematical relations of rotational and translation stiffness, the dynamic characteristics of a beam can be modeled. By implementing proper control strategies, the dynamic behavior of a beam on MRE boundary support can be modified in response to the external disturbing source. Later, this approach can be extended to realize a plate on MRE boundary support.

8.4 Contributory effect on the design process of a MRE device

MRE is a potential material to realize the concept of semi-active vibration mitigation device. The success of MRE based device relies on the understanding of the material properties. The experimental based approach is more effective as the properties can be evaluated at different

operating condition. However, these approaches are complex in terms of number of variable and this process can be simplified by adopting a material modelling technique.

The shear mode and the translation or compression mode are the commonly used configurations in a MRE based device. The translation mode is most widely used as its exhibits a high load bearing capacity. Moreover, for viscoelastic boundary damping applications, the translation stiffness is critical as it controls the transition of boundary support conditions. The translation status of loading is not an ideal configuration to characterize the viscoelastic properties as it fails to satisfy the volume preserving state of deformation. On the contrary, the shear mode is most effective in characterizing the properties of filled rubber under different dynamic loading to rheological elastomer. However, the conversions of viscoelastic properties of MRE between the shear mode to translation mode are not accurate as the mechanism of interaction between the fillers are the matrix are distinctly different.

The translation stiffness of MRE is a function of frequency, magnetic field, strain, preload and the temperature. The preload and the temperature effects can be neglected for the devices operating under room temperature and subjected to lighter pre-compression. For semi-active control applications, the material behavior should be represented in a mathematical form. Most often viscoelastic constitutive relations are used for mathematical modelling of MRE. However, the fractional derivative order viscoelastic relation is more convenient to simulate the behavior of a filled rubber. The semi-empirical model based on theory of viscoelasticity demands experimental results to obtain the model parameters of the model. These parameters vary with the input conditions, and it needs to be generalized using polynomial equations. A linear variation is most preferred as it simplifies the control algorithm.

However, models based on viscoelastic relations can only represent the frequency and the magnetic field dependency. The amplitude dependency behavior is incorporated

in the model by including the hysteresis components. The Bouc-Wen element more versatile as it simulates the strain hardening and strain softening phenomenon effectively. However, under moderate strain levels a stochastically linearized Bouc-Wen element can be coupled with the viscoelastic model to represent dynamic viscoelastic behavior of MRE at varying operating conditions. A good model should be able to represent the material response of MRE with fewer parameters over a wide range of operating conditions in a simple form.

REFERENCES

Aho, J. (2011). *Rheological characterization of polymer melts in shear and extension: Measurement reliability and data for practical processing*. Doctoral Theses, Tempere University of Technology.

Aga, Z. and Faidley, L. (2008). "Characterization of the magnetostriction of magnetorheological elastomers." Proceedings of *SMASIS*. 1, 447–52.

Aishah, S. et al. (2016). "Effects of multiwall carbon nanotubes on viscoelastic properties of magnetorheological elastomers." *Smart Materials and Structures*, 25, 77001.

Aloui, S. and Klüppel, M. (2015). "Magneto-rheological response of elastomer composites with hybrid-magnetic fillers." *Smart Materials and Structures*, 24(2), 25016.

Alkhatib, F.(2013). *Techniques for Engine Mount Modeling and Optimization*.Theses and Dissertations. University of Wisconsin Milwaukee.

ASTM standard E756-04, Standard Test Method for Measuring Vibration-Damping Properties of Materials.

Ausanio, G., Hison, C.L., Iannotti, Iannotti, V and Lanotte, L. (2011) " Magneto-piezoresistance in elastomagnetic composites." *Journal of Applied Physics*, 110, 063903.

Basdogon, I. and Dikmen, E. (2011). "Modelling viscoelastic response of vehicle door seal." *Experimental techniques*, 35, 29-35.

Bagley, R. L. and Torvik, P. J. (1983). "A Theoretical Basis for the Application of Fractional Calculus to Viscoelasticity." *Journal of Rheology*, 27, 201–210.

Bednarek, S. (1999). "The giant magnetostriction in ferromagnetic composites within an elastomermatrix." *Applied Physics A Materials Science & Processing*. 68, 63–67.

Behrooz, M., Wang, X. and Gordaninejad, F. (2014). "Performance of new magnetorheological elastomer isolation system." *Smart Materials and Structures*, 23, 045014.

Behrooz, M. et al. (2015). "Behavior of magnetorheological elastomers with coated particles.", *Smart Materials and Structures*,24(3), 35026.

Berg, M.(1997). "A model for rubber springs in the dynamic analysis of rail vehicles." *Proceedings of the Institution of Mechanical Engineers - Part F -Journal of Rail & Rapid Transit*. 211, 95-108.

Berg, M. and Kari, L. (2003). "Nonlinear Isolator Dynamics at Finite Deformations: An Effective Hyperelastic, Fractional Derivative, Generalized Friction Model." *Nonlinear Dynamics,* 33, 323–336.

Bica, I., Anitas, E. M., Bunoiu, M., Vatzulik, B. and Juganaru, B. (2014). " Hybrid magnetorheological elastomer: Influence of magnetic field and compression

pressure on its electrical conductivity." *Journal of Industrial and Engineering Chemistry*. 20, 3994–3999.

Boczkowska, A. and Awietjan, S. F. (2009). "Smart composites of urethane elastomers with carbonyl iron." *Journal of Materials Science,* 44, 4104–4111.

Boczkowska, A., Awietjan, S. F., Pietrzko, S., Kurzydłowski, K. J.(2012). "Mechanical properties of magnetorheological elastomers under shear deformation." *Composites: Part B*. 43, 636–640.

Borin, D. Y., Stepanov, G. V. and Odenbach, S. (2013). "Tuning the tensile modulus of magnetorheological elastomers with magnetically hard powder." *Journal of Physics: Conference Series*, 412 , 012040.

Bose, H. and Roder, R. (2009) " Magnetorheological Elastomers with High Variability of Their Mechanical Properties." *Journal of Physics: Conference Series*, 149, 012090.

Bossis,G., Abbo, C., Cutillas,S., Lacis S. and Metayer, C. (2001). " Electroactive and electrostructured elastomers." *International Journal of Modern Physics B*, 15, 564-573.

Brown, R.P. (1996). *Physical Testing of Rubber*. Chapman & Hall,2-6 Boundary Row, London, 144-150.

Bruni, S. and Collina, A. (2000). "Modelling the Viscoelastic Behaviour of Elastomeric Components: An Application to the Simulation of Train-Track Interaction." *Vehicle System Dynamics*, 34(4), 283–301.

Caterino, N., Azmoodeh, M. B. and Occhiuzzi, A. (2014). "Mediumto long term behavior of MR dampers for structural control." *Smart Materials and Structures*. 23, 117005.

Carboni, B. and Lacarbonara, W. (2015). "Dynamic Response of Nonlinear Oscillators With Hysteresis." *Proceedings of the ASME 2015 International Design Engineering Technical Conferences & Computers and Information in Engineering Conference*. doi:10.1115/DETC2015-46352

Chazeau, L. et al. (2000). "Modulus recovery kinetics end other insights into the Payne effect for filled elastomers." *Polymer Composites*, 21(2), 202–222.

Chen, D., Yu, M., Zhu, M., et al. (2016). "Carbonyl iron powder surface modification of magnetorheological elastomers for vibration absorbing application." *Smart Materials and Structures*, 25(11):115005.

Chen, L., Gong, X. L. and Li, W. H. (2007a). "Microstructures and Viscoelastic Properties of Anisotropic Magnetorheological Elastomers." *Smart Materials and Structures*, 16(6), 2645–0.

Chen, L., Gong, X.L., Jiang, W., Yao, J., Deng, H. and Li, W. (2007b). " "Investigation on Magnetorheological Elastomers Based on Natural Rubber." *Journal of Materials Science* 42, 5483–5489.

Chen, L., Gong, X. L. and Li, W. H., (2008a) "Damping of magnetorheological elastomers." *Chinese Journal of Chemical Physics*, 21(6):581-585.

Chen, L., Gong, X. L. and Li, W. H., (2008b). “Effect of carbon black on the mechanical performances of magnetorheological elastomers.” *Polymer testing*, 27, 340-345.

Chen, L. and Jerrams, S. (2011). "A Rheological Model of the Dynamic Behaviour of Magnetorheological Elastomers." *Journal of Applied Physics*, 110, 013513 (2011).

Chen, Y. and Xu, C. (2011). "Specific nonlinear viscoelasticity behaviors of natural rubber and zinc dimethacrylate composites due to multi-crosslinking bond interaction by using rubber process analyzer 2000." *Polymer Composites*, 32, 1593–1600.

Cesmeci, Ş. and Engin, T. (2010). "Modeling and testing of a field-controllable magnetorheological fluid damper." *International Journal of Mechanical Sciences*, 52(8), 1036–1046.

Collette,C., Kroll, C., Saive, G., Guillemier, V. and Avraam, M. (2010). " On Magnetorheologic Elastomers for Vibration Isolation, Damping, and Stress Reduction in Mass-varying Structures *Journal of Intelligent Material Systems and Structures*, 21,1463–1467.

Collyer, A. A. and Clegg, D. W. (1998). *Rheological measurement*. 2nd edition. Chapman & Hall, London, 1998, 327-353.

Cosson, P. and Michon, C.J. (1996). " Identification by a non-integer order model of the mechanical behaviour of an elastomer." *Chaos, Solitons & Fractals*, 7(11), 1807-1824.

Cho, K. S., Hyun K, Ahn, K. H. and Lee S. J. (2005). “A geometrical interpretation of large amplitude oscillatory shear response.” *Journal of Rheology*, 49, 747–758.

Cho, H. J. and Youn, S. K. (2006). "A viscoelastic constitutive model of rubber under small oscillatory load superimposed on large static deformation considering the Payne effect." *Archive of Applied Mechanics*, 75, 275–288.

Christensen, R. M. (1982). *Theory of viscoelasticity—An introduction* (2nd ed.). New York: Academic Press.

Damiani, R. and Sun, L. Z. (2016). “Microstructural characterization and effective viscoelastic behavior of magnetorheological elastomers with varying acetone contents.” *International Journal of Damage Mechanics*, DOI: 10.1177/1056789516657676.

Demchuk, S. A. and Kuz’min, V. A. (2002). ”Viscoelastic properties of magnetorheological elastomers in the regime of dynamic deformation.” *Journal of Engineering Physics and Thermophysics*, 75(2), 104–107.

Davis, L. C. (1999). "Model of magnetorheological elastomers." *Journal of Applied Physics*, 85(6), 3348–3351.

Deshpande, A. P., Krishnan, J. M. and Kumar, S. (2010). *Rheology of Complex Fluids*. Springer.

Dong, X., Ma, N. Qi, M., Li, J., Chen, R. and Qu, J.(2012). "The pressure-dependent MR effect of magnetorheological elastomers." *Smart Materials and structures*, 21, 075014.

Du, G. and Chen, X. (2012). "MEMS magnetometer based on magnetorheological elastomer. Measurement." 45,54–58.

Eem, S. H., Jung, H. J. and Koo, J. H. (2012). "Modeling of magneto-rheological elastomers for harmonic shear deformation." *IEEE Transactions on Magnetics*. 48(11), 3080–3083.

Eldred, B. L. et al. (1995). " Kelvin-Voigt vs fractional derivative model as constitutive relations for viscoelstic materials." *AIAA Journal*, 33(3), 547-550.

Emri, I. and Gergesova, M. (2010). "Time-dependent behavior of solid polymers. In: Gallegos, C. (ed.) Encyclopedia of Life Support Systems (EOLSS)." *Rheology*, 1, 247–330.

Ewoldt, R. H., Hosoi, A. E. and Mckinley, G. H.(2010). "New measures for characterizing nonlinear viscoelasticity in large amplitude oscillatory shear." *Journal of Rhoelogy*, 52:1427-1458.

Fan,R., Meng, G., Yang, M. J. and He, C. (2009). "Experimental study of the effect of viscoelastic damping materials on noise and vibration reduction within railway vehicles ." *Journal of Sound and Vibration*, 319, 58–76.

Fan, Y. C. et al. (2011). "Interfacial friction damping properties in magnetorheological elastomers." *Smart Materials and Structures*, 20(3),35007.

Fan, Z.J., Lee, J. H., Kang, K. H. and Kim, K. J. (1998). "The forced vibration of a beam with viscoelastic boundary supports." *Journal of sound and vibration*, 210(5), 673-682.

Fay J. J., C. J. Murphy, D. A. Thomas and L. H. Sperling,1991, Effect of Morphology, Crosslink Density, and Miscibility on Interpenetrating Polymer Network Damping Effectiveness, Polymer Engineering and Science, 31,1734-1741.

Filipcsei G., Csetneki I., Szilágyi A., Zrínyi M.,(2007). " Magnetic Field-Responsive Smart Polymer Composites." *Advances in Polymer Science*. (2007), 206, 137–189.

Figliola, R. S. and Beasley, D. E.(1995). *Theory and Design for Mechanical Measurements,* Wiley, New York.

Franchek, M. A., Ryan, M. W. and Bernhard, R. J. (1995). "Adaptive Passive Vibration Control." *Journal of Sound and Vibration,* 189, 565-585.

Foliente, C.G., Singh, M. P.and Noori, M. N. (1996). "Equivalent linearization of generally pinching Hysteretic, degrading systems." *Earthquake engineering and structural dynamics*, 25, 611-629.

Fu, J., Zheng, X., Yu, M., Ju, B. X.,(2013). "A New Magnetorheological Elastomer Isolator in Shear -Compression Mixed Mode. *IEEE/ASME International Conference on Advanced Intelligent Mechatronics*, Wollongong, Australia.

Fuente, J. L. et al. (2002*).* "Viscoelastic behaviour in a Hydroxyl-Terminated Polybutadiene gum and its highly filled composites: Effect of the type of filler on the relaxation process." *Journal of applied polymer science,*88,1705-1712.

Funt, J. M. (1988). "Dynamic Testing and Reinforcement of Rubber." *Rubber Chemistry and Technology*, 61, 842-865.

Furst, E. M. and Gast, A. P. (2000). "Micromechanics od magnetorheoogical suspensions." *Physical Review E*, 61(6), 6732-6739.

Gade, S. et al. (1994). "Damping measurements – from impulse response functions – from resonance and non-resonance excitation techniques."*Tech Rev,* 2, 28–44.

García Tárrago, M. J. et al. (2007). "Torsion stiffness of a rubber bushing: a simple engineering design formula including the amplitude dependence." *The Journal of Strain Analysis for Engineering Design*, 42, 13–21.

Gauthier , C. et al. (2004). " Analysis of the non-linear viscoelastic behaviour of silica filled styrene butadiene rubber." *Polymer*, 45, 2761–2771.

Garnier, P. et al.(2013). "The influence of cyclic loading conditions on the viscoelastic properties of filled rubber." *Mechanics of Materials*, 56 , 84–94.

Ge,L., Fan, Y. and Xuan, S. (2013). "Preparation and mechanical properties of the magnetorheological elastomer based on natural rubber/rosin glycerin hybrid matrix." *Smart Materials and structures,* 22, 115029.

Ginder, J. M., Clark, S. M., Schlotter, W. F. and Nichols, M. E. (2002). "Magnetostrictive Phenomena in Magnetorheological Elastomers." *International Journal of Modern Physics B*, 16, 2412-2418.

Ginic, M et al.(2000). " Viscoelastic behaviour of filled, and unfilled, EPDM elastomer." *Thermomechanica Acta*, 357, 211-216.

Gil-Negrete, N., Viñolas, J. and Kari, L. (2006). "A simplified methodology to predict the dynamic stiffness of carbon-black filled rubber isolators using a finite element code." *Journal of Sound and Vibration*, 296(4–5), 757–776.

Gil-Negrete, N., Vinolas, J. and Kari, L. (2009). "A Nonlinear Rubber Material Model Combining Fractional Order Viscoelasticity and Amplitude Dependent Effects." *Journal of Applied Mechanics*, 76(1), 11009.

Giaralis, A and Spanos, P. D. (2013). "Derivation of equivalent linear properties of Bouc-Wen hysteretic systems for seismic response spectrum analysis via statistical linearization." *10th HSTAM International Congress on Mechanics* Chania, Crete, Greece.

Glenn, E W. (1963). "Dynamic Strain Effects in Elastomers." *rubber chemistry technology*, 36, 407-421.

Gong, X. L., Zhang, X.Z., and Zhang, P. Q. (2005). "Fabrication and characterization of isotropic magnetorheological elastomers." *Polymer Testing,* 24, 669–676.

Gong, X.L., Chen, L. and Li, J. F. (2007). "Study of Utilizable Magnetorheological Elastomers." *International Journal of Modern Physics*, 16(2), 337–351.

Gong, X. L., Xu, Y., Xuan, S., Guo, C. and Zong, L. (2012a). "The investigation on the nonlinearity of plasticine-like magnetorheological material under oscillatory shear rheometry" Journal of Rheology, 56(6), 1375-1391.

Gong, X, Fan,Y, Xuan, S., Xu, Y., and Peng, Chao. (2012b). "Control of the Damping Properties of Magnetorheological Elastomers by Using Polycaprolactone as a Temperature-Controlling Component." *Industrial and Engineering Chemistry Research*, 51(18), 6395–6403.

Gordaninejad, F., Wang, X. and Mysore, P. (2012). "Behavior of thick magnetorheological elastomers." *Journal of Intelligent Material Systems and Structures*, 23(9), 1033–1039.

Greco, R., Marano, G.C. and Mezzina, M. (2001). "The Performance of HDRB Devices in Base Isolation: a Stochastic Sensitivity Analysis." *Journal of Structural Control*, 8(2), 203-217.

Guan, X. C., Dong, X. F. and Ou, J. P. (2008). "Magnetostrictive effect of magnetorheological elastomer." *Journal of Magnetism and Magnetic Materials*. 320, 158–63.

Guo F, Du C, Li R (2014) Viscoelastic Parameter Model of Magnetorheological Elastomers Based on Abel Dashpot. *Advances in Mechanical Engineering* 629386.

Han, Y., Hong, W. and Faidley, L. E. (2013), "Field-stiffening effect of magneto-rheological elastomers." *International Journal of Solids and Structures*, 50, 2281–2288.

Hegde, S., K . Kiran, K. V. Gangadharan , 2014, A novel approach to investigate effect of magnetic field on dynamic properties of natural rubber based isotropic thick magnetorheological elastomers in shear mode, *Journal of Central South University of Technology* , 21, 2612−2619.

Heinrich, G and Vilgis, T.A. (1995). " Effect of filler networking on the dynamic mechanical properties of crosslinked polymer solids." *Macromolecule symposium*, 93, 253-260.

Hofer, P. and Lion, A (2009). "Modelling of frequency- and amplitude-dependent material properties of filler-reinforced rubber." *Journal of the Mechanics and Physics of Solids*, 57, 500–520.

Hu, G., Guo, M., Li, W., Du, H. and Allici, G. (2011a). "Experimental investigation of the vibration characteristics of a magnetorheological elastomer sandwich beam under non-homogeneous small magnetic fields." *Smart Materials and Structures,* 20, 127001.

Hu. S, Chen, W. and Gou, X. (2011b). "Modal analysis of fractional derivative damping model of frequency-dependent viscoelastic soft matter." *Advances in Vibration Engineering*, 10, 187–196.

Hu, W. and Wereley, N. M. (2007). "Distributed Rate-Dependent Elastoslide Model for Elastomeric Lag Dampers." *Journal of Aircraft*, 44(6), 1972–1984.

Hu, Y. et al. (2005). "New Magnetorheological Elastomers Based on polyurethane/Si-Rubber Hybrid." *Polymer Testing*, 24(3), 324–29.

Huang, X. G., Yan, Z. Y., Liu, C. Li, G. H. and & Wang, J. (2015). "Study on the resistance properties of magnetorheological elastomer." *Materials Research Innovations*, 19, 924 -928.

Hurtado, J. E. and Barbat, A. H. (2000). "Equivalent linearization of the Bouc-Wen hysteretic model." *Engineering Structures*, 22(9), 1121–1132.

Ikhouane, F. and Rodellar, J. (2007). *Systems with Hysteresis Analysis, Identification and Control using the Bouc–Wen Model.* John Wiley & Sons Ltd.

Ismail, R. et al. (2016). "Dynamic mechanical behavior magnetorheological nanocomposites containing CNTs: A review." *AIP Conference Proceedings*, 1733. doi: 10.1063/1.4948878.

Ismail, M., Ikhouane, F. and Rodellar, J. (2009). "The hysteresis Bouc-Wen model, a survey." *Archives of Computational Methods in Engineering*, 16(2), 161–188.

ISO 10846-1:2008 Acoustics and vibration-Laboratory measurement of vibro-acoustic transfer properties of resilient elements-Part 01: principles and guidelines.

ISO 10846-2:2008 Acoustics and vibration-Laboratory measurement of vibro-acoustic transfer properties of resilient elements-Part 02: dynamic stiffness of elastic supports for translator motion-direct method.

ISO 10846-3:2008 Acoustics and vibration-Laboratory measurement of vibro-acoustic transfer properties of resilient elements-Part 02: dynamic stiffness of elastic supports for translator motion-indirect method.

Jalili, N. (2002). " A Comparative Study and Analysis of Semi-Active Vibration-Control Systems." *Journal of Vibration and Acoustics*, 124, 593-605.

Jian-feng, L. and Gong, X.L. (2009). "Dynamic damping property of magnetorheological elastomer ." *Journal of Central South University*, 15, 261−265.

Jin, Q. et al. (2014). "Influence of the Particle Size on the Rheology of Magnetorheological Elastomer." *Materials Science Forum*, 809–810, 757–763.

Jolly, M. R., J., Carlson, D. B., Muñoz, C and Bullions, T. A. (1996). "The Magneto viscoelastic Response of Elastomer Composites Consisting of Ferrous Particles Embedded in a Polymer Matrix". *Journal of intelligent material systems and structures*, 7, 613-622.

Jolly, M. R., Carlson, J. D. and Muñoz, B. C. (1999). "A model of the behaviour of magnetorheological materials." *Smart Materials and Structures*, 5(5), 607–614.

Jong, L. (2005). " Viscoelastic properties of Ionic polymer composites reinforced by Soy protein isolate." *Journal of Polymer Science Part B: Polymer Physics,* 43, 3503–3733.

Jrad, H. et al. (2013). "Experimental Characterization, Modeling and Parametric Identification of the Hysteretic Friction Behavior of Viscoelastic Joints." *International Journal of Applied Mechanics*, 5(2), 1350018.

Ju, B. et al. (2015). "Temperature-Dependent Dynamic Mechanical Properties of Magnetorheological Elastomers under Magnetic Field." *Journal of Magnetism and Magnetic Materials*, 374, 283–88.

Ju, B. X., Yu, M., Fu,J., Yang, Q., Liu, X. Q. and Zheng, X. (2012). "A novel porous magnetorheological elastomer preparation and evaluation." *Smart Materials and Structures*.,21, 035001.

Jung, H.-J. et al. (2009). "Dynamic Characterization of Magneto-Rheological Elastomers in Shear Mode." *IEEE Transactions on Magnetics*, 45(10), 3930–3933

Kaleta, J., Krolewicz, M. and Lewandowski, D. (2011). "Magnetomechanical properties of anisotropic and isotropic magnetorheological composites with thermoplastic elastomer matrices." *Smart Materials and Structures*, 20, 085006.

Kalfus, J and Jancar, J. (2007). "Viscoelastic response of nanocomposite poly(vinyl acetate)-hydroxyapatite with varying particle shape—dynamic strain softening and modulus recovery." Polymer Composites, 28, 743-747.

Kallio, M. 2005. "The elastic and damping properties of magnetorheological elastomers." *PhD Thesis* VTT, Finland.

Kallio, M. et. al (2007). "Dynamic compression testing of a tunable spring element consisting of a magnetorheological elastomer." *Smart Materials and Structures*. 16, 506–514.

Kang, K.H. and Kim, K.(1996). " Modal properties of beams and plates on resilient supports with rotational and translational complex stiffness ." *Journal of Sound and Vibration.* 190(2), 207-220.

Kashima, S., Miyasaka, F. and Hirata, K. (2012). "Novel Soft Actuator Using Magnetorheological Elastomer." *IEEE Transactions on Magnetics*, 48(4), 1649–1652.

Kchit, N and Bossis, G. (2009). " Electrical resistivity mechanism in magnetorheological elastomer." *Journal of Physics D: Applied Physics*. 42, 105505.

Khairi, M. H. A. et al. (2016). "Effect of Sucrose Acetate Isobutyrate Ester on the Epoxidised Natural Rubber Based Magnetorheological Elastomers." *Journal of Physics: Conference Series*, 776:12034.

Kim, S. Y. and Lee, D.H. (2009). "Identification of fractional-derivative-model Parameters of viscoelastic materials from measured FRFs." *Journal of Sound and Vibration,* 324, 570–586.

Koblar ,D. and Boltezar, M. (2013) "Evaluation of the frequency-dependent Young's modulus and damping factor of rubber from experiment and their

implementation in a finite-element analysis.” *Experimental Techniques*, DOI: 10.1111.

Koh, C.G. and Kelly, J.M. (1990). "Application of fractional derivatives to seismic analysis of base isolated models." *Earthquake Engineering and Structural Dynamics*, 19, 229-241.

Koo, J. H., Khan, F., Jang,D., and Jung, H. (2010) "Dynamic characterization and modeling of magneto-rheological elastomers under compressive loadings." *Smart Materials and Structures*. 19, 115026.

Koo, J. H., Dawson, A. and Jung, H. J. (2012). "Characterization of actuation properties of magnetorheological elastomers with embedded hard magnetic particles." *Journal of Intelligent Material Systems and Structures*, 23,1049-1054.

Koutsawa, Y. and Daya, E. M. (2007)."Static and free vibration analysis of laminated glass beam on viscoelastic supports." *International Journal of Solids and Structures*. 44 , 8735–8750.

Kramarenko, E. Y., Chertovich, A. V., Stepanov, G.V., Semisalova., Makarova, L.A., Perov, N.S. and Khokhlov, A. R. (2015)." Magnetic and viscoelastic response of elastomers with hard magnetic filler." *Smart Materials and Structures*, 24, 035002.

Lakes, R. (2009). *Viscoelastic Materials*. Cambridge university press.

Lejon, J. and Kari, L. (2009). “Preload, frequency, vibrational amplitude and magnetic field strength dependence of magnetosensitive rubber.” *Plastics, Rubber and Composites*, 38(8), 321–326.

Lectez, A.S. and Verron, E. (2016). “Influence of large strain preloads on the viscoelastic response of rubber-like materials under small oscillations.” *International Journal of Non-Linear Mechanics,* 81,1–7.

Leng, D. et al (2015). “The dynamic performance of magnetic-sensitive elastomers under impact loading.”*Smart Materials and structures,* **24**,045023.

Le´opolde`s, J. et al. (2002). "Influence of Filler–Rubber Interactions on the Viscoelastic Properties of Carbon-Black-Filled Rubber Compounds. " *Journal of Applied Polymer Science*, 91, 577–588.

Lewandowski, R. and Chorążyczewski, B. (2007). “Remarks on modelling of passive viscoelastic dampers.” *9th International Conference* , Vilnius, Lithuania.

Lewandowski, R. and Chorazyczewski, B. (2010). "Identification of the parameters of the Kelvin–Voigt and the Maxwell fractional models, used to modeling of viscoelastic dampers." *Computers and Structures*, 88, 1–17.

Liao, G. J., Gong, X., Xuan, S., Guo, C. and Zong, L. (2012). " Magnetic-field-induced normal force of magnetorheological elastomer under compression status." *Industrial & Engineering Chemistry Research,* 51, 3322–3328.

Lijun, Z., Zengliang, Y. and Zhuoping, Y. (2010). "Novel Empirical Model of Rubber Bushing in Automotive Suspension System." *Proceedings of ISMA*, 20-22 September, No. 0170, 2010.

Li, R. and Sun, L. Z. (2011). "Dynamic mechanical behavior of magnetorheological nanocomposites filled with carbon nanotubes." *Applied Physics Letters*, 99, 2012–2015.

Li, W., Kostidis, K., Zhang, X. and Zhou, Y. (2009). " Development of a Force Sensor Working with MR Elastomers." *IEEE/ASME International Conference on Advanced Intelligent Mechatronics*.

Li, W., Zhou, Y., Tian, T and Alici, G. et al. (2010a). "Creep and recovery behaviors of magnetorheological elastomers". *Frontiers in Mechanical Engineering*, 5, 341–346.

Li, W. H., Zhou, Y. and Tian, T.F, (2010b). "Viscoelastic properties of MR elastomers under harmonic loading." *Rheologica Acta*, 49, 733–740.

Li, W., Zhang, X. and Du, H. (2012). "Development and simulation evaluation of a magnetorheological elastomer isolator for seat vibration." *Journal of Intelligent Material Systems and Structures*, 23(9) 1041–1048.

Li Y, Li J, Li W and Samali, B (2013) Development and characterization of a magnetorheological elastomer based adaptive seismic isolator. *Smart Materials and Structures*, 2013, 22:035005.

Lin T.R., Farag, N. H., Pan, P.(2003). "Evaluation of frequency dependent rubber mount stiffness and damping by impact test." *Applied Acoustics*, 66, 829–844.

Lion, A. and Kardelky, C. (2004). "The Payne effect in finite viscoelasticity: constitutive modelling based on fractional derivatives and intrinsic time scales." *International Journal of Plasticity*, 20, 1313–1345.

Liu, Y., Matsuhisa H and Utsuno H. (2008). "Semi-active vibration isolation system with variable stiffness and damping control." *Journal of Sound and Vibration*, 313 , 16–28.

Lockette, P., Lofland, S. E., 2, Biggs, J., Roche, J., Mineroff, J. and Babcock, M. (2011) "Investigating new symmetry classes in magnetorheological elastomers: cantilever bending behavior." *Smart Materials and Structures*, 20, 105022.

Lokander, M. and B. Stenberg, 2003a, "Performance of isotropic magnetorheological rubber materials." *Polymer Testing*, 22, 245–51.

Lokander, M. and Stenberg, B. (2003b). "Performance of Isotropic Magnetorheological Rubber Materials." *Polymer Testing*, 22(6), 677–80.

Love, J. S., Tait, M. J. and Toopchi-Nezhad, H. (2011). "A hybrid structural control system using a tuned liquid damper to reduce the wind induced motion of a base isolated structure." *Engineering Structures*, 33(3), pp. 738–746.

Lu, X. S. et al. (2012). "Mechanical and structural investigation of isotropic and anisotropic thermoplastic magnetorheological elastomer composites based on

poly(styrene-b-ethylene-co-butylene-b-styrene) (SEBS).” *Rheologica Acta,* 51, 37–50.

Luo, W. et al. (2010). ‘Frequency and strain amplitude dependent dynamic mechanical properties and hysteresis loss of CB filled vulcanlized natural rubber.” *International Journal of Mechanical Sciences.* 52, 168-174.

Malecki, P. et al. (2015). “Dynamic mechanical analysis of magnetorheological composites containing silica-coated carbonyl iron powder.” *Journal of Intelligent Material Systems and Structures*, 26(14), 1899–1905.

Malecki, P. et al. (2016). "Influence of carbonyl iron particle coating with silica on the properties of magnetorheological elastomers." *Smart Materials and Structures*, 25, 105030.

Mallik, A.K., Kher, V., Puri, M. and Hatwal, H. (1999). "On the modeling of non-linear elastomeric vibration isolators." *Journal of Sound and vibration*, 219, 239–53.

Makris, N. and Constantinou, M. (1991). "Fractional-derivative maxwell model for viscous dampers." *Journal of Structural Engineering*, 117(9), 2708-2724.

Marano, G. C. and Greco, R. (2003). "Efficiency of base isolation systems in structural seismic protection and energetic assessment." *Earthquake Engineering and Structural Dynamics*, 32(10), pp. 1505–1531.

Makris, N. and Constantinou, M. (1991). "Fractional-derivative maxwell model for viscous dampers." *Journal of Structural Engineering*, 117(9), 2708-2724.

Markovitz, H. (1977). “Boltzmann and the beginnings of linear viscoelasticity.” *Transactions of The Society of Rheology*, 21(3):381-398.

Martinelli, B. and Augusto E.(2005). “*Rubber bearings for precision positioning systems*.” M.S. Thesis, Massachusetts Institute of Technology.

McConnel, K.G. (1995). “*Vibration testing theory and practice.”* John Wiley & Sons, Inc.

Menard, P.H (2008). *Dynamic Mechanical Analysis, A Practical Introduction*, Second Edition, Taylor & Francis Group. NW.

Medalia, A. I. (1978). “ Effect of carbon black on dynamic properties of rubber vulcanizates.” *Rubber Chemistry and Technology*, 51, 437-523.

Melenev, P., Raikher,R., Stepanov, G., Rusakov, V. and Polygalova, L. (2011). "Modeling of the Field-Induced Plasticity of Soft Magnetic Elastomers." *Journal of Intelligent Material Systems and Structures*, 22, 531-538.

Meral, F. C., Royston, T. J. and Magin, R. (2010). "Fractional calculus in viscoelasticity: An experimental study." *Communications in Nonlinear Science and Numerical Simulation*. 15(4), pp. 939–945.

Molchanov, et al. (2014). " Viscoelastic Properties of Magnetorheological Elastomers for Damping Applications." *Macromolecular Matererials and Engineering*, DOI: 10.1002/mame.201300458.

Nakra, B. C.(1998). "Vibration control in machines and structures using viscoelastic damping." *Journal of Sound and Vibration* . 211(3), 449-465

Nadeau. S, and Champoux, Y. (2000). "Application of the direct complex stiffness method to engine mounts." *Experimental techniques*, 21–23.

Nakra, B. C.(2000). " Structural dynamic modification using additive damping." *SADHANA*, 25(3), 277-289.

Nakara, B. C.(2001) " Vibration damping." *PINSA*, 67(4 &5), 461-478.

Nikitin, L.V., Stepanov, G.V. , Mironova, L.S.and Gorbunov, A.I. (2004). "Magnetodeformational effect and effect of shape memory in magnetoelastics." *Journal of Magnetism and Magnetic Materials*, 272–276, 2072–2073.

Ng,T. S. K., McKinley, G. H. and Ewoldt, R. H. (2010). "Large amplitude oscillatory shear flow of gluten dough: A model power-law gel." *Journal of Rhoelogy*, 54, 627-654.

Noll, S., Dreyer, J. and Singh, R.(2014). "Complex eigensolutions of coupled flexural and longitudinal modes in a beam with inclined elastic supports with non-proportional damping."*Journal of Sound and Vibration*. 333, 818–834.

Norouzi M et al. (2015). "A new approach for modeling of magnetorheological elastomers." *Journal of Intelligent Material Systems and Structures.* 27:1121–1135.

Olabide, I. A., Berasategui, J., . Elejabarrieta, M. J. and Ali,M.M.B. (2014). "Characterization of the linear viscoelastic region of magnetorheological elastomers." *Journal of Intelligent Material Systems and Structures*, 25, 2074–2081.

Ooi, L. E. and Ripin, Z. M. (2011). "Dynamic stiffness and loss factor measurement of engine rubber mount by impact test." *Materials and Design*, 32, 1880–1887.

Özkaya, N. and Nordin, M.(1998). *Fundamentals of biomechanics*. New York, Springer.

Osman, M.A. and Atallah, A. (2006). "Effect of the particle size on the viscoelastic properties of filled polyethylene." *Polymer*, 47, 2357-2368.

Padalka, O., Song, H. J., Wereley, N. M., File, J. A. and Bell, R. C. (2010)."Stiffness and Damping in Fe, Co, and Ni Nanowire-Based Magnetorheological Elastomeric Composites."*IEEE Transactions on Magnetics*, 46(6), 2275-2277.

Park, S.W. (2001). "Analytical modeling of viscoelastic dampers for structural and vibration control." *International Journal of Solids and Structures* 38,8065-8092.

Park, J., Mongeau, L. and Siegmund, T. (2003)." Influence of support properties on the sound radiated from the vibrations of rectangular plates." *Journal of Sound and Vibration*, 264, 775–794.

Payne, A.R. (1966). *Physical properties of natural rubber*, Masters theses, Durham University.

Perales-Martínez, I.A. et al. (2017). “Enhancement of a Magnetorheological PDMS Elastomer with Carbonyl Iron Particles.” *Polymer Testing*, 57,78–86.

Popp, K.M., Kroger, M., Li, W. H., Zhang, X. Z., Kosasih, P. B. (2009). "MRE Properties under shear and squeeze modes and applications." *Journal of Intelligent Material Systems and Structures,*21,1471-1477.

Pritz, T. (1996). “Analysis of four-parameter fractional derivative model of real solid materials.” *Journal of Sound and Vibration* 195 (1): 103-115.

Pritz, T. (2003). “Five-parameter fractional derivative model for polymeric Damping materials.” *Journal of Sound and Vibration,* 265,935–952.

Possinger, T., Bolzmacher, C., Bodelot, L., Triantafyllidis, N. (2014). "Influence of interfacial adhesion on the mechanical response of magnetorheological elastomers at high strain." Microsystem Technologies, 20,803–814.

Qiao, X. *et al.*(2012). "Microstructure and magnetorheological properties of the thermoplastic magnetorheological elastomer composites containing modified carbonyl iron particles and poly(styrene- b -ethylene- ethylenepropylene- b-styrene) matrix.", *Smart Materials and Structures,* 21, 115028.

Rabindranath, R. and Böse, H. (2013). “On the Mobility of Iron Particles Embedded in Elastomeric Silicone Matrix.” *Journal of Physics: Conference Series*, 412:12034.

Rajhana, N.H, Hamida, H. A., Ibrahim , A, Ismai, R. (2013). “Experimental Study on Mechanical Properties of Magnetorheological Elastomer.” *Journal of the Japan Society of Engineering Geology*.11, 91–96.

Ramallo, J. C., Johnson, E. A., ASCE, A.M., Spencer Jr, B. F. and ASCE, M. (2002). ‘‘Smart Base Isolation Systems.” *Journal of Engineering Mechanics*, 128(10), 1088-1099.

Ramier, J. et al.(2006). “Payne effect in silica filled styrene butadiene Rubber: Influence of surface treatment.” *Journal of Polymer Science Part B: Polymer Physics,* 45,286-297.

Ramorino, G., Vetturi, D., Cambiaghi, D., Pegoretti, A. and Ricco, T. (2003). “Developments in Dynamic Testing of Rubber Compounds: Assessment of Non-Linear Effects.” *Polymer Testing,* 22, 681–687.

Rao, M.D. (2004). "Recent applications of viscoelastic dampingfor noise control in automobiles and commercial airplanes." *Journal of Sound and Vibration*. 262,457–474.

Rao, S.S. (2004) *Mechanical Vibrations Pearson* Prentice Hall, Upper Saddle River, N.J.

Ren, J. and Krishnamoorti, R. (2003). "Nonlinear viscoelastic properties of Layered – Silicate-based intercalated Nanocomposites." *Macromolecules*. 36: 4443-4451.

Renou, F., Stellbrink, J. and Petekidis,G. (2010). "Yielding processes in a colloidal glass of soft star-like micelles under large amplitude oscillatory shear (LAOS)." *Journal of Rhoelogy* , 54, 1219-1242.

Riande, E. et al. (2000). *Polymer Viscoelasticity: Stress and Strain in Practice*. Dekker, Inc., New York.

Roylance, D. (2001). *Engineering Viscoelasticity*. MIT Press: Cambridge, MA, 2001.

Sasso, M. et al. (2011). " Application of fractional derivative models in linear viscoelastic problems." *Mechanics of Time-Dependent Materials*, 15,367–387.

Schubert, G. and Harrison, P. (2016). "Magnetic induction measurements and identification of the permeability of Magneto-Rheological Elastomers using finite element simulations." *Journal of Magnetism and Magnetic Materials*, 404, 205–214.

Schmidt, A. and Gaul, L. (2008). "Experimental investigation and numerical treatment of viscoelastic materials**."** *IMAC-XXVI: Conference & Exposition on Structural Dynamics*.

Shahsavari, R. and Ulm, F. (2009),"Indentation analysis of fractional viscoelastic solids." *Journal of Mechanics of Materials and Structures*, 4(3), 523-549.

Shaw, M.T. and MacKnight, W.J. (2005). *Introduction to Polymer Viscoelasticity* (3rd ed.). John Wiley & Sons Inc, New Jersey.

Shen, J. J. et al. (2013). "Fractional order viscoelasticity in characterization for atrial tissue." *Korea Australia Rheology Journal*, 25(2), 87–93.

Shen, Y. et al. (2004). "Experimental Research and Modeling of Magnetorheological Elastomers." *Journal of Intelligent Material Systems and Structures,* 15, 27-35.

Sireteanu, T., Giuclea, M. and Mitu, A. M. (2009). "An analytical approach for approximation of experimental hysteretic loops by Bouc-Wen model." *Proceedings of the Romanian Academy Series A - Mathematics Physics Technical Sciences Information Science*, 10(1), 1–12.

Sireteanu, T., Giuclea, M. and Solomon, O. (2010). "On the Liniarization of Experimental Hysteretic Loops." *Revue Roumaine des Sciences Techniques*, **55**, 63–71.

Sireteanu, T. et al. (2013). "A statistical linearization method of hysteretic systems based on rayleigh distribution." *Proceedings of the Romanian Academy Series A - Mathematics Physics Technical Sciences Information Science*, 14(4), 335–342.

Sjöberg, M. M. and Kari, L. (2002). "Non-Linear Behavior of a Rubber Isolator System Using Fractional Derivatives." *Vehicle System Dynamics*, 37(3), 217–236.

Song , H.J., Padalka, O. and Wereley, N. M. (2009). "Impact of Nanowire versus Spherical Microparticles in Magnetorheological Elastomer Composites." 50th AIAA/ASME/ASCE/AHS/ASC Structures, Structural Dynamics, and Materials Conference.

Spaldin, N. A. (2011). *Magnetic Materials Fundamentals And Applications*, Cambridge University Press, UK.

Stacer,R. G. et al. (1990). "Binder/Filler Interaction and the Nonlinear Behavior of Highly-Filled Elastomers." *Rubber Chemistry and Technology*, 63, 488-502.

Stelandre, L. L. et al.(2003). “ Dynamic mechanical properties of precipitated silica filled rubber: influence of morphology and coupling agent.” *Rubber Chemistry and Technology,* 76, 145-160.

Stelzer, G. J., Schulz, M. J., Kim, J. and Allemang, R. J.(2003). “A Magnetorheological Semi-Active Isolator to Reduce Noise and Vibration Transmissibility in Automobiles.” *Journal of Intelligent Material Systems and Structures*, 14, 743-765.

Stepanov, G.V., Abramchuk, S.S., Grishin, D.A. , Nikitin, L.V, Kramarenko, E.Y. and Khokhlov, A.R.(2007). "Effect of a homogeneous magnetic field on the viscoelastic behavior of magnetic elastomers." *Polymer*, 48, 488-495.

Stepanov, G.V., Borin, D Y, Raikher, Y. L., Melenev, P. V. and Perov, N. S. (2008). "Motion of ferroparticles inside the polymeric matrix in magnetoactive elastomers." *Journal of Physics: Condensed Matter*, 20, 204121.

Stepanov, G., Borin, D. and Odenbach, S. (2009). "Magnetorheological effect of magneto-active elastomers containing large particles." *Journal of Physics: Conference Series*, 149, 12098.

Stepanov ,G.V., Chertovich, A.V. and Kramarenko, E.Y. (2012). "Magnetorheological and deformation properties of magnetically controlled elastomers with hard magnetic filler."*Journal of Magnetism and Magnetic Materials* , 324, 3448–3451.

Stepanov , G.V., Borin, D.Yu. and Storozhenko, P.A.(2017). "Rotation of magnetic particles inside the polymer matrix of magnetoactive elastomers with a hard magnetic filler." *Journal of Magnetism and Magnetic Materials*, 431,138–140.

Sun, T. L. et al. (2008). "Study on the damping properties of magnetorheological elastomers based on cis-polybutadiene rubber." *Polymer Testing*, 27(4), 520–526.

Sun, S., Deng, H., Yang, Y., Li, W., Du, H. and Alici, G. (2014). "Performance evaluation and comparison of magnetorheological elastomer absorbers working in shear and squeeze modes." *Journal of Intelligent Material Systems and Structures* , 26 (14), 1757-1763.

Suzuki, N., Ito, M. and Yatsuyanagi, F. (2005). "Effects of rubber/filler interactions on deformation behavior of silica filled SBR systems." *Polymer*.46, 193–201.

Tariq, S. et al. (1998), "Nonlinear viscoelasticity of cheese." *Biorheology*,35, 171-191.

Thompson, J. D. (1998). “Developments of the indirect method for measuring the high frequency dynamic stiffness of resilient elements.” *Journal of Sound and Vibration*, 213, 169-188.

Thaijaroen, W. and Harrison, A. J. L. (2010). "Nonlinear dynamic modelling of rubber isolators using six parameters based on parabolic spring, springpot, and smooth-slip friction element." *Polymer Testing*, 29(7), 857–865.

Tian, T. F. et al. (2011). “Microstructure and magnetorheology of graphite-based MR elastomers.” *Rheologica Acta*, 50(9–10), 825–836.

Tian, T. F., Li, W. H. and Alici, G. (2013a). "Study of magnetorheology and sensing capabilities of MR elastomers."*Journal of Physics: Conference Series*, 412, 012037.

Tian, T. F. et al. (2013b). "Study of PDMS based magnetorheological elastomers." *Journal of Physics: Conference Series*, 412, 12038.

Tillema, H. G., 2003, *Noise reduction of rotating machinery by viscoelastic bearing supports*, Doctoral thesis, University of Twente, Enschede, The Netherlands.

Torvik, P.J. and Bagley, R.L. (1983). “On the Appearance of the Fractional Derivative in the Behavior of Real Materials.” *Transactions of the ASME***,** 51,294-298.

Tsai, M.,S. Huang,P. Chiang, C. Chen,2007, Morphology, Dynamic Mechanical Properties, and Gas Separation of Crosslinking Silica-Containing Polyimide Nanocomposite Thin Film, *Journal of Applied Polymer Science.*, 106, 3185–3192.

Tsai, M., W. Whang, 2003, Dynamic Mechanical Properties of Polyimide/Poly(silsesquioxane)-Like Hybrid Films, *Journal of Applied Polymer Science,* 81, 2500–2516.

Uthayakumaran S, Newberry, M., Phan-Thien, N. and Tanner,R. (2002). " Small and large strain rheology of wheat gluten." *Rheolocica Acta*,41,62–172.

Wang, K. and Tang, J. (2008). *Nonlinear High Precision Robust Control With Hysteresis Compensation. In: Adaptive Structural Systems with Piezoelectric Transducer Circuitry*, Springer Publishing.

Wang, X., Gordaninejad, X., Calgar, M., Liu, Y., Sutrisno, J. and Fuchs, A. (2009). "Sensing Behavior of Magnetorheological Elastomers." *Journal of Mechanical Design*, 131, 091004-6.

Wang, X and Robertson, C.G. (2005). "Strain-induced nonlinearity of filled rubber." *Physical review*, 72, 031406.

Wang, Y. et al. (2006). "Effects of rubber/magnetic particle interactions on the performance of magnetorheological elastomers." *Polymer Testing*, 25, 262–267.

Wang, Y. et al. (2007)." Preparation and Properties of Magnetorheological Elastomers Based on Silicon Rubber/Polystyrene Blend Matrix." *Journal of Applied Polymer Science*, 103, 3143–3149.

Wang, Y., Zhang, X., Oh, J. and Chung, K. (2015). “Fabrication and Properties of Magnetorheological Elastomers Based on CR/ENR Self-Crosslinking Blends.” *Smart Materials and Structures*, 24(9), 95006.

Wei, B., Gong, X.L. and Jiang, W. (2010). "Influence of Polyurethane Properties on Mechanical Performances of Magnetorheological Elastomers." *Journal of Applied Polymer Science*, 116, 771–778.

Wei, S. D., Gang, C.,Yu, G. and Eberhard, P. (2009). "Modeling and parameter identification of amplitude- and frequency-dependent rubber isolator." *Journal of Central South University of Technology*, 18, 672−678.

Wilhelm, M., Reinheimer, P., Ortseifer, M., Neidhöfer, T. and Spiess, H. (2000), " The crossover between linear and non-linear mechanical behavior in polymer solutions as detected by Fourier-transform rheology." *Rheologica Acta*, 39,241–246.

Winthrop, M.F., Baker, W.P. and Cobb, R.G. (2005) . "A variable stiffness device selection and design tool for lightly damped structures." *Journal of Sound and Vibration*, 287, 667–682.10.1177/1045389X14568819.

Wollscheid, D. (2014). *Predeformation and frequency dependence of filler-reinforced rubberunder vibration*, Ph D theses, University of the Bundeswehr Munich.

Wren, G. G. and Kinra, V. K., (1992). "Modeling and Measurement of Axial andFlexural Damping in Metal-Matrix Composites," *M3 D: Mechanics and Mechanisms of Material Damping, ASTM STP*, 1169*,* 282-315.

Wu, J., Gong, X.L., Chen, L., Xia, H. and Hu, Z. (2009). " Preparation and Characterization of Isotropic Polyurethane Magnetorheological Elastomer Through In Situ Polymerization " *Journal of Applied Polymer Science*, 114, 901–910.

Wu, J., Gong, X.L., Fan, Y. and Xia, H. (2012). " Improving the Magnetorheological Properties of Polyurethane Magnetorheological Elastomer Through Plasticization." *Journal of Applied Polymer Science*, 123, 2476–2484.

Xu, Y., Gong, X., Xuan, S., Zhange,W. and Fan, Y. (2011). " A high-performance magnetorheological material: preparation, characterization and magnetic-mechanic coupling properties." *Soft Matter*, 2011, 7, 5246–5254.

Xu, Z. and Chen, W. (2013). "A fractional-order model on new experiments of linear viscoelastic creep of Hami Melon." *Computers and Mathematics with Applications*. 66(5), 677–681.

Xu, Z.D., Xu, C. and Hu, J. (2015). "Equivalent fractional Kelvin model and experimental study on viscoelastic damper". Journal of Vibration and Control. 21(13),2536-2552.

Yang, C., Fu, J., Yu, M., Zheng, X. and Ju,B. (2015). "A New Magnetorheological Elastomer Isolator in Shear-Compression Mixed Mode." *Journal of Intelligent Material Systems and Structures*, 26(10), 1290–1300.

Yang, J., Gong, X.L. Deng, X., Qin, L. and Xuan, S.(2012). "Investigation on the Mechanism of Damping Behavior of Magnetorheological Elastomers." *Smart Materials and Structures*, 21, 125015.

Yang, J., Gong, X.L., Zong, L., Peng, C., Huan, S.X. (2013a) "Silicon Carbide-Strengthened Magnetorheological Elastomer: Preparation and Mechanical Property." *Polymer Engineering and Science*, doi: 10.1002/pen

Yang, M. G., Li, C. Y. and Chen, Z. Q. (2013b). "A new simple non-linear hysteretic model for MR damper and verification of seismic response reduction experiment." Engineering Structures, 52, pp. 434–445.

Yang, J. et al. (2013c). "Experimental study and modeling of a novel magnetorheological elastomer isolator." *Smart Materials and Structures,* 22,117001

Yao, G.Z., Yap, F.F, Chen, G., Li, W. H. and Yeo, S. H. (2002). "MR damper and its application for semi-active control of vehicle suspension system." *Mechatronics*, 12, 963–973.

Yoshioka,H., Ramallo, J. C. and Spencer Jr, B. F. (2002). " SmartBase Isolation Strategies Employing Magnetorheological Dampers." *Journal of Engineering Mechanics*, 128(5), 540-551.

Yu. M., Ju, B., Fu, J., Liu, X. and Yang, Q. (2012). "Influence of composition of carbonyl iron particles on dynamic mechanical properties of magnetorheological elastomers."*Journal of Magnetism and Magnetic Materials*, 324 , 2147–2152.

Yu, M. et al. (2017). "Understanding the reinforcing behaviors of polyaniline-modified carbonyl iron particles in magnetorheological elastomer based on polyurethane/epoxy resin IPNs matrix." *Composites Science and Technology*, 139, 36–46.

Yu, M., Qi, S., Fu, J. Fu, Yang, P. A. and Zhu, M. (2015). "Preparation and Characterization of a Novel Magnetorheological Elastomer Based on Polyurethane/epoxy Resin IPNs Matrix." *Smart Materials and Structures*, 24(4),45009.

Yu, Y., Naganathan, N.G. and Dukkipati, R.V. (2001). "A literature review of automotive vehicle engine mounting Systems." *Mechanism and Machine Theory*, 36, 123-142.

Yurkeli, K. (2001). "Structure dynamics of carbon black filled elastomer." *Journal of Polymer Science Part B: Polymer Physics,* 39,256-275.

Yunus, N. A. et al. (2016). "Rheological Properties of Isotropic Magnetorheological Elastomers Featuring an Epoxidized Natural Rubber." *Smart Materials and Structures*, 25(10),107001.

Zajac, P. et al. (2010). "Isotropic magnetorheological elastomers with thermoplastic matrices: structure, damping properties and testing." *Smart Materials and Structures,*19, 045014.

Zilli, D. et al. (2005)." Magnetic properties of multi-walled carbon nanotube-epoxy composites." *Polymer*, 46(16), 6090–6095.

Zhang, J. and Richards, C. M. (2006). "Dynamic Analysis and ParameterIdentification of a Single Mass Elastomeric Isolation System Using a Maxwell-Voigt Model." *Journal of Vibration and Acoustics,* 128,713-721.

Zhang, X. et al. (2007). "Existence of bound-rubber in magnetorheological elastomers and its influence on material properties." *Chinese Journal of Chemical Physics*, 20, 173-179

Zhang, W. et al., (2010). "Effect of Cyclic Deformation on Magnetorheological Elastomers." *Chinese Journal of Chemical Physics*.23, 226-230.

Zhang, W., Gong, X. L., Jiang,W. Q. and Fan,Y. C. (2010). "Investigation of the Durability of Anisotropic Magnetorheological Elastomers Based on Mixed Rubber." *Smart Materials and Structures* 19:85008.

Zhang, X. X. et al. (2001). " Magnetic properties of Fe nanoparticles trapped at the tips of the aligned carbon nanotubes." *Journal of Magnetism and Magnetic Materials*, 231, 9–12.

Zhu, J. T, Xu, Z. D. and Guo, Y. Q (2012). "Magnetoviscoelasticity parametric model of an MR elastomer vibration mitigation device". *Smart Materials and Structures*, 21, 075034.

Zhu, J. T, Xu, Z. D. and Guo, Y. Q. , 2013, "Experimental and Modeling Study on Magnetorheological Elastomers with Different Matrices". *Journal of materials in civil engineering*, 25, pp. 1762-1771.

List of Publications based on PhD Research Work

Sl. No.	Title of the paper	Authors (in the same order as in the paper. Underline the Research Scholar's name)	Name of the Journal/ Conference, Vol., No., Pages	Month, Year of Publication	Category*
1.	Dynamic blocked transfer stiffness method of characterizing the magnetic field and frequency dependent dynamic viscoelastic properties of MRE	Umanath R Poojary, Sriharsha Hegde, K.V. Gangadharan	Korea-Australia Rheology Journal , Volume 28, Issue 4, pp 301–313.	November, 2016	1
2.	Dynamic deformation–dependent, magnetic field–induced force transmissibility characteristics of magnetorheological elastomer	Umanath R Poojary, Sriharsha Hegde, K.V. Gangadharan	Journal of Intelligent Material Systems and Structures, Volume: 28 issue: 11, page(s): 1491-1500.	November, 2016	1
3.	Experimental investigation on the effect of magnetic field on strain dependent dynamic stiffness of magnetorheological elastomer	Umanath R Poojary and K.V. Gangadharan	Rheologica Acta Volume 55, Issue 11–12, pp 993–1001.	December, 2016	1
4.	Magnetic field and frequency dependent LVE limit characterization of magnetorheological elastomer	Umanath R Poojary and K.V. Gangadharan	Journal of the Brazilian Society of Mechanical Sciences and Engineering.Volume 39, Issue 4, pp 1365–1373	April, 2017	1
5	Integer and fractional order based viscoelastic constitutive modelling to predict the frequency and magnetic field induced properties of MRE	Umanath R Poojary and K.V. Gangadharan	Journal of Vibration and Acoustics, 041007, , doi: 10.1115/1.4039242	February, 2018	1
6	Experimental investigation on the effect of carbon nanotube additive on the field-induced viscoelastic properties of magnetorheological elastomer	Umanath R Poojary, Sriharsha Hegde, K.V. Gangadharan	Journal of Materials Science, Volume 53, Issue 6, pp 4229–4241	March, 2018	1

*Category: 1: Journal paper, full paper reviewed 2: Journal paper, Abstract reviews 3: Conference/Symposium paper, full paper reviewed
4:Conference/Symposium paper, abstract reviewed 5: others(including papers in Workshops, NITK Research Bulletins, Short notes etc.)

Umanath R Poojary

Research Scholar
Name & Signature, with Date

Dr. K V Gangadharan

ResearchGuide
Name & Signature, with Date